

# Initial Benchmarks of UV LEDs and Comparisons with White LEDs

U.S. Department of Energy—Lighting R&D Program

November 2021

(This page intentionally left blank)

## Disclaimer

This report was prepared as an account of work sponsored by an agency of the United States Government. Neither the United States Government nor any agency thereof, nor any of its employees, makes any warranty, express or implied, or assumes any legal liability or responsibility for the accuracy, completeness, or usefulness of any information, apparatus, product, or process disclosed, or represents that its use would not infringe privately owned rights. Reference herein to any specific commercial product, process, or service by trade name, trademark, manufacturer, or otherwise does not necessarily constitute or imply its endorsement, recommendation, or favoring by the United States Government or any agency thereof. The views and opinions of authors expressed herein do not necessarily state or reflect those of the United States Government or any agency thereof.

## Authors

The authors of this report are:

J. Lynn Davis, Kelley Rountree, Roger Pope, Clint Clayton, Andrew Dart, Michelle McCombs, and Abdal Wallace, RTI International

## Acknowledgments

This material is based upon work supported by the U.S. Department of Energy's Office of Energy Efficiency and Renewable Energy (EERE) under the National Energy Technology Laboratory (NETL) Mission Execution and Strategic Analysis (MESA) contract, award number DE-FE0025912.

## Nomenclature or List of Acronyms

$\lambda_{\max}$	wavelength of maximum emission
$^{\circ}\text{C}$	degree Celsius
$a$	in-plane lattice constant of a wurtzite crystal structure
A	amps
ACGIH	American Conference of Governmental Industrial Hygienists
AlGaN	aluminum gallium nitride
AlGaInN	aluminum gallium indium nitride
AlGaInP	aluminum gallium indium phosphide
AlN	aluminum nitride
CCT	correlated color temperature
DOE	U.S. Department of Energy
DUT	device under test
$e$	charge on an electron
EERE	Office of Energy Efficiency and Renewable Energy
$E_g$	band gap energy
eV	electronvolt
FWHM	full-width at half maximum
GaN	gallium nitride
GUV	germicidal ultraviolet radiation
HP-LED	high-power LED
$I_f$	forward current
InGaN	indium gallium nitride
InN	indium nitride
IR	infrared
I-V	current-voltage measurement
K	Kelvin
LED	light-emitting diode
LPM	low-pressure mercury

LSRC	LED Systems Reliability Consortium
mA	milliampere
MC-PCB	metal-core printed circuit board
MESA	Mission Execution and Strategic Analysis
mm	millimeter
MPM	medium-pressure mercury
mV	millivolt
mW	milliwatt
NETL	National Energy Technology Laboratory
nm	nanometer
PCB	printed circuit board
pc-LED	phosphor-converted LED
QW	quantum well
$R_{\text{serial}}$	serial resistance
SARS-CoV-2	severe acute respiratory syndrome coronavirus 2
SPD	spectral power distribution
SRH	Shockley-Read-Hall
SSL	solid-state lighting
t	time
$T_a$	ambient temperature
TAT	trap-assisted tunneling
TE	transverse electric mode of radiation
$T_j$	junction temperature
TM	transverse magnetic mode of radiation
$T_{\text{sp}}$	solder point temperature
UV	ultraviolet radiation
UV-A	a band of UV radiation with wavelengths between 315 nm and 380 nm
UV-B	a band of UV radiation with wavelengths between 280 nm and 315 nm
UV-C	a band of UV radiation with wavelengths between 100 nm and 280 nm

UV-x	identification code for UV products used in this report; x is a number between 1 and 14
V	volt
V(t)	change in voltage with time at a fixed $I_f$ value
$V_{br}$	breakdown voltage
$V_f$	forward voltage
$V_{th}$	threshold voltage
W	watt

## Executive Summary

Light-emitting diodes (LEDs) can emit radiation that spans the range from near infrared (IR) to all three bands of ultraviolet (UV) radiation (i.e., UV-A, UV-B, UV-C). These emission sources are fabricated by varying doping levels of the aluminum gallium indium nitride (AlGaInN) alloy system, which tunes the emission wavelength of the semiconductor. During the past 20 years, the blue LED, made from InGaN, has advanced technologically to the point that it now provides the backbone for the solid-state lighting revolution that is occurring in general illumination. With proper doping, the InGaN alloy system can be extended to UV-A emission wavelengths as low as 362 nanometers (nm); however, producing LEDs that emit in the UV-B and UV-C bands requires the use of AlGaN alloys. Unfortunately, AlGaN semiconductors are not at the same level of technological development as InGaN, and LEDs made from AlGaN suffer from a variety of inefficiencies arising from electrical and optical limitations of the current technology. This report is aimed at benchmarking the performance of UV LEDs across all three bands in an effort to understand the current state of the technology.

UV sources have many industrial applications, and their total market exceeds \$750 million. Examples of applications for UV sources include ink and polymer curing (primarily UV-A sources), medical treatments (primarily UV-B sources), and disinfection (primarily UV-C sources). While UV-A applications are the largest market today, the increased need for surface and air disinfection is expected to create a significant market opportunity for UV-C sources in the near future. The current technology most widely used for UV sources in all three bands is the mercury discharge lamp, which has moderate energy efficiency but also has a number of limitations including compatibility with compact form factors, long-term reliability, and end-of-life issues associated with disposing a glass tube containing mercury without creating environmental contamination. UV LEDs have the potential to displace mercury lamps in UV applications in much the same way that white LEDs have displaced fluorescent lamps in many commercial and residential lighting markets.

The primary goal of this report is to benchmark the initial level of performance of a selection of commercial UV LEDs across all three bands (i.e., UV-A, UV-B, UV-C). To provide the initial performance benchmarks, a test matrix containing 13 different UV LED products was created in association with the LED Systems Reliability Consortium (LSRC). The products in this test matrix were all commercially available as of June 2021, and at least 22 samples of each product were tested. In addition, two common, commercial white LEDs were tested to provide a benchmark against blue-pumped white LEDs. Testing of the samples included electrical performance testing (e.g., current-voltage measurements) and photometric testing in a calibrated integrating sphere capable of measuring devices in the UV-A, UV-B, and UV-C bands. The electrical testing provided insights into the performance of the semiconductor layers in the LEDs, allowing parameters such as the threshold voltage ( $V_{th}$ ) and serial resistance ( $R_{serial}$ ) of each sample to be determined. The photometric testing provided insights into emission wavelengths, peak shapes, and radiant efficiencies for each sample. Combined, the information from these

tests permits the overall device efficiencies to be compared and provides insights into the electrical and optical performance of the technology.

The  $V_{th}$  value required to initiate light emission from an LED is dependent on the bandgap energy ( $E_g$ ) of the semiconductor and any additional voltages that are needed to compensate for parasitic voltage losses (i.e., inefficiencies). Values of  $V_{th}$  near  $E_g$  indicate a semiconductor that is approaching peak electrical performance, but does not provide any insights into the optical performance of the LED. As shown in **Figure ES-1**, the  $V_{th}$  values for the white LEDs tested in this study are approximately equal to the  $E_g$  value for an ideal 450 nm emitter. Likewise, for the four UV-A products tested in the study (i.e., identified as UV-11, UV-12, UV-13, UV-14), the average  $V_{th}$  was approximately equal to the  $E_g$  value of an ideal 365 nm emitter. Differences in the  $V_{th}$  and  $E_g$  values for these products are likely due to thermal effects arising from room temperature operation of the LEDs. This finding is not surprising given that both UV-A and blue LEDs share the InGaN alloy systems.

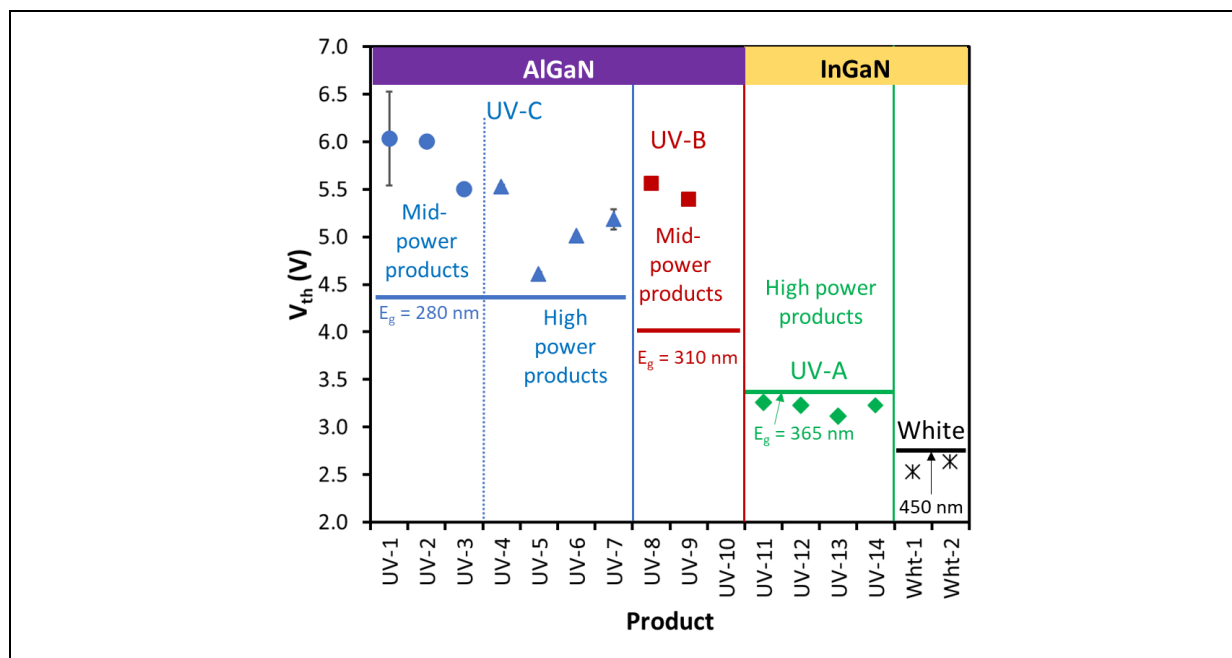


**Figure ES-1:** Average  $V_{th}$  values for each product examined in this study. Error bars represent measurement standard deviation for each product and are calculated for at least 20 samples. The solid horizontal lines are the approximate  $E_g$  for an ideal emitter at 280 nm (blue), 310 nm (red), 365 nm (green), and 450 nm (black).

In contrast, the UV-B and UV-C LEDs examined in this study exhibited a  $V_{th}$  value that was significantly higher than the  $E_g$  value of an ideal emitter at 280 nm (blue line in **Figure ES-1**) or an ideal emitter at 310 nm (red line in **Figure ES-1**). The additional voltages above  $E_g$  that are required to compensate for the parasitic voltage losses varied from 0.18 volts (V; UV-5) to greater than 1.5 V (UV-1, UV-2, and UV-9). The necessity of these additional voltages can be traced to the  $R_{serial}$  values of the electrical contacts used in the devices and the quality of the semiconductor (e.g., carrier concentration and mobility, dislocation density). For comparison, in the year 2000, the difference between  $V_{th}$  and the  $E_g$  for blue AlGaInN was 0.5 to 1.0 V.

The radiant efficiency of InGaN LEDs emitting in the blue is high and can exceed 70% in some cases. Likewise, the radiant efficiency of UV-A LEDs utilizing InGaN chemistry can also be high and can exceed 50% at low currents. However, the radiant efficiency of AlGaN LEDs is significantly lower due to the electrical and optical challenges yet to be solved with this semiconductor system. As shown in **Figure ES-2**, the total radiant efficiencies of UV-B and UV-C products examined in this study varied from 2% to 5%, and showed a strong inverse dependence on  $V_{th}$  below 5.5 V. The lone exception to this trend was UV-3 where unknown factors raised the radiant efficiency to 5% despite a high  $V_{th}$  value. The unknown factors responsible for the performance of UV-3 are not likely electrical in nature because  $V_{th}$  and  $R_{serial}$  are high. Instead, it is likely that this LED's improved radiation efficiency was achieved through improvements in radiation extraction efficiency such as a reduction in the absorbance of the p-contact layer or improved contact reflectivity.

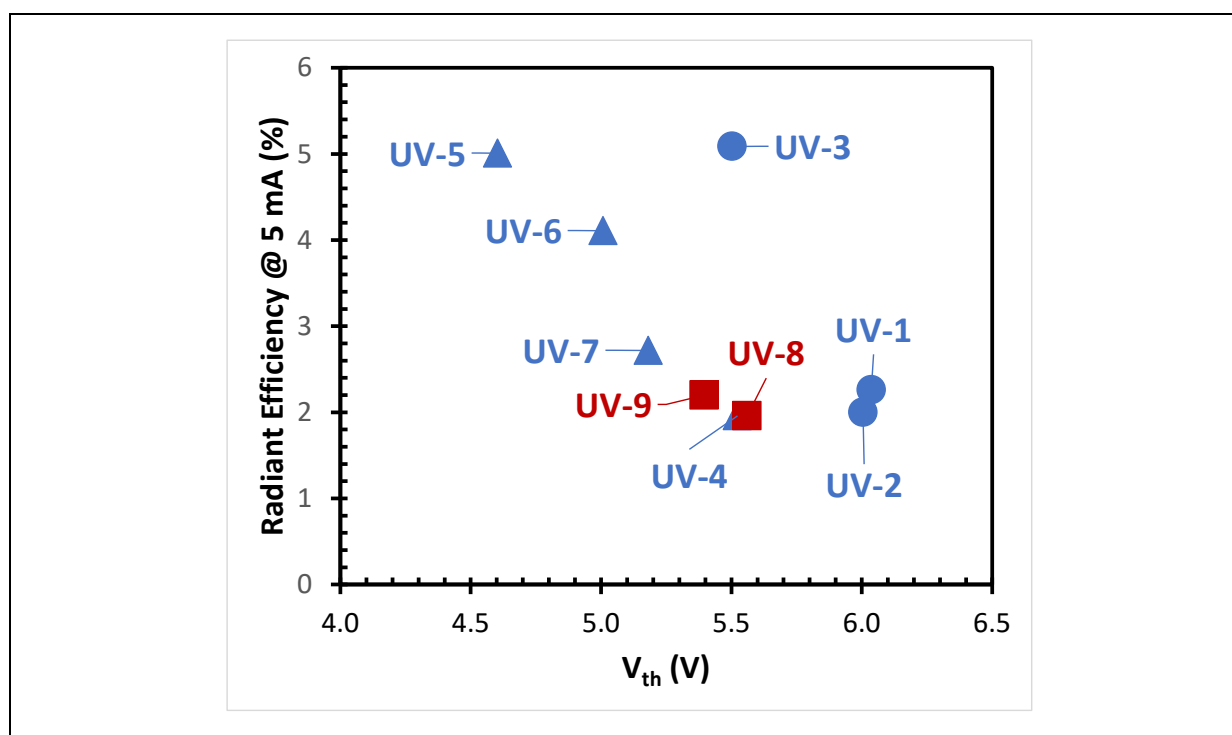


**Figure ES-2:** Radiant efficiency at an  $I_f$  value of 5 mA versus  $V_{th}$  for the UV-B (red squares), mid-power UV-C (blue circles), and high-power UV-C (blue triangles) products examined in this report.

This study provides initial benchmarks on the electrical and optical performance of UV-A, UV-B, and UV-C LEDs. A future report will provide lifetime performance data on these same LEDs when operated for extended periods at room temperature and in an elevated temperature and humidity environment. Although the more advanced InGaN technologies used in UV-A LEDs produce devices with relatively high efficiencies, the less mature AlGaN technology required to make LEDs that emit in the UV-B or UV-C bands currently produces devices with low efficiencies. This report underscores that there are electrical and optical challenges to be solved in the AlGaN system to improve efficiency and reduce energy consumption. Overcoming these

limitations will produce UV LEDs that eliminate the environmental issues and other limitations of mercury discharge lamps that are currently used as a UV source. In addition, UV LEDs may spark a wave of innovative lighting products that combine illumination and UV LEDs to create new, energy efficient, multifunctional products for office, commercial, and possibly residential use.

## Table of Contents

Executive Summary .....	vii
1 Introduction.....	1
1.1 Industrial Uses of Ultraviolet Radiation.....	1
1.2 Sources for UV Radiation .....	2
1.2.1 Mercury Discharge Lamps.....	2
1.2.2 Light-Emitting Diodes .....	3
1.3 Other UV Sources .....	6
1.4 UV Radiation Safety .....	6
1.5 Goals of This Study.....	7
2 LED Samples .....	8
3 Experimental Methods and Procedures .....	10
3.1 Current-Voltage Measurements .....	11
3.2 Voltage over Time Measurements .....	13
3.3 Radiometric Measurements.....	15
4 Results and Discussion .....	17
4.1 LED Package Structures.....	17
4.2 Initial I-V Measurements .....	18
4.3 Initial Radiometric Measurements .....	22
4.4 Device Radiant Efficiencies.....	25
5 Conclusions.....	28
References.....	29

## Appendices

Appendix A: Initial Benchmarks for UV LEDs .....	31
Appendix B: Initial V(t) Measures for LEDs in This Study.....	46

## List of Figures

ES-1:	Average $V_{th}$ values for each product examined in this study. Error bars represent measurement standard deviation for each product and are calculated for at least 20 samples. The solid horizontal lines are the approximate $E_g$ for an ideal emitter at 280 nm (blue), 310 nm (red), 365 nm (green), and 450 nm (black). .....	viii
ES-2:	Radiant efficiency at an $I_f$ value of 5 mA versus $V_{th}$ for the UV-B (red squares), mid-power UV-C (blue circles), and high-power UV-C (blue triangles) products examined in this report.....	ix
1-1:	Mercury lamps designed for general illumination (bottom) and for UV radiation dosing (top). .....	3
1-2:	Variation in band gap of the AlInGaN materials system as a function of lattice constant of the doped alloy. First principles calculations of $E_g$ and $a$ were used to create this graph [10]. .....	4
1-3:	Some technical challenges to be solved in the maturation of UV-B and UV-C LED technology. ....	5
1-4:	Eight-hour exposure limits for UV radiation based on relative spectral effectiveness values from the ACGIH [15]. .....	7
2-1:	Extruded aluminum heat sinks used for all UV LEDs included in the study. ....	9
3-1:	I-V measurement for White-2, a representative white, high-powered LED.....	11
3-2:	Log-linear version of the I-V profile given in Figure 3-1.....	12
3-3:	Representation example of a voltage vs. time measurement for a UV-C LED operated at 5 mA.....	14
3-4:	Small integrating sphere used in initial measurements.....	16
3-5:	Larger integrating sphere used in these measurements. The sphere measured 10 inches in diameter. ....	16
4-1:	Breakout of the LED package architectures found for the UV LEDs examined in this study. ....	17
4-2:	Average $V_{th}$ values for each product examined in this study. Error bars representing measurement standard deviation for each product and are calculated for at least 20 samples. The solid horizontal lines are the approximate $E_g$ for an ideal emitter at 280 nm (blue), 310 nm (red), 365 nm (green), and 450 nm (black). .....	19
4-3:	Average $R_{serial}$ values for each product examined in this study. Errors bars are also included and represent the measurement standard deviation of at least 20 samples. ....	20
4-4:	Current measured at 0.5 V below average $V_{th}$ for each product.....	21
4-5:	UV-C product (UV-7) with a main emission peak and a weaker secondary emission peak arising from deep-level luminescence. The relative spectra is shown for two different DUTs of UV-7. ....	23
4-6:	Radiant efficiency at an $I_f$ value of 5 mA versus $V_{th}$ for the UV-B (red squares), mid-power UV-C (blue circles), and high-power UV-C (blue triangles) products examined in this report.....	26

4-7: Radiant efficiency change with drive current ( $I_f$ ) for a representative DUT of each UV-B and UV-C product examined in this report. ....27

4-8: Radiant efficiency change with drive current ( $I_f$ ) for a representative DUT of each UV-A product examined in this report. ....28

## List of Tables

1-1:	Market sizes (in \$ millions) of applications using UV radiation [2].	2
2-1:	Basic properties of the UV LEDs examined in this study. <sup>a</sup>	8
2-2:	Construction practices used in the LEDs examined in this study.	10
3-1:	Wavelengths and associated band gaps for sources examined in this study.	13
3-2:	Calculated temperature rise during 5 mA operation of the LEDs in this study.	14
4-1:	Initial photometric properties of the UV LEDs examined in this study. <sup>a</sup>	22
4-2:	Relative amounts of UV-C radiation at $I_f = 5$ ma for products with $\lambda_{max}$ between 270 nm and 280 nm.	24
4-3:	Relative amounts of UV-A radiation when operated at 5 mA.	25

# 1 Introduction

## 1.1 Industrial Uses of Ultraviolet Radiation

Electromagnetic radiation in the form of light is widely used in illumination applications throughout the world. The band of visible radiation known as light is defined by the response of the photoreceptors in the human retina and occurs at wavelengths between 380 nanometer (nm) and 780 nanometers (nm). Ultraviolet (UV) radiation occurs at shorter wavelengths between 100 nm and 380 nm, and this radiation is not directly imaged by the human eye. UV radiation is produced naturally by the sun, though it is not visible to humans. Commercially, UV radiation has many useful applications and also some potentially harmful side effects due to its significant impact on humans, plants, and animals [1].

UV radiation is typically divided into three bands, UV-A spanning the wavelengths between 315 nm and 380 nm, UV-B spanning the wavelengths between 280 nm and 315 nm, and UV-C radiation spanning the wavelengths between 100 nm and 280 nm. Earth's atmosphere, especially ozone and carbon dioxide, absorb all UV-C radiation and most UV-B radiation produced by the sun. In contrast, UV-A radiation undergoes significantly less attenuation when passing through the atmosphere. As a result, plants, animals, viruses, bacteria, and other organisms are naturally exposed to UV-A radiation and some UV-B radiation, but are generally not exposed to UV-C radiation at ground level. This may be part of the reason why UV-C radiation is such an effective disinfectant.

There are numerous manmade sources for UV radiation across the three bands (see **Section 1.2**). These sources are widely used in many industrial processes, some of which are shown in **Table 1-1** [2]. Of these industrial applications, UV curing, which mainly involves UV-A radiation, has reached the broadest commercial use at this time. UV-B radiation is used in medical phototherapy for treatment of certain skin diseases, and UV-C radiation is receiving a significant amount of attention because of its germicidal capabilities, especially against viruses such as severe acute respiratory syndrome coronavirus 2 (SARS-CoV-2). Revenue growth in UV-A products has been slowing recently due to oversupply issues, and the average selling prices for UV-A products are decreasing as a result [2]. In contrast, the growth in the UV-C market since 2020 has been significant, and total market size is expected to increase 10-fold between 2019 and 2025 [2]. There is generally less demand for UV-B sources due to limited commercial opportunities. As a result of these forces, UV-C LEDs are expected to become the dominant market for UV LEDs over the next decade.

**Table 1-1: Market sizes (in \$ millions) of applications using UV radiation [2].**

Application of UV	Typical UV Band	2019 Lamp Market Size (\$ millions)
UV curing	UV-A	269
Disinfection (low to high power)	UV-C	216
Tanning	UV-A	96
Analytical instruments	UV-A, UV-B, UV-C	81
Medical phototherapy	UV-B	51
Black lighting	UV-A	34
Photocatalytic purification	UV-A	6
Counterfeit detection	UV-A	3

## 1.2 Sources for UV Radiation

### 1.2.1 Mercury Discharge Lamps

Gas-discharge lamps based on the emission spectrum of mercury vapor have been widely used as sources in lighting applications for decades. The relative intensities of the emission lines in the mercury-vapor spectrum depends upon the construction of the lamp including the mercury vapor pressure. In this way, the partial pressure of the mercury vapor contained within the lamp determines the emission spectrum. Mercury lamps with higher mercury vapor pressures are direct emitters of blue, green, and yellow radiation and are used as high intensity sources in outdoor lighting. Low-pressure mercury-vapor lamps (LPM) can emit radiation with sharp peaks at 185 nm and 254 nm, whereas medium-pressure mercury-vapor lamps (MPM) emit radiation between 185 and 600 nm in varying proportions [3].

Perhaps the most common mercury-vapor lamp is the fluorescent tube used widely in generally illumination applications. In the construction of this lamp, a mixture of phosphors is coated on the interior surface of the glass tube and the primary radiation from the mercury-vapor arc excites the phosphors and produces secondary radiation in the visible light spectrum. Fluorescent tubes have been widely used in indoor lighting for decades and are commonly found in troffers and compact fluorescent lamps [3]. In general, fluorescent tubes have a relatively good energy efficiency, but are usually available only in linear formats. Breakage of the glass tube can be a significant issue that makes disposal of mercury-vapor lamps problematic because the mercury contained by the glass tube is hazardous to the environment [4].

An energy efficient UV source can be produced when the phosphor is removed from the glass tube of an LPM source. LPM lamps emit primarily in the UV-C band at 185 and 254 nm, with the 254 nm line being the most common. Radiation at 185 nm can produce ozone, so ozone-free lamps use special glass tubes to filter out this radiation. MPMs can be constructed to emit primarily in the UV-A or UV-C bands. As with fluorescent lamps, mercury-vapor UV lamps are

typically available as linear or round glass tubes, which limits the potential luminaire form factors and sizes. Examples of a fluorescent lamp and a low-pressure mercury lamp are shown in **Figure 1-1**.

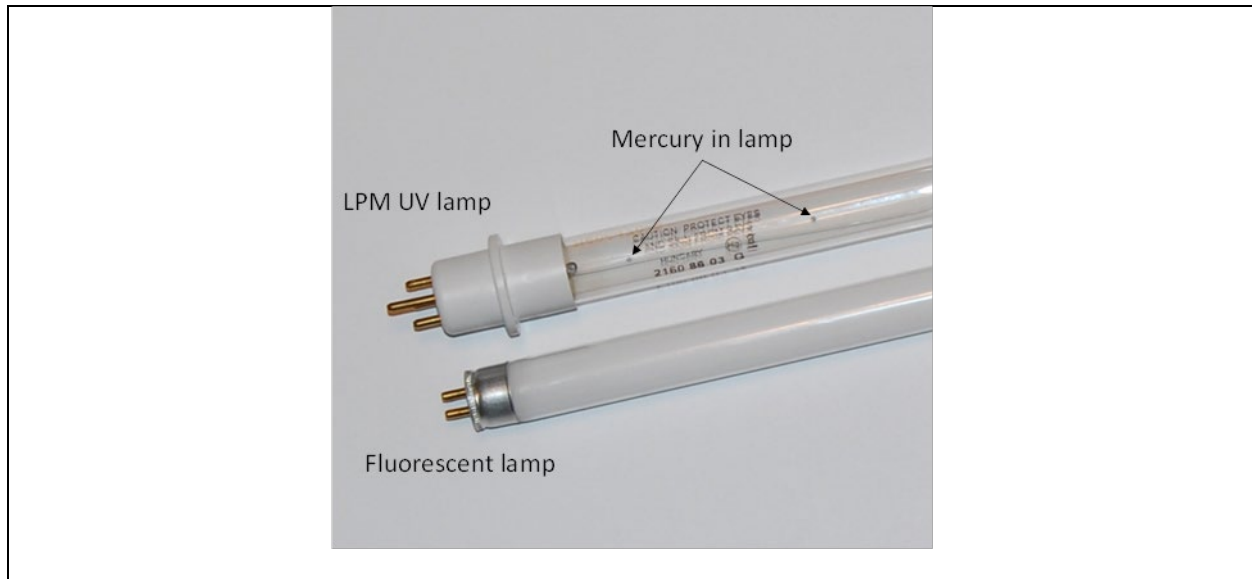


**Figure 1-1:** Mercury lamps designed for general illumination (bottom) and for UV radiation dosing (top).

### 1.2.2 Light-Emitting Diodes

Over the past 20 years, light-emitting diodes (LEDs) have transformed from a nascent source of low-level light used for indicator lamps and small backlights into the dominant lighting source in the industry. LED-based lighting is displacing fluorescent lamps in most product categories including indoor lights, outdoor lighting, backlights for monitors and mobile displays, and signage. This transformation is being driven by significant improvements in the field performance (e.g., efficiency, stability, reliability) and manufacturability of white and visible light LEDs and a corresponding drop in the average selling price of these sources by several orders of magnitude [5, 6].

The underlying chemistry responsible for the development of the blue LEDs used in solid-state lighting (SSL) is the III-V semiconductor system. Some of the most prominent III-V materials are indium nitride (InN), gallium nitride (GaN), and aluminum nitride (AlN), which form the alloy system shown in **Figure 1-2**. The bandgap energy ( $E_g$ ) of pure InN is 0.77 electron volts (eV), the  $E_g$  value of pure GaN is 3.42 eV, and the  $E_g$  value of pure AlN is 6.28 eV. This corresponds to photon emission wavelengths of 1,610 nm (InN), 362.5 nm (GaN), and 197.4 nm (AlN) [7-10]. All three semiconductors have wurtzite crystal structures, and the in-plane lattice constants ( $a$ ) of these structures are 0.354 nm (InN), 0.319 nm (GaN), and 0.311 nm (AlN).

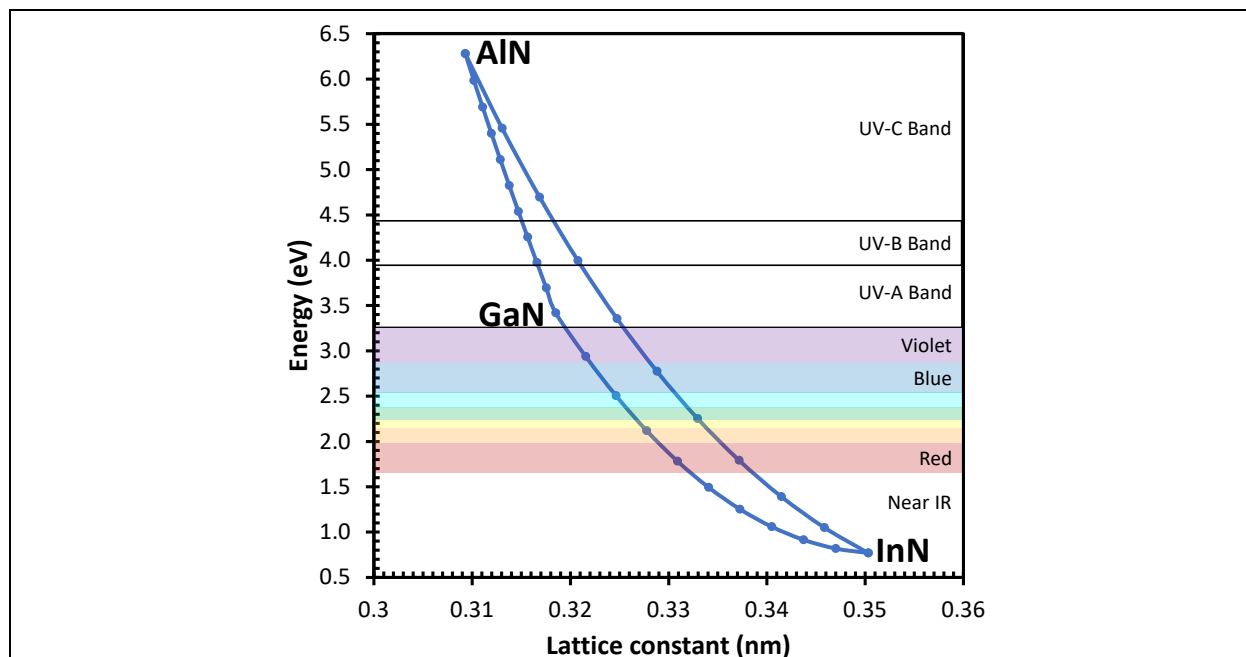


Figure 1-2: Variation in band gap of the AlInGaN materials system as a function of lattice constant of the doped alloy. First principles calculations of  $E_g$  and  $a$  were used to create this graph [10].

Perhaps one of the most important features of the III-V semiconductors is the ability to achieve different direct bandgaps through a continuous alloy system formed from InN, GaN, and AlN. As a result of the ability to tailor the bandgap energy, the emission wavelengths of this materials system can be tuned from infrared (IR) to UV wavelengths. For example, combining GaN with In to form InGaN alloys allows semiconductors with emissions in the visible to UV-A wavelengths to be produced, whereas alloying GaN with Al to form AlGaN alloys results in semiconductors with emissions in the UV-B and UV-C bands.\*

InGaN alloys have been studied extensively due to their use in SSL applications. There is typically an optimal value for the alloy composition that is the most efficient, and for InGaN alloys the emission wavelength of the most efficient material occurs at blue wavelengths; longer wavelengths (e.g., green, yellow) are less efficient. This phenomenon is responsible for the green gap, which refers to the efficiency drop in InGaN semiconductors at green and yellow wavelengths. A key implication of the data shown in **Figure 1-2** is that the InGaN materials system used to make LEDs for SSL applications are limited to wavelengths longer than the bandgap of GaN (i.e., 362 nm). This spectral range covers part of the UV-A band and visible light, but the InGaN materials system is not able to produce UV LEDs in the UV-B and UV-C bands.

To make UV-B and UV-C LEDs, GaN must be doped with Al to create AlGaN alloys as shown in **Figure 1-3**. As this is a different materials system from the heavily studied InGaN

\* The alloys are most accurately represented by the stoichiometric equation  $\text{In}_x\text{Ga}_{1-x}\text{N}$  and  $\text{Al}_x\text{Ga}_{1-x}\text{N}$  where  $x$  is the mole fraction. For brevity, we have adopted the shorthand notation of InGaN and AlGaN, respectively.

semiconductors, new research is needed to develop optimized products for UV-B and UV-C applications. Therefore, the development of AlGaN alloys for use in UV LEDs is not as well understood as the InGaN alloys used for visible LEDs employed in SSL. Consequently, the efficiency and radiant flux levels of UV-B and UV-C LED is not equal to their blue LED counterparts.

There is significant research underway to improve the performance of AlGaN UV LEDs with the expectation that large price reductions will occur within the next few years for sources for UV-B and UV-C radiation. However, there are significant technical challenges impacting the performance and reliability of AlGaN UV LEDs that need to be addressed including developing a transparent p-contact material, reducing the defect density of both n-doped and p-doped materials, improving radiation extraction efficiency, and developing a mirror with high reflectivity between 220 and 340 nm [7, 11–14]. These technical challenges can be largely divided into electrical and optical challenges and some examples are given in **Figure 1-3**. Electrical challenges are those that impact carrier concentrations, conductance, and operational voltages, whereas optical challenges are those that impact radiation extraction from the LED. Some breakthroughs in optical structures, such as a transparent p-layer have recently been incorporated into commercial products resulting in an increase in device efficiency [7]. In addition, there are package-level challenges that will also need to be solved to improve the efficiency and radiant flux delivery of UV-B and UV-C LEDs. These improvements include management of the heat produced by the UV LED, determining whether a hermetic package is required (because AlGaN is susceptible to corrosion), improving the outcoupling of UV radiation from the LED die to the package exterior, and increasing the reflectivity of package structures.

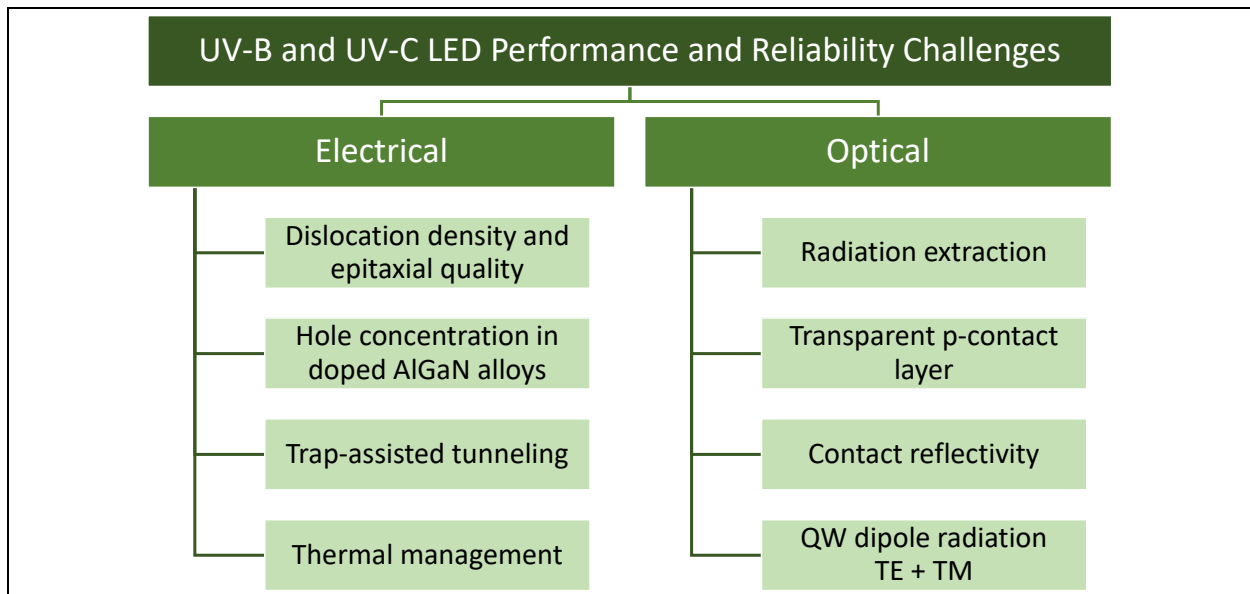


**Figure 1-3:** Some technical challenges to be solved in the maturation of UV-B and UV-C LED technology. (Note: QW = quantum well; TE = transverse electric mode of radiation; TM = transverse magnetic mode of radiation.)

### 1.3 Other UV Sources

Several other sources of UV radiation exist, including cold plasma tubes and excimer lamps. Discharge excimer lamps, such as krypton-chloride, are receiving a significant amount of attention due to their ability to produce radiation around 222 nm, which is a wavelength that is believed to have minimal human safety risk compared to UV-B and UV-C radiation [15, 16]. However, both cold plasma and discharge excimer sources emit multiple wavelengths spanning the UV-B and UV-C bands, and only sources that have appropriate radiation filters to absorb unwanted UV-B radiation should be used in most applications.

### 1.4 UV Radiation Safety

Excessive exposure to UV radiation is known to damage living tissues. Damage to skin tissues can include sun burn and blistering in worst case scenarios, whereas damage to the eyes can cause photokeratitis. In some cases, overexposure to UV radiation can cause melanoma later in life. However, the exposure risks from UV radiation vary with the different bands in relation to the level of tissue damage that the radiation causes and the depth of penetration that the radiation has in the tissue. This information has been compiled by several sources, such as the American Conference of Governmental Industrial Hygienists (ACGIH), into sensitive and exposure curves, and the 8-hour exposure limits for UV radiation are given in **Figure 1-4**. UV-A radiation has the lowest energy and usually causes minimal damage to tissues. UV-C radiation has higher energies, but its penetration into tissues is much lower because much of the radiation is absorbed by dead skin cells residing on top of living tissue, so the net risk is moderate. However, UV-B radiation has sufficient energy to cause tissue damage and can also penetrate deeply into the skin. Consequently, radiation from 280–315 nm should be used judiciously, although any UV radiation is a potential risk. Safety measures are already established to use UV radiation indoors and information on the risks and safety measures can be found elsewhere [15–17]. In addition, adequate personal protective equipment (e.g., lab coat, gloves, goggles, face mask, head covering) is available to prevent overexposure to UV radiation in any band and should be used.

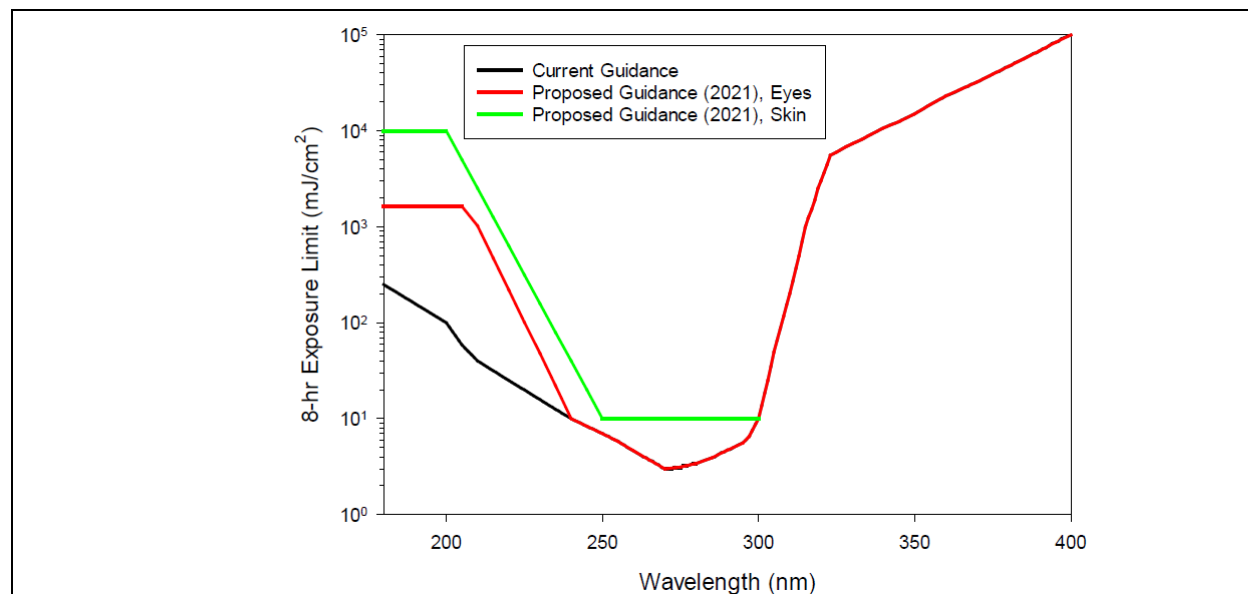


Figure 1-4: Eight-hour exposure limits for UV radiation based on relative spectral effectiveness values from the ACGIH [15].

## 1.5 Goals of This Study

Mercury-discharge lamps have been used as UV sources in a variety of building systems including heat, ventilation, and air conditioning equipment, upper-room germicidal UV (GUV) systems, and robotic disinfection systems for decades [3, 7]. Although mercury-discharge tubes have reasonable energy efficiency in these applications, they suffer from several limitations including environmental issues associated with the use of mercury, limitations on form factors due to the need to accommodate a linear tube, and limited lifetime.

Because of these limitations, LED-based UV sources are being viewed as the ultimate replacement for mercury-discharge lamps. LED-based UV systems will allow new form factors for UV systems including the potential to integrate UV and visible sources into a building's lighting system to provide an integrated smart network that leverage sensors (e.g., occupancy, particle sensors) and controls commonly found in lighting systems. However, before this vision can be realized on a large scale, the efficiency of UV LEDs needs to improve.

The goal of this study is to compare the initial performance and long-term reliability of UV LEDs with that of phosphor-converted white LEDs. This report focuses on the construction and initial performance benchmarks of a group of 13 UV LEDs spanning the range from UV-A to UV-C. A future report will examine the long-term performance of this same set of LEDs at room temperature and in an elevated temperature and humidity environment. In both studies, the behavior of the UV LEDs will be compared across the different bands and with two representative white LEDs. The intent of this work is to provide information to facilitate the use of UV LEDs in combination with lighting systems for commercial and residential buildings.

## 2 LED Samples

Based on feedback from the LED Systems Reliability Consortium (LSRC), a sample matrix of 14 different UV LED products was developed for this study. The sample matrix contained representative examples of UV-A, UV-B, and UV-C products spanning both low-power and high-power products. For convenience, the identity of each product was anonymized and labels of the format UV-x (where x is a number between 1 and 14 that uniquely identifies the product) are used in this report. We were not able to source adequate quantities of UV-10, so that product is not included in this testing matrix. Basic properties of the remaining 13 products are given in **Table 2-1**. In addition to the UV LEDs, two white high-power LED (HP-LED) products were also included in the test matrix for comparison. These products, which are common, mass-produced phosphor converted LEDs (pc-LEDs), are labeled as White-1 and White-2. The properties of these white HP-LEDs are also included in **Table 2-1**.

**Table 2-1: Basic properties of the UV LEDs examined in this study.<sup>a</sup>**

Product Number	UV Band	Nominal Peak Wavelength (nm)	Maximum DC Current (mA)	Maximum Radiant Flux (mW)	Maximum Use Temperature (°C) <sup>b</sup>
UV-1	UV-C	275	30	2.8	$T_a < 60$
UV-2	UV-C	275	30	2.5	$T_{sp} < 80$
UV-3	UV-C	275	40	4.7	$T_a < 60$
UV-4	UV-C	275	200	15.0	$T_a < 60$
UV-5	UV-C	280	500	119	$T_a < 85$
UV-6	UV-C	275	500	47	$T_a < 60$
UV-7	UV-C	275	800	88	$T_j < 100$
UV-8	UV-B	310	30	1.2	$T_a < 60$
UV-9	UV-B	310	30	2.7	$T_{sp} < 80$
UV-11	UV-A	365	500	1,000	$T_j < 90$
UV-12	UV-A	365	700	1,050	$T_a < 85$
UV-13	UV-A	365	4,000	3,800	$T_j < 125$
UV-14	UV-A	365	1,000	1,375	$T_{sp} < 70$
White-1	White	453 <sup>c</sup>	1,500	550 <sup>d</sup>	$T_j < 150$
White-2	White	450 <sup>c</sup>	700	350 <sup>d</sup>	$T_j < 135$

<sup>a</sup> Reported values are based on manufacturer's specifications.

<sup>b</sup>  $T_a$  = ambient temperature,  $T_{sp}$  = solder point temperature, and  $T_j$  = junction temperature.

<sup>c</sup> Denotes blue LED maximum emission wavelengths.

<sup>d</sup> Value at 350 mA instead of maximum current value.

Pictures of each UV LED and the white LED products are shown in **Appendix A** along with representative electrical and radiometric measurements. Details on the experimental techniques used for these measurements are given in **Section 3** of this report. At least 25 samples of each product were obtained from outside electrical supply providers except for Product UV-1 of which only 22 samples could be purchased due to supply limitations.

Most of the products examined in this study were purchased with the LED package mounted on a metal-core printed circuit board (MC-PCB). Consequently, the test samples are limited by the quality of the soldering operations performed by the supplier, and there were some noticeable examples of the supplier not following the manufacturers recommendations for solder pad size and solder paste volume. For example, the large amount of the copper pad that is visible around the solder joint for UV-1 and UV-5 (see **Figure A-1** and **Figure A-13** in **Appendix A**) suggests that the pad design and solder printing was not optimal. Five products (UV-3, UV-6, UV-7, UV-8, UV-14) could only be purchased as LED packages. We contracted with a local design and prototyping company to design custom MC-PCBs for each of these five products according to the manufacturer's specifications. For these five products, one LED was soldered to each custom MC-PCB using solder thicknesses and stencil patterns recommended by each LED manufacturer.

The MC-PCB of all samples, regardless of operational current, were mounted on extruded aluminum heat sinks such as the ones shown in **Figure 2-1**. Each heat sink measures 1.813 inches  $\times$  2 inches  $\times$  1.25 inches and weighted approximately 89 grams. The heat sink contains six tapered fins of 0.95 inches in length. The LEDs were attached to the heat sinks using a combination of thermally conductive tape (thermal conductivity of 1.5 watts [W]/meter Kelvin [K]) and mounting screws.

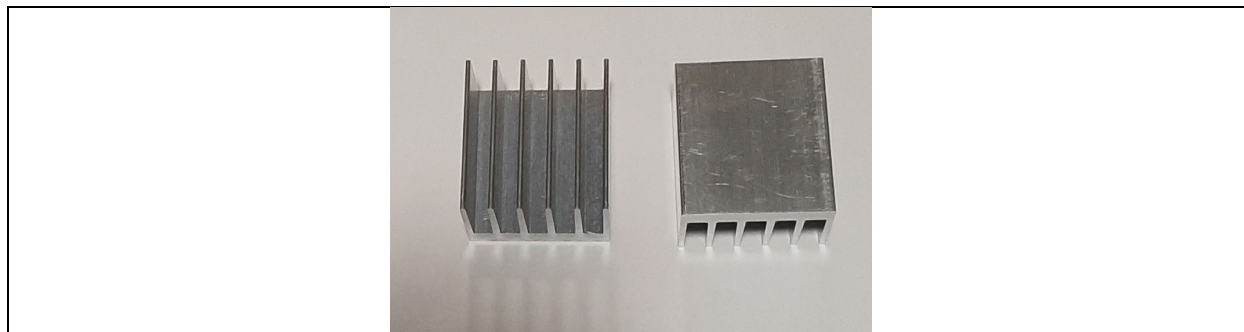


**Figure 2-1:** Extruded aluminum heat sinks used for all UV LEDs included in the study.

Additional classification of the products was conducted to determine the LED package properties and construction methods used in the UV and white LED products. Although all LED products examined in this study were housed in ceramic packages, other packaging features varied widely including the lens and LED-to-package interconnect method. For example, many of the UV-B and UV-C LEDs used a flat, fused quartz lens that was bonded to the outer surface of the package. This resulted in visible bond lines for the various lenses, an example of which is shown in **Figure A-34**. Among the UV-B and UV-C LEDs, only UV-5 had a hermetically sealed package with the lens being part of a metal lid (incorporating a glass-to-metal seal) that could be

soldered to the package to create the hermetic seal. The manufacturer for UV-3 and UV-6 used a fused quartz lens integrated into the ceramic package that is subsequently bonded to the package base; however, the manufacturer states that the seal is not hermetic. Most of the UV-A LEDs have dome lenses made from either silicones or glass, although UV-13 has a flat glass lens that is attached to the package with adhesives. A short list of construction practices that may affect overall product performance is provided in **Table 2-2**.

**Table 2-2: Construction practices used in the LEDs examined in this study.**

Product Number	Reflector	Lens	Interconnections	Package Size (mm x mm x mm)	Chip Size (mm x mm)	Per Unit Cost
UV-1	Gold	Moisture-resistant encapsulant	Flip chip + wire bonds	3 x 3 x 0.92	0.5 x 0.5	\$10–\$20
UV-2	Gold	Flat, glued lens	Flip chip	3.5 x 3.5 x 1.01	0.6 x 0.6	> \$50
UV-3	Gold	Flat, integrated lens	Flip chip	3.6 x 3.6 x 1.33	0.3 x 0.5	\$5–\$10
UV-4	Gold	Flat, glued lens	Flip chip	3.5 x 3.5 x 1.3	0.6 x 1.0	\$20–\$30
UV-5	Gold	Flat, hermetic lens	Flip chip	6.8 x 6.8 x 2.12	1.7 x 1.7	> \$50
UV-6	Gold	Flat, integrated lens	Flip chip	3.6 x 3.6 x 1.33	1.2 x 1.2	\$40–\$50
UV-7	Gold	Flat, glued lens	Flip chip	3.25 x 3.25 x 1.22	1.0 x 1.0	\$10–\$20
UV-8	Gold	Flat, glued lens	Flip chip	3.5 x 3.5 x 1.2	0.5 x 0.5	\$10–\$20
UV-9	Gold	Flat, glued lens	Flip chip	3.5 x 3.5 x 1.01	0.5 x 0.6	> \$50
UV-11	Gold	Silicone dome	Wire bonds	3.5 x 3.5 x 2.02	1.4 x 1.4	\$5–\$10
UV-12	Gold	Silicone encapsulant	Wire bonds	3.5 x 3.5 x 0.875	1.0 x 1.0	< \$5
UV-13	Gold	Flat, glued lens	Wire bonds	6.8 x 6.8 x 1.0	1.3 x 1.3 (each die)	> \$50
UV-14	Silver	Glass dome	Wire bonds	4.4 x 4.4 x 2.7	2.0 x 2.0	\$10–\$20
White-1	Silver	Silicone dome	Wire bonds	3.45 x 3.45 x 2.4	1.5 x 1.5	< \$5
White-2	Silver	Silicone dome	Flip chip	2 x 2 x 1.35	1.2 x 1.2	< \$5

Note: mm = millimeter.

### 3 Experimental Methods and Procedures

A series of electrical and radiometric measurements were conducted on each device under test (DUT) to determine the initial level of performance. In all cases, measurements were taken after each DUT had cooled to room temperature, which is typically  $22 \pm 2$  degrees Celsius ( $^{\circ}\text{C}$ ). Room temperature was monitored during all tests to track the impact of any temperature change on electrical and radiometric properties of the LEDs. Because there are 15 different UV and white

LED products examined in this study and each product had at least 20 samples, more than 300 different DUTs are part of this study.

### 3.1 Current-Voltage Measurements

Measuring the current-voltage (I-V) profile of an LED provides significant insight into the performance of the diode because the shape of the I-V profile is determined by the transport of charge carriers. I-V measurements are typically performed with a programmable source meter that changes the forward voltage ( $V_f$ ) in a linear ramp between an initial value and a final value. For this study, a calibrated Keithley 2400 source meter was used for all I-V measurements. An example I-V profile taken from a representative white, HP-LED is given in **Figure 3-1**. In performing this measurement, the voltage was linearly ramped between -2 volts (V) and +3 V (or higher), and the corresponding current was measured with the source meter. The source meter is capable of measuring currents as low as  $10^{-12}$  amps (A).

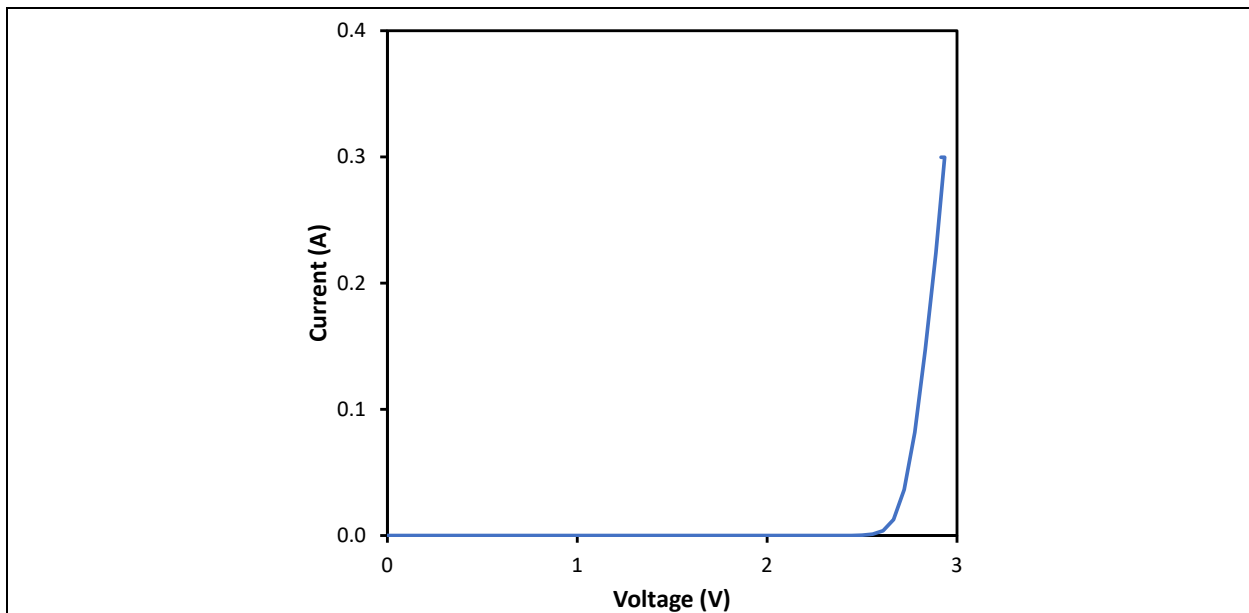


**Figure 3-1:** I-V measurement for White-2, a representative white, high-powered LED.

Three distinct regions can be defined in **Figure 3-2**. The operational region, which for this product occurs above +2.5 V, is the region when the LED is consuming a large forward current ( $I_f$ ) and is emitting light. Above the threshold voltage ( $V_{th}$ ), electrons and holes recombine to produce radiation, and the amount of radiation produced is proportional to the recombination rate of the charge carriers through radiative pathways, assuming droop effects are low.  $V_{th}$  is defined as the minimum voltage required for forward conduction to occur. In an ideal diode, no conduction would occur below  $V_{th}$  but for a real diode, a small current occurs, typically on the order of nanoamps or less. Therefore, in practical terms,  $V_{th}$  is calculated as the  $x$ -axis intercept of the tangent line where current is most linear (once conduction starts) and is equal to 2.683 V in **Figure 3-1**.

The second region of the I-V profile occurs between 0 V and  $V_{th}$ . In this region the current flow is zero for an ideal diode, but for a real diode, a small current occurs, typically on the order of nanoamps or less. In **Figure 3-2**, which is the logarithmic version of **Figure 3-1**, the current flow in this product could not be detected by the source meter below 1.55 V, so the device is approaching ideal behavior below this voltage. Between 1.55 V and  $V_{th}$ , a small leakage current, increasing from  $7 \times 10^{-11}$  A to 0.01 A was measured. The small current flow before  $V_{th}$  is indicative of defects in the epitaxial layer that promote non-radiative recombination of electrons and holes mostly through Shockley-Read-Hall (SRH) processes. Trap-assisted tunneling (TAT) is the main mechanism responsible for the SRH currents in UV LEDs [13].

Below 0 V, the LED is reversed biased and minimal current flow occurs in this region until the LED breakdown voltage ( $V_{br}$ ) is reached. The maximum reverse bias on the LED in **Figure 3-1** was intentionally set below  $V_{br}$  to prevent damage to the diode. If  $V_{br}$  had been reached, a large negative current would have occurred. Many LEDs, including most of the UV LEDs examined in this study have a protective diode (often set to approximately -0.7 V) to prevent excess overvoltage from being applied to the LED. The negative current flow from the protective diode is readily apparent in some of the I-V curves (e.g., UV-1, UV-2) given in **Appendix A**.

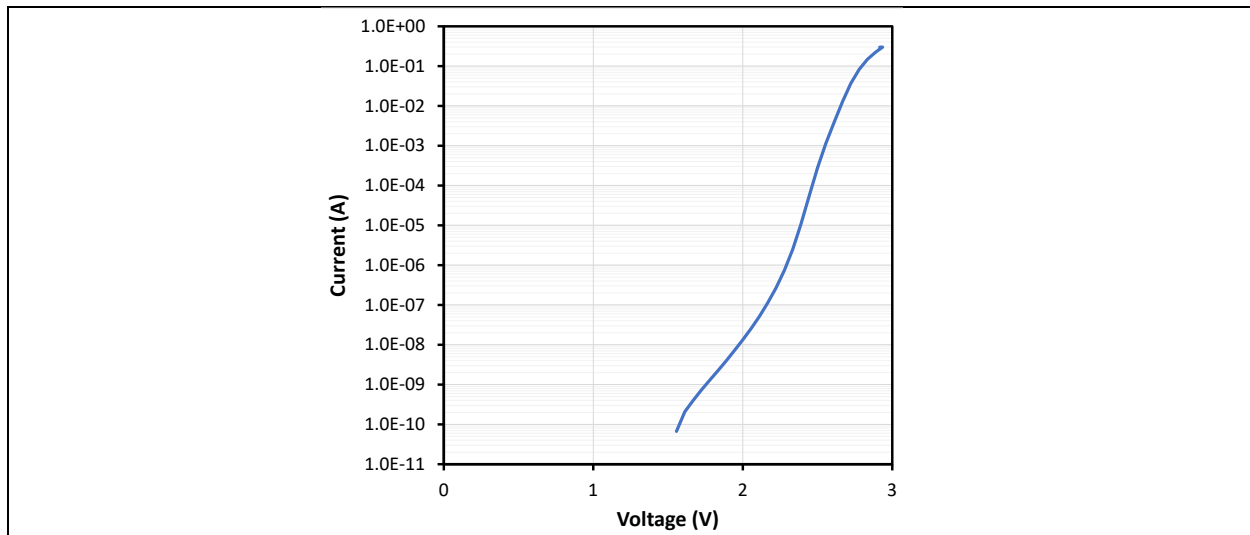


**Figure 3-2: Log-linear version of the I-V profile given in Figure 3-1.**

Several critical parameters can be determined from the shape of the I-V curve. The instantaneous slope of the forward current with voltage is inversely proportional to the serial resistance ( $R_{serial}$ ) in the diode arising from the contacts, buffer layers, and other structures. An ideal diode with zero parasitic resistances operating in the forward conduction mode would have an I-V profile above  $V_{th}$  that is represented by a vertical line. For real LEDs, the I-V profile has a non-vertical slope when operated in the forward bias mode due to serial resistances in the structure [8]. The higher this slope, the lower the resistance. Another critical parameter that can be obtained from an I-V profile is  $V_{th}$ , which is the minimum voltage required for forward conduction to occur in the LED. Ideally, the value of  $V_{th}$  depends on the  $E_g$  value of the emitter (i.e., photon energy) and can be approximated by using **Equation 1**:

$$V_{th} \sim E_g/e \quad (\text{Eq. 1})$$

where  $e$  is the electron charge. However, there are additional voltage drops in the LED structure arising from large bandgap discontinuities in the nitride system [7, 8]. In addition, both serial (e.g., contact resistance) and parallel resistances (e.g., TAT channels that bypass the p-n junction) in the structure can produce additional voltage drops. Values of  $V_{th}$  near  $E_g$  indicate less serial parasitic voltages in the LED structure and likely a higher efficiency. Typical values of the maximum emission wavelength ( $\lambda_{max}$ ) and the corresponding  $E_g$  values (in eV) are given in **Table 3-1**. For convenience, I-V measurements for each DUT examined in this study are given in **Appendix A** along with the average value for  $V_{th}$  for each product studied.  $V_{th}$  values for each product are discussed in detail in the **Section 3.1** of this report.

**Table 3-1: Wavelengths and associated band gaps for sources examined in this study.**

Wavelength (nm)	Band gap (eV)
254	4.881
275	4.509
280	4.428
310	3.999
365	3.397
450	2.755

### 3.2 Voltage over Time Measurements

At a constant current, the  $V_f$  value of the LED changes in response to the  $T_j$  of the diode. As  $T_j$  rises,  $V_f$  drops and vice versa. The change in  $V_f$  is typically between 2 and 17 millivolts (mV) per degree change (in degrees Celsius) in  $T_j$ , and the value will depend upon the materials used in the LEDs, the band gap, and how effectively the LED package is able to dissipate thermal energy. However, for UV LEDs, there is also a transient voltage effect when the LED is first turned on that can distort the value of  $V_f$  by 1 V or more, especially in the first milliseconds of operation, but does not impact the amount of radiation that is produced. The transient voltage is typically caused by a thyristor effect that acts as a capacitance in series with the LED junction. Fortunately, the transient voltage effect decays rapidly, and its effect on  $V_f$  can be minimized by waiting a set period of time after the pulse is applied.

When performing radiometric measurements, it is important that  $T_j$  be known since the amount of radiant flux that is produced will vary with  $T_j$ . This is especially important for UV LEDs where the lower diode efficiencies result in greater waste heat production than blue LEDs, can significantly increase  $T_j$ , and negatively impact radiant flux.

To choose the right  $I_f$  value for radiometric measurements, the change in voltage over time following a step change in current was measured for all LEDs examined. A typical example is shown in **Figure 3-3** for a UV-C LED operated at 5 milliamp (mA) in which the  $V_f$  value was

4.4795 V at the first measurement time (at 0.9 seconds) after application of the pulse so as to lessen the impact of the transient voltage effect. After 120 seconds,  $V_f$  has decreased to 4.4745 V, a difference of only 5 mV from the first measurement. Because this LED has a temperature coefficient of  $V_f$  value of  $-5.6 \text{ mV}/^\circ\text{C}$ , the  $T_j$  value is within  $0.9^\circ\text{C}$  of the starting temperature, which was room temperature ( $22^\circ\text{C}$ ). Typical values of  $V(t)$  for all samples examined in this study are given in **Appendix B**. These measurements were used to calculate the temperature rise occurring in all samples during operation at 5 mA and the results are given in **Table 3-2**. The largest temperature rise was measured for UV-1 where the change in  $V_f$  at an  $I_f$  value of 5 mA indicated a  $4.7^\circ\text{C}$  temperature rise during 3 minutes of operation. For the remainder of the LEDs, operation at an  $I_f$  value of 5 mA produced less than a  $2^\circ\text{C}$  increase in temperature above the ambient temperature.

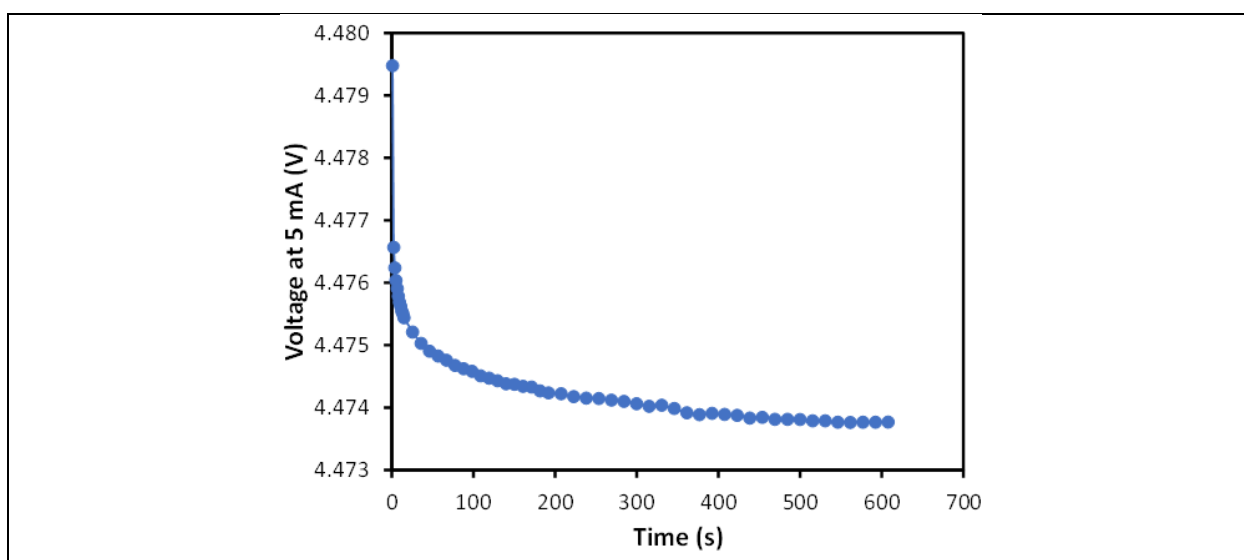


Figure 3-3: Representation example of a voltage vs. time measurement for a UV-C LED operated at 5 mA.

Table 3-2: Calculated temperature rise during 5 mA operation of the LEDs in this study.

Product	Temperature Coefficient of $V_f$	Drive Current	$\Delta V_f$	Temperature Rise Above Ambient <sup>a</sup>
UV-1	$-5.7 \text{ mV}/^\circ\text{C}$	5 mA	26.7 mV	$4.7^\circ\text{C}$
UV-2	$-7.3 \text{ mV}/^\circ\text{C}$	5 mA	7.8 mV	$1.1^\circ\text{C}$
UV-3	$-12 \text{ mV}/^\circ\text{C}$	5 mA	11.0 mV	$0.9^\circ\text{C}$
UV-4	$-6.3 \text{ mV}/^\circ\text{C}$	5 mA	4.7 mV	$0.8^\circ\text{C}$
UV-5	$-5.6 \text{ mV}/^\circ\text{C}$	5 mA	5.3 mV	$0.9^\circ\text{C}$
UV-6	$-6.9 \text{ mV}/^\circ\text{C}$	5 mA	3.2 mV	$0.5^\circ\text{C}$
UV-7	$-9.1 \text{ mV}/^\circ\text{C}$	5 mA	10.1 mV	$1.1^\circ\text{C}$
UV-8	$-16.6 \text{ mV}/^\circ\text{C}$	5 mA	23.3 mV	$1.4^\circ\text{C}$
UV-9	$-7.3 \text{ mV}/^\circ\text{C}$	5 mA	11.0 mV	$1.4^\circ\text{C}$

Product	Temperature Coefficient of $V_f$	Drive Current	$\Delta V_f$	Temperature Rise Above Ambient <sup>a</sup>
UV-11	-3.3 mV/°C	5 mA	0.1 mV	< 0.1°C
UV-12	-2.4 mV/°C	5 mA	0.1 mV	< 0.1°C
UV-13	Not given in specification sheet	5 mA	0.1 mV	< 0.1°C
UV-14	-2.7 mV/°C	5 mA	1.6 mV	0.6°C
White-1	-1.3 mV/°C	5 mA	0.3 mV	< 0.1°C
White-2	-1.7 mV/°C	5 mA	0.4 mV	0.2°C

<sup>a</sup> The temperature rise is calculated after 3 minutes of operation at an  $I_f$  value of 5 mA.

### 3.3 Radiometric Measurements

Measurements of the radiometric properties of the LEDs examined in this study were taken with integrating spheres using the procedures given in LM-79-19 [18, 19]. When performing integrating sphere measurements for UV LEDs, several experimental factors need to be considered that are not normally a problem with white LEDs. First, UV-B and UV-C LEDs can damage the typical interior coating used in most integrating spheres that measure white light. Only integrating spheres containing Teflon-based interior coatings should be used for UV-B and UV-C LEDs. A Teflon-coated integrating sphere can also be used for UV-A and white LEDs. The second consideration in radiometric measurements of UV LEDs is the availability of calibration standards for the UV band. The traditional tungsten filament-based calibration sources set to a correlated color temperature (CCT) value of 3,000 K do not have sufficient radiant flux below 350 nm to provide an accurate calibration. Instead, other calibration sources such as a xenon lamp are needed to provide an accurate calibration standard for UV sources. The final consideration is the relative inefficiency of UV sources compared to white LEDs. This inefficiency can result in increases in  $T_j$  values during measurement that can adversely affect the radiant flux produced by the LEDs. Consequently, it is essential to conduct radiometric measurements of UV LEDs at conditions where a stable  $T_j$  can be achieved [18, 19].

For these measurements, two integrating spheres were used, both of which were coated with Teflon-based materials. Initial measurements were conducted in a small integrating sphere (38 mm diameter) in which the LEDs were mounted external to the integrating sphere and measurements were taken in the  $2\pi$  geometry. A picture of this sphere is shown in **Figure 3-4**. A calibration source was not available for this integrating sphere, so only raw, uncorrected measurements could be obtained. However, a subset of the UV DUTs were used as standards and measured whenever the 38 mm sphere was used. These standards were also measured in the calibrated 10-inch sphere (described in the next paragraph), allowing an indirect calibration of the 38-millimeter (mm) sphere.



**Figure 3-4: Small integrating sphere used in initial measurements.**

The second integrating sphere that was used in this study was larger and equipped with a xenon lamp calibration source that permits calibration of UV and visible sources between 210 nm and 800 nm. The xenon lamp, which is a  $2\pi$  source, served as both the calibration source and the auxiliary lamp for all measurements and allowed calibrated measurements of radiant flux, traceable to standards at the National Institute for Standard and Technology. All samples were mounted in the center of the larger integrating sphere and all measurements were taken in the  $4\pi$  geometry. This sphere is shown in **Figure 3-5**.

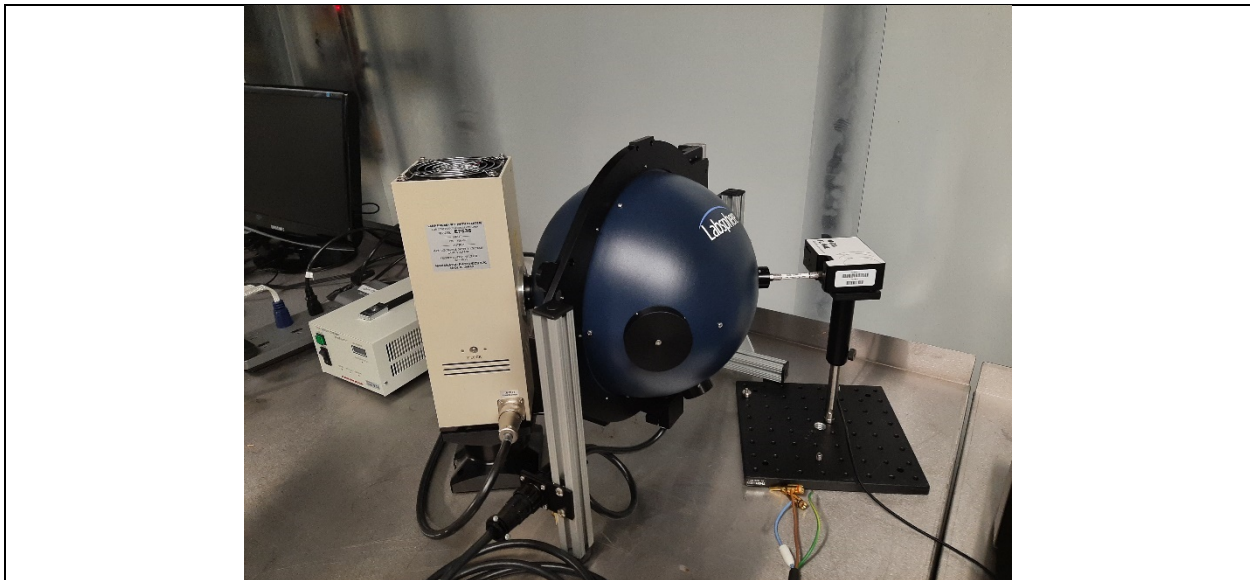


**Figure 3-5: Larger integrating sphere used in these measurements. The sphere measured 10 inches in diameter.**

In performing radiometric measurements, all samples were measured at an  $I_f$  value of 5 mA. As described in **Section 3.2**, this current was chosen to minimize heating of the samples and to keep the  $T_j$  values near room temperature. For all DUTs examined in this study,  $T_j$  was  $22^\circ\text{C} \pm 3^\circ\text{C}$  during radiometric testing, although higher  $T_j$  values will occur during life testing when higher  $I_f$

values are used. One coincidental advantage of performing radiometric tests at low  $I_f$  values is that parasitic luminescence is usually higher at low currents. Parasitic luminescence arises from deep-level defects (e.g., vacancies, impurities, dislocations) and can reduce quantum yield if present [20, 21].

## 4 Results and Discussion

### 4.1 LED Package Structures

The LED packages examined in this study are intended to provide protection from environmental stress and to dissipate heat levels ranging from 0.15 W to 11 W. To be an effective UV LED package, the structure must be able to withstand the radiation and heat produced by the LED with minimal changes in the package materials. UV radiation is more energetic than visible light, and UV-C and UV-B LEDs made from AlGaN are likely to generate more waste heat, per current setting, than UV-A LEDs made with more mature InGaN materials. Consequently, the packaging requirements for UV-C products are the most demanding, while UV-A products can utilize many of the packaging breakthroughs found in white LEDs.

The package structure of the UV LEDs examined in this study can be roughly classified according to the radiation band of the product, and a breakout of the package structures of the products is given in **Figure 4-1**. Pictures of all LEDs examined in this study are given in **Appendix A**. Ceramic packages are used in all products examined in this study. However, beyond this first layer of similarity, many differences exist between packaging for UV-A and UV-B/UV-C products.

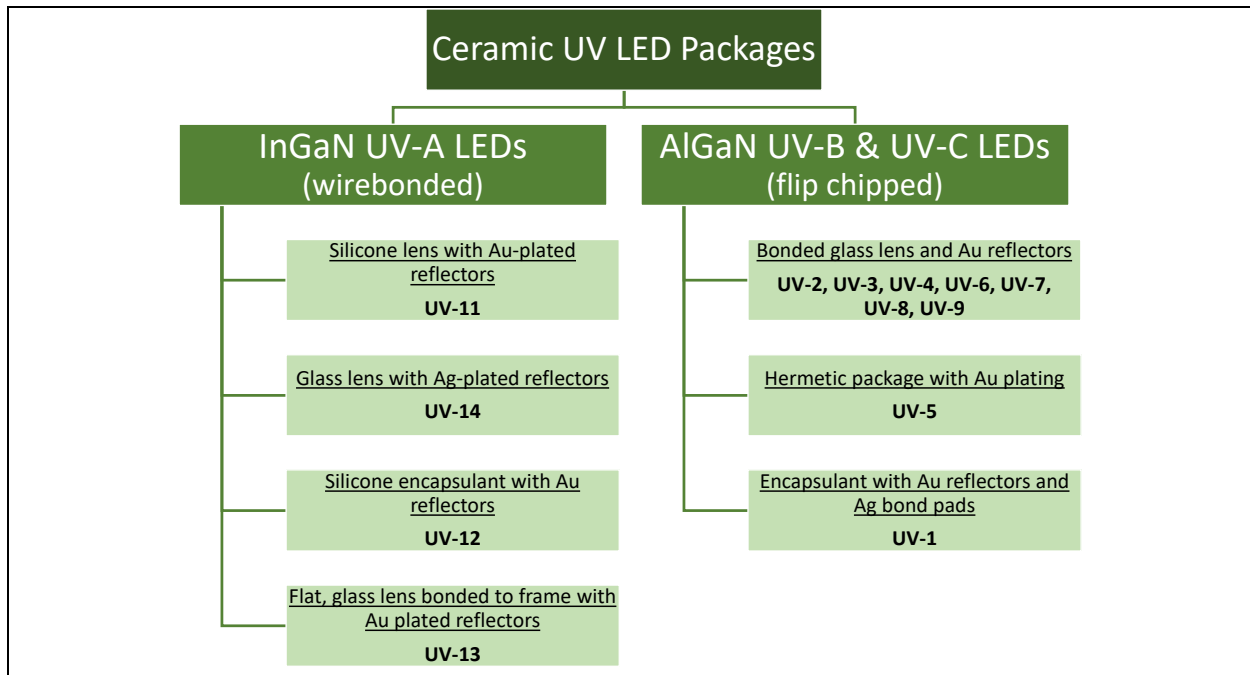


Figure 4-1: Breakout of the LED package architectures found for the UV LEDs examined in this study.

The four UV-A LED packages each had a distinct construction feature, although three of the packages likely use silicones in assembly (UV-11, UV-12, and UV-14). UV-11 is a single die package that uses a silicone dome to protect the LED and to provide optical collection of the emitted radiation. UV-14 is also a single die package that has a dome lens, but the dome is made from glass according to the manufacturer's specification. For UV-14, it is possible that the glass lens is held in place with a silicone adhesive. UV-12 has a silicone encapsulant, according to the manufacturer's specification, but the silicone is applied as a conformal coating and not formed into a dome.

The package for UV-13 is entirely different from the other UV-A products. First, UV-13 contains four LED die and each die has two wire bonds connected to the cathode. Connection to the anode is presumably through the backside of each die. In addition, UV-13 has a glass lens that is bonded to the lid of the ceramic package. In some cases, the bonding adhesive spilled onto the gold plating on the top of the package and became visible. This type of structure closely resembles the most common LED package structure found in UV-B and UV-C LEDs.

The most widely used LED architecture structure for the UV-B and UV-C LEDs was a black ceramic base, with gold-plated reflectors and side walls, capped by a flat, glass lens bonded to the top flange of the package base. This package architecture was used in seven different LED products made by four different manufacturers with only minor variations. As with UV-13, the flat lid (presumably a fused glass or quartz) is bonded to the package lid using an adhesive and, in some cases, a slight change in the color of the gold can be observed to indicate the presence of the adhesive. While gold interconnects are widely used in electronics packaging, the reflectance of gold in the UV wavelength region is modest at best with a typical value of approximately 0.4 [22].

UV-1 has a unique LED package structure in which the die is mounted to bonding pads in a gold cavity using flip chip technology, and the pads in the gold cavity are connected to an exposed lead frame in the package through wire bonds. The entire assembly is covered in a moisture-resistant encapsulant, according to the manufacturer's specification, although the identity of this encapsulant is not given.

UV-5 is the only LED package examined in this study that is known to be hermetically sealed. Hermetic sealing is achieved using a solder to connect the lens cover (containing a glass-to-metal seal) with the package body. The lone die in this package is flip chip bonded to the substrate and is surrounded by gold plating, which provides a reflector function.

## 4.2 Initial I-V Measurements

I-V measurements were taken for all DUTs in the test matrix, and the results for each individual measurement are given in **Appendix A**. The shape of an I-V measurement can be used to identify any circuit abnormalities such as shunt resistances, series resistances, or parasitic diodes using the scheme given by Schubert [8]. All the LEDs examined in the study have serial resistance ( $R_{\text{serial}}$ ) values that produce a sloping I-V profile at high currents. The current from

these LEDs was typically low ( $< 10^{-6}$  A) at voltages much lower than  $V_{th}$ , but steadily increased until  $V_{th}$  was reached (or surpassed). However, one LED (UV-1) exhibited sub-threshold turn-on for most samples, and the characteristic “hump” between 2V and 5V was observed for these samples at currents up to 1 mA. Some of the other products had a few samples that exhibited sub-threshold turn-on with  $I_f$  values as high as 1 mA. One sample of UV-2 exhibited this behavior as shown in **Appendix A**. Other products (e.g., UV-4, UV-6, UV-7, UV-8, UV-12, UV-14) exhibited some part-to-part variation in the I-V profile at low currents (i.e.,  $< 10^{-4}$  A), which suggests some differences in the level of TAT occurring in the devices due to variations in the quality of the semiconductor layers.

The I-V measurements were also used to determine the  $V_{th}$  and  $R_{serial}$  values for each DUT. These average  $V_{th}$  and  $R_{serial}$  values were determined by the  $x$ -axis intercept ( $V_{th}$ ) and slope of the I-V signal above  $V_{th}$  using the methods described by Schubert [8]. The average values for  $V_{th}$  and  $R_{serial}$  for each product in this study are provided in **Figure 4-2** and **Figure 4-3**, respectively. Also included in **Figure 4-2**, is the approximate  $E_g$  value of an ideal LED emitting at various wavelengths as calculated using **Equation 1**. These values are represented by a horizontal blue line for 280 nm emission, a horizontal red line for 310 nm emission, a horizontal green line for 365 nm emission, and a horizontal black line for 450 nm emission.

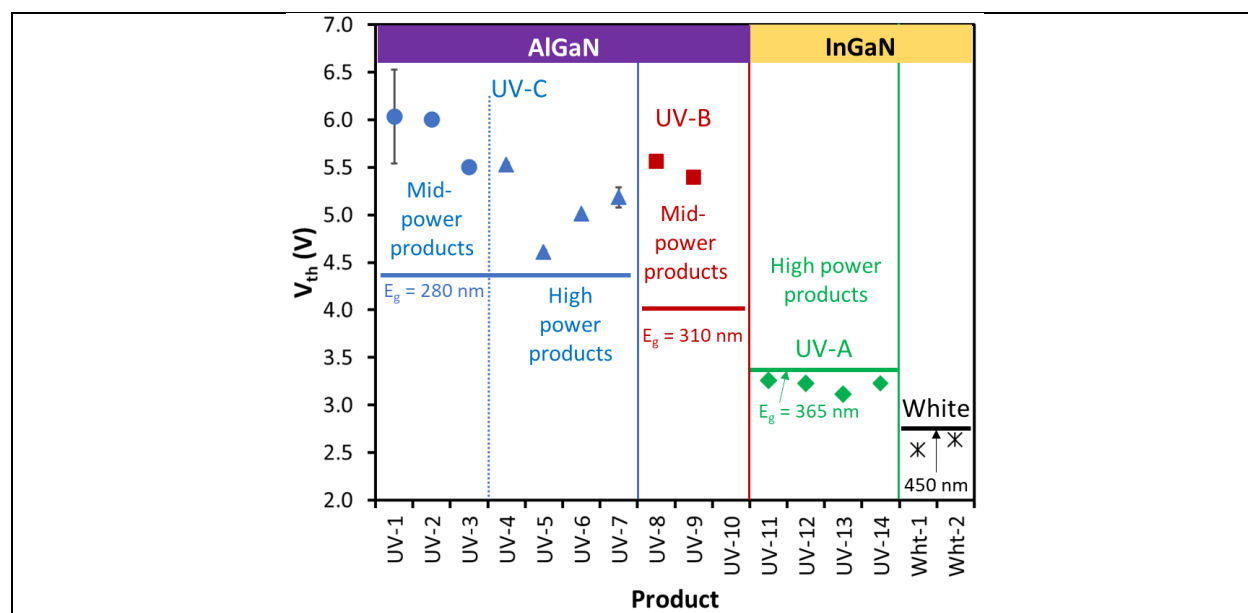


**Figure 4-2: Average  $V_{th}$  values for each product examined in this study. Error bars representing measurement standard deviation for each product and are calculated for at least 20 samples. The solid horizontal lines are the approximate  $E_g$  for an ideal emitter at 280 nm (blue), 310 nm (red), 365 nm (green), and 450 nm (black).**

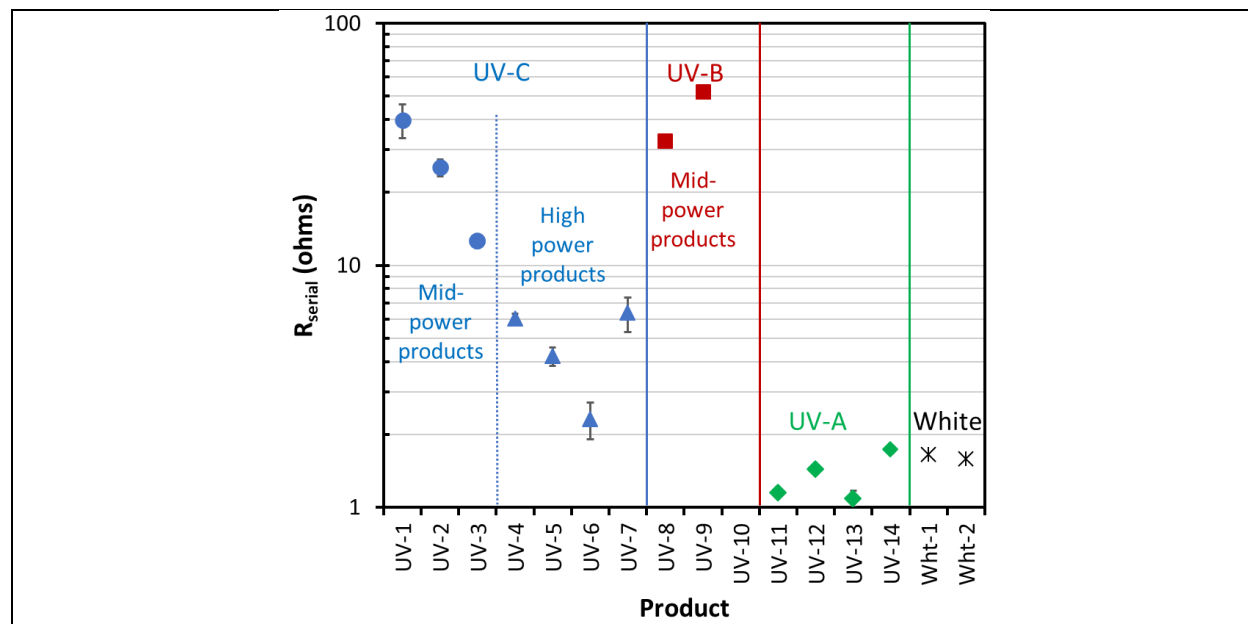


**Figure 4-3: Average  $R_{\text{serial}}$  values for each product examined in this study. Errors bars are also included and represent the measurement standard deviation of at least 20 samples.**

The standard deviations for most products shown in **Figure 4-2** is small and barely visible. The one exception is UV-1 where a difference of more than 1 V was found in the  $V_{\text{th}}$  values for some products. A closer look at I-V characteristics of these samples (see **Figure A-2**), shows that there are at least two separate sample populations for the product. The population with the fewer samples exhibited minimal tunnelling below 3 V with a sharp rise in  $I_f$  above 3 V resulting in  $V_{\text{th}}$  values in the 5.3–5.4 V range. In contrast, UV-1 samples that exhibited sub-threshold turn-on had significant leakage currents between 2.2 V and 5 V. For this population,  $V_{\text{th}}$  was delayed until at least 5.9 V with some samples exhibiting  $V_{\text{th}}$  values as high as 6.4 V.

When compared to the band gap, the measured  $V_{\text{th}}$  values for the UV-A and white LEDs were just below the estimated photon emission energy for the respective  $E_g$  values. This behavior is in line with measurements for other compound semiconductor materials such as AlGaInP [20], and the finding that  $V_{\text{th}}$  is slightly lower than  $E_g$  can be attributed to thermal energy in the sample at the time of measurement [8]. Since both UV-A and white LEDs with a blue pump use InGaN semiconductors, the relative maturity of the technology in the materials systems used in these products likely accounts for the  $V_{\text{th}}$  value being so close to  $E_g$ . However, for the UV-B and UV-C LEDs,  $V_{\text{th}}$  is significantly higher than  $E_g$ , indicative of electrical inefficiencies causing parasitic voltages in the semiconductor stack that must be compensated with high  $V_f$  values. The difference between  $V_{\text{th}}$  and  $E_g$  varies from 0.18 V (UV-5) to greater than 1.5 V (UV-1, UV-2, and UV-9). For comparison, the difference between  $V_{\text{th}}$  and  $E_g$  for blue AlGaInN semiconductors was 0.5 to 1.0 V in 2000 [20].

Part of the parasitic voltages found in the UV-B and UV-C LEDs arise from contact resistance and other resistances (e.g., p-layer resistance, n-layer resistance) in the stack and represent inefficiencies in the LED structure [7, 8, 14]. As shown in **Figure 4-3**, the products with high  $V_{\text{th}}$

values also have high  $R_{\text{serial}}$  values. The largest  $R_{\text{serial}}$  values were found for UV-9, which exhibited a value that is nearly 50 times larger than that observed for the UV-A and white LED products. In contrast, the  $R_{\text{serial}}$  values are significantly lower in the high-power UV-C products likely through better design and current spreading. As a result, the measured  $R_{\text{serial}}$  value for UV-6 is approximately twice that measured for the UV-A and white LEDs products demonstrating that significant improvements in  $R_{\text{serial}}$  values is possible with today's technology.

There is a definite dependence on LED power level for  $V_{\text{th}}$  and  $R_{\text{serial}}$ . As noted above, both of these values tend to be lower in the higher power products than in the mid-power products. A closer look at the packaging materials reveals that the same package were used for UV-2, UV-4, UV-8, and UV-9 although the LEDs are made by different manufacturers. Likewise, UV-3 and UV-6 also used the same package. As a result, there is little if any difference in packaging between mid-power and high-power UV LED products in contrast to white LEDs. Consequently, differences in  $V_{\text{th}}$  and  $R_{\text{serial}}$  for the UV LED products can be attributed to the semiconductor and not the package.

One way to assess the quality of the semiconductor in the different products is to compare the leakage current measured before  $V_{\text{th}}$ . This measurement provides some information on the level of TAT occurring in the epitaxial layer. For this analysis, we arbitrarily chose a value of 0.5 V below average  $V_{\text{th}}$  for each product and measured the current for each DUT. The results are shown in **Figure 4-4**.

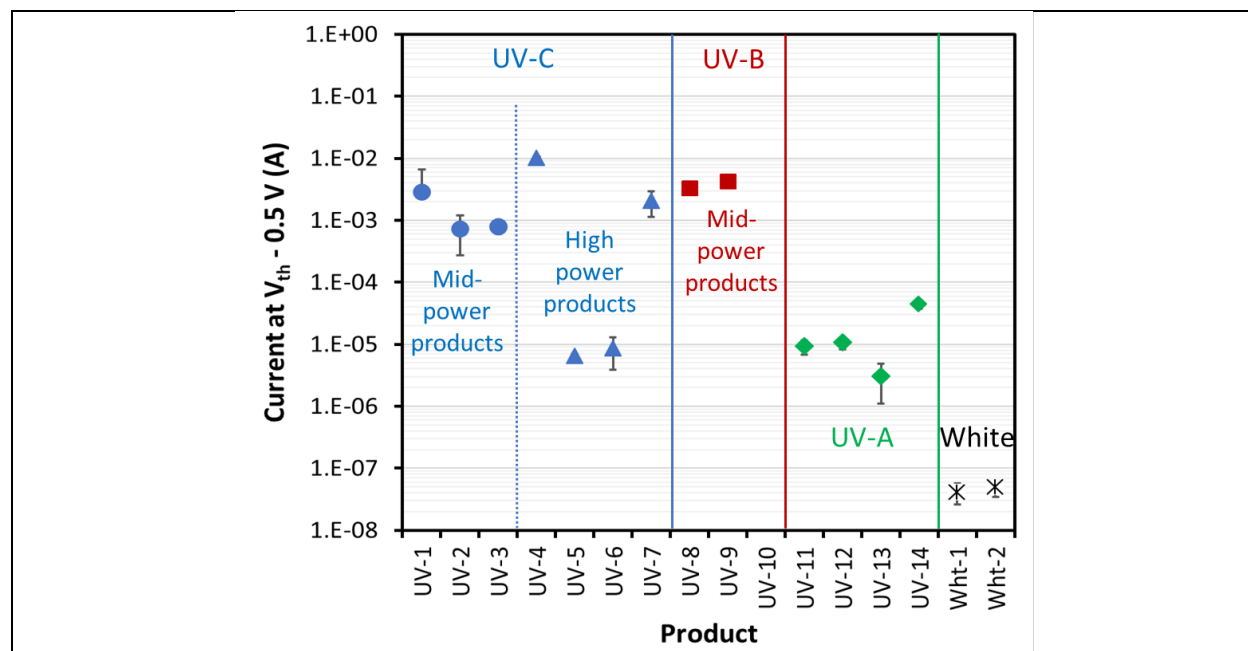


**Figure 4-4:** Current measured at 0.5 V below average  $V_{\text{th}}$  for each product.

In this analysis, the leakage current at 0.5 V below  $V_{\text{th}}$  measured for the white LEDs was very low ( $< 10^{-7}$  A) as expected for the mature commercial white LED products. For UV-A LEDs, the leakage current was roughly two orders of magnitude higher ( $\sim 10^{-5}$  A). Both UV-A and the white LEDs use the InGaN system, so further improvements in leakage current for UV-A LEDs

will likely occur through process optimization leveraging knowledge gained in the manufacturing of white LEDs. For the UV-B and UV-C LEDs, there is an approximately three orders of magnitude variation in average leakage current across the different products. The best performance was shown by UV-5 and UV-6, which demonstrated leakage currents on the order of  $10^{-5}$  A at 0.5 V below  $V_{th}$ , comparable to the leakage currents for the UV-A LEDs. In contrast, the leakage current at 0.5 V below  $V_{th}$  was typically on the order of  $10^{-2}$  A for the other UV-B and UV-C products, indicating significant leakage currents flowing through defects in the structure likely involving TAT and possibly other mechanisms.

### 4.3 Initial Radiometric Measurements

Radiometric measurements were taken for all UV LEDs in the test matrix and a summary of the emission peak ( $\lambda_{max}$ ), the full-width at half-maximum (FWHM), and radiant flux for each product is given in **Table 4-1**. Spectra for each product are given in **Appendix A**. These measurements were taken using the 10-inch integrating sphere with a  $2\pi$  calibration source. The acquisition time for each product is set to a value that produced a response that is approximately 70% of the detector maximum response. Consequentially, acquisition time varied with radiant flux. Each reported spectral power distribution (SPD) was the average of 10 scans and no smoothing has been applied. For products with long acquisition times, it could take up to a minute to complete the measurement including acquiring the 10 scans. For products with short acquisition times, measurements could be completed in less than 5 seconds.

**Table 4-1: Initial photometric properties of the UV LEDs examined in this study.<sup>a</sup>**

Product	$\lambda_{max}$ (nm)	FWHM (nm)	Radiant Flux (mW) at 5 mA <sup>b</sup>
UV-1	278.7 ± 2.4	10.4 ± 0.4	0.686 ± 0.090
UV-2	271.6 ± 1.0	10.9 ± 0.2	0.598 ± 0.063
UV-3	275.5 ± 0.8	10.8 ± 0.1	1.369 ± 0.035
UV-4	272.8 ± 0.9	9.9 ± 0.3	0.476 ± 0.186
UV-5	280.2 ± 0.1	8.7 ± 0.2	1.117 ± 0.029
UV-6	275.0 ± 0.7	11.2 ± 0.3	1.005 ± 0.049
UV-7	279.1 ± 0.6	10.0 ± 0.4	0.664 ± 0.157
UV-8	308.6 ± 0.6	13.5 ± 0.2	0.533 ± 0.039
UV-9	309.7 ± 1.1	9.2 ± 0.2	0.580 ± 0.027
UV-11	365.0 ± 0.8	10.7 ± 0.6	8.338 ± 1.022
UV-12	367.4 ± 0.6	10.7 ± 1.6	1.621 ± 0.142
UV-13	366.4 ± 0.4	12.2 ± 0.3	1.561 ± 0.356
UV-14	371.4 ± 0.8	19.7 ± 0.8	9.214 ± 1.307

<sup>a</sup> All measurements were taken at an  $I_f$  value of 5 mA.

<sup>b</sup> Peak integration was performed using the trapezoidal rule.

The  $\lambda_{\max}$  for the nominal UV-C products varied from 271 nm to 280 nm, which covers the upper end of the UV-C band and the lower end of the UV-B band. Products UV-2 and UV-4 exhibited the lowest  $\lambda_{\max}$  values (approximately 271–272 nm) while products UV-1, UV-5, and UV-7 exhibited the highest (approximately 279–280 nm). The FWHM values of the emission peak for each product was generally in the 9–11 nm range for UV-1 through UV-7. Product UV-5 exhibited the smallest FWHM (8.7 nm), and UV-6 exhibited the largest (11.2 nm).

In addition to main peak, some products exhibited a secondary peak at a higher wavelength. This effect is most pronounced for all of the UV-7 products, as shown in **Figure 4-5**, although the intensity of this peak varied from DUT to DUT. This second emission peak was broader and weaker than the main emission peak and also occurred at a wavelength that is approximately 50 nm higher than the  $\lambda_{\max}$  position. Because of the absence of overlap of the primary and secondary peak emissions, the latter did not impact the FWHM value of the main peak but it still made a significant contribution to the total radiation. This secondary peak likely arises from deep-level states in the epitaxial layer resulting from defects (e.g., magnesium-acceptor traps) [8, 13, 21]. This effect was most pronounced for UV-7 (see **Figure A-21** in **Appendix A**). All samples of UV-B and UV-C products exhibited some deep-level luminescence, but the amounts are significantly lower than those observed for UV-7. The relative percentage of these deep-level luminescent peaks diminishes as  $I_f$  value increase [21], and we also observed this effect at high  $I_f$  values (see **Figure 4-5**). However, there is still significant radiant flux in the deep level luminescent peak at higher  $I_f$  values. At 25 mA, 1.994 mW is involved in the main emission peak of UV-7 and 0.247 mW from the deep level luminescent peak.

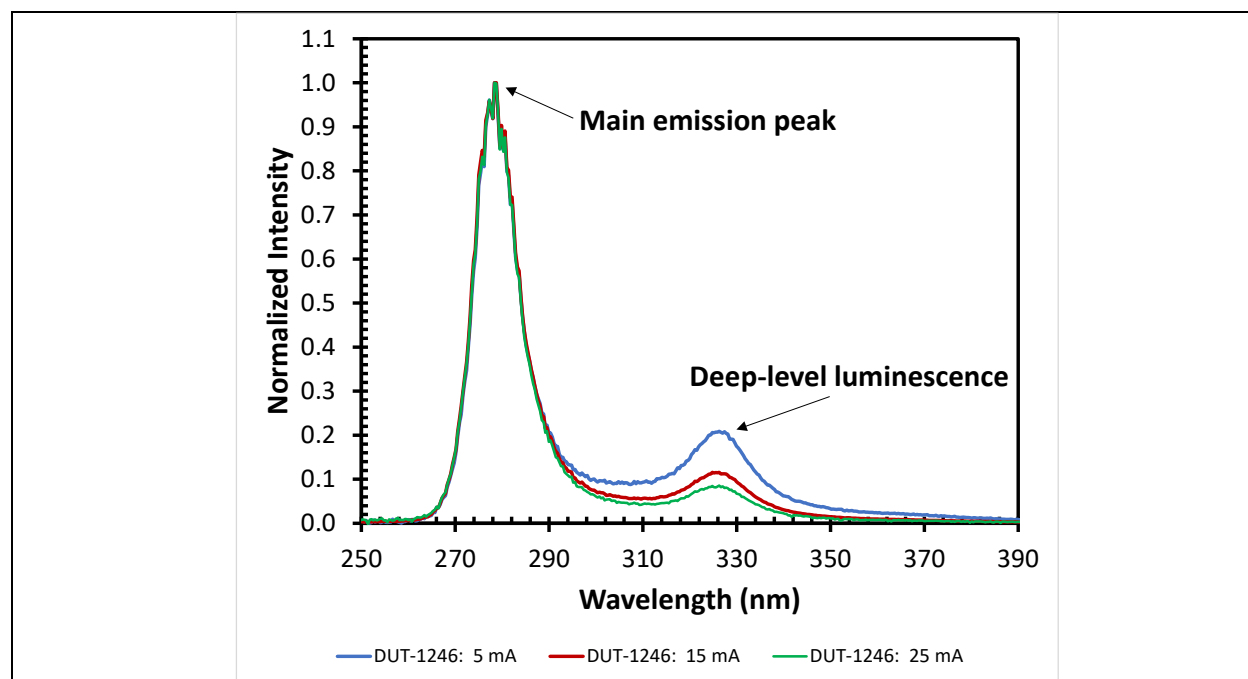


**Figure 4-5:** UV-C product (UV-7) with a main emission peak and a weaker secondary emission peak arising from deep-level luminescence. The relative spectra is shown for two different DUTs of UV-7.

The radiometric properties of the UV-A and UV-B products also exhibited interesting trends. For the two UV-B products (i.e., UV-8 and UV-9), the  $\lambda_{\max}$  values were similar but the FWHM values were different with the value for UV-8 being 4.3 nm larger than the value for UV-9. The net result is a higher total radiant flux for UV-9 at an  $I_f$  value of 5 mA even though the FWHM is smaller. The UV-A products tended to fall into two groups: those displaying high radiant flux at 5 mA and those with low radiant flux at 5 mA. UV-11 and UV-14 exhibited the highest radiant flux at 5 mA; however, the  $\lambda_{\max}$  value for UV-14 is 6 nm higher than that of UV-11, and the FWHM is 9 nm larger resulting in more radiation falling in the visible band. UV-12 and UV-13 exhibited similar radiant flux values at 5 mA drive currents. The  $\lambda_{\max}$  values were also similar (367.4 nm vs. 366.4 nm), but the FWHM of UV-13 was larger than that of UV-12. As discussed in **Section 4.4**, the efficiency of UV-12 and UV-13 exhibited the largest change when  $I_f$  was increased from 5 mA.

Based on the spectral shapes, the amount of radiation in the UV-C band (i.e., < 280 nm) and in the UV-B band (i.e., > 280 nm) can be calculated for products UV-1 through UV-7, and the results are shown in **Table 4-2** for  $I_f$  values of 5 mA. The products with the highest percentage of UV-C radiation were UV-2, UV-3, UV-4, and UV-6. These products, which are from three different manufacturers, have average  $\lambda_{\max}$  values of 275.5 nm or less. In contrast, UV-1, UV-5, and UV-7 exhibited the highest percentages of UV-B radiation but for two different reasons. Much of the UV-B radiation produced by UV-7 DUTs was the result of deep-level luminescence. This finding is consistent with the fact that UV-1 and UV-7 have similar  $\lambda_{\max}$  and FWHM values, but the relative amount of UV-C radiation produced by UV-1 is 14.4% higher. For UV-5, the lower  $\lambda_{\max}$  value of this product resulted in much of the radiation falling in the UV-B band even though this product exhibited the emission peak with the smallest FWHM. As there is a strong decrease in dermal exposure risk for UV-C radiation relative to UV-B radiation, knowing the relative amounts of radiation in these two bands is important in applications where human exposure to the UV radiation can occur. For applications where the risk of human exposure is minimal (e.g., ventilation ductwork, enclosed chambers), the amount of radiant flux is likely the more important quantity than the radiation band.

**Table 4-2: Relative amounts of UV-C radiation at  $I_f = 5$  ma for products with  $\lambda_{\max}$  between 270 nm and 280 nm.**

Product	% UV-C Radiation
UV-1	56.5 ± 12.8%
UV-2	88.3 ± 1.2%
UV-3	74.8 ± 1.0%
UV-4	85.3 ± 2.5%
UV-5	36.1 ± 0.4%
UV-6	74.3 ± 4.3%
UV-7	42.1 ± 5.3%

For the UV-A products, the radiant power produced by each DUT was significantly higher than for the UV-B and UV-C products (aside from UV-3), suggestive of higher radiant efficiencies. The UV-A products also exhibited a small amount of deep-level luminescence that resulted in emissions in the visible band, which were especially pronounced for UV-14 due to its large FWHM. As a result, the distribution of the radiation between UV-A wavelengths (i.e.,  $\lambda_{\text{max}} < 380$  nm) and visible wavelengths (i.e.,  $\lambda_{\text{max}} > 380$  nm) varied as shown in **Table 4-3**. In general, the radiation from UV-11, UV-12, and UV-13 exhibited similar percentages of UV-A and visible radiation. This finding is not surprising because the average  $\lambda_{\text{max}}$  and FWHM of these products were similar. UV-14 exhibited a much higher percentage of visible radiation in the radiant flux, which can be attributed to the higher  $\lambda_{\text{max}}$  value and significantly broader peak width that were measured for this product.

**Table 4-3: Relative amounts of UV-A radiation when operated at 5 mA.**

Product	% UV-A Radiation
UV-11	93.9 ± 0.8%
UV-12	92.8 ± 0.3%
UV-13	91.3 ± 0.5%
UV-14	72.6 ± 3.8%

#### 4.4 Device Radiant Efficiencies

The International Commission on Illumination defines radiant efficiency as the quotient of the radiant flux of the emitted radiation and the power consumed by the source. For the LEDs examined in this report, the radiant efficiencies varied greatly depending upon the band and the  $I_f$  value. For the UV-B and UV-C products, the radiant efficiency generally has an inverse correlation with  $V_{\text{th}}$  as shown in **Figure 4-6**. There appears to be a baseline efficiency of approximately 2%, which was exhibited by products UV-1, UV-2, UV-4, and UV-8, all of which had  $V_{\text{th}}$  values of 5.5 V or higher. For products with  $V_{\text{th}}$  values below 5.5 V, the efficiency steadily increased as  $V_{\text{th}}$  decreased. This finding is consistent with increasing the radiant efficiency of a UV LED by improving the electrical characteristics of the constituent semiconductors and connections. The lone exception to this behavior was UV-3, which exhibited one of the highest radiant efficiency values for the UV-B and UV-C products and also a high  $V_{\text{th}}$  value.

The root cause for the higher efficiency of UV-3, compared to the other LEDs with high  $V_{\text{th}}$  values, is unknown. **Figure 1-3** demonstrates that the path to improving the performance of UV-B and UV-C LEDs involves either addressing the electrical or optical shortcomings of the technology. The electrical performance of UV-3 is modest at best resulting in high values for  $V_{\text{th}}$  and  $R_{\text{serial}}$ . Consequently, an unknown improvement in the electrical performance is not likely to account for the higher than expected efficiency of UV-3. Instead, it is more likely that UV-3 is incorporating an improvement in radiation extraction efficiency that is producing the higher than

expected efficiency of UV-3. It is possible that UV-3 is utilizing a structure that has less absorbance of UV radiation such as a transparent p-contact layer. However, the incorporation of such technology into UV-3 has not been confirmed.

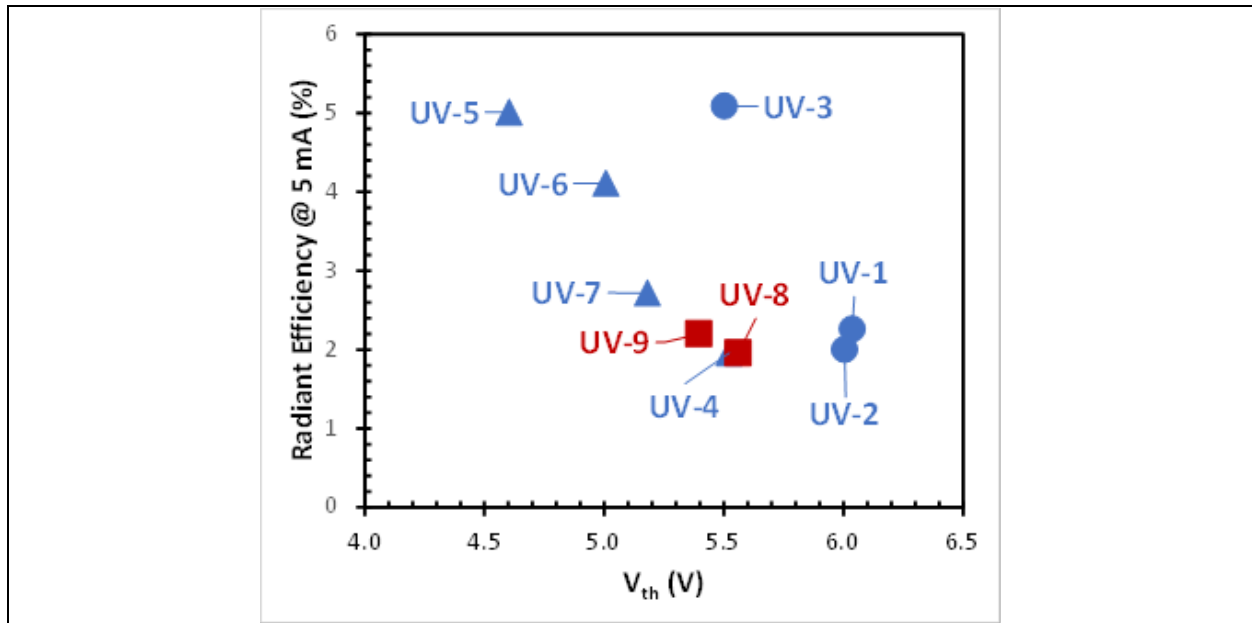


Figure 4-6: Radiant efficiency at an  $I_f$  value of 5 mA versus  $V_{th}$  for the UV-B (red squares), mid-power UV-C (blue circles), and high-power UV-C (blue triangles) products examined in this report.

To assess the change in radiant efficiency with  $I_f$ , the radiant efficiency of one DUT from each product (UV-1 to UV-7) was measured at different  $I_f$  values, and the findings are presented in **Figure 4-7**. In order for the tested DUT to represent the entire population, the DUTs chosen for this analysis were those with radiant efficiencies similar to the average value of the product population. As shown in **Figure 4-7**, there is only minor changes in radiant efficiency with  $I_f$  for most products. The one exception is UV-3, where the radiant efficiency dropped as  $I_f$  increases. However, the maximum  $I_f$  value of UV-3 is 40 mA, so it will likely have better efficiency than all the tested UV-C and UV-A products over its operational range, except for products UV-5 and UV-6. In contrast, there is much less variation in radiant efficiency with  $I_f$  for the other products. Slightly higher radiant efficiencies are possible at higher currents but the differences are minimal. As a result, we concluded that 5 mA is a reasonable  $I_f$  value that balances radiant efficiency with minimal  $T_j$  changes. This finding indicates that improvement in the electrical efficiency of the UV-B and UV-C LED materials will, in general, improve efficiency if they also lower  $V_{th}$ . In addition, the findings from UV-6 suggest that improvements in optical performance could also significantly impact overall device efficiency. Therefore, further improvements in electrical and optical performance (see **Figure 1-3**) are also needed to drive radiant efficiency higher.

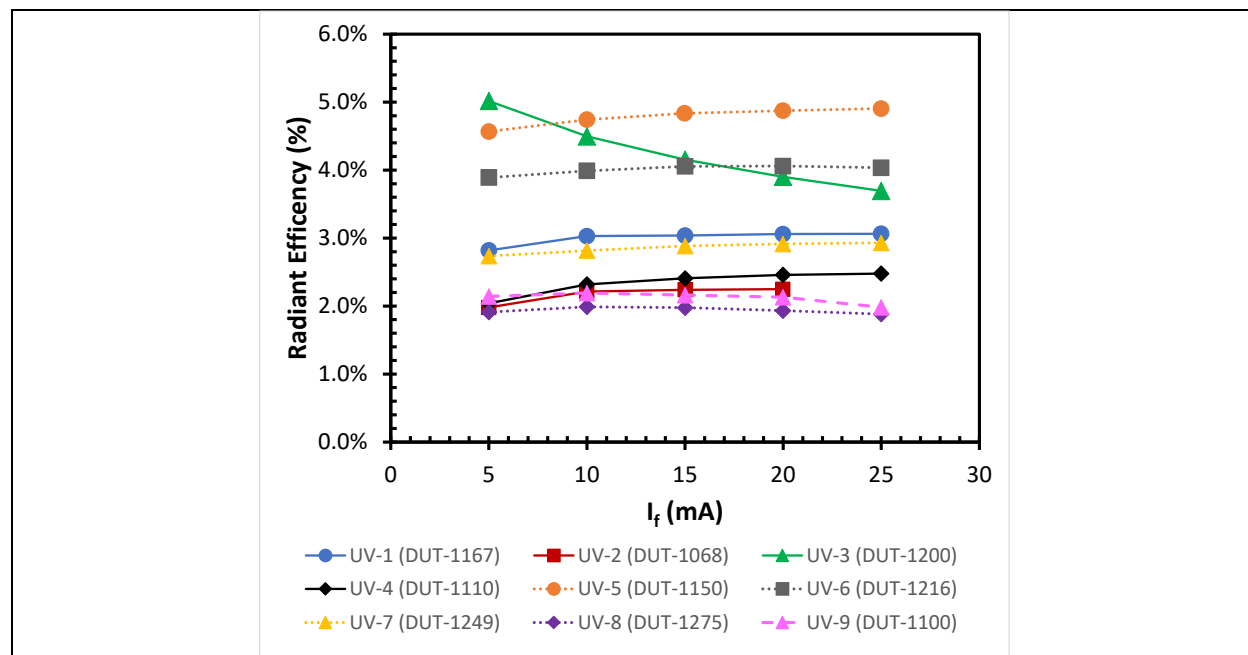


Figure 4-7: Radiant efficiency change with drive current ( $I_f$ ) for a representative DUT of each UV-B and UV-C product examined in this report.

The radiant efficiencies of the UV-A products exhibited different characteristics, as shown in **Figure 4-8**. First, the radiant efficiencies of the UV-A products were significantly higher than the UV-B and UV-C products, which may be expected given the relative maturity of the InGaN semiconductor chemistry. Second, the radiant efficiency of the UV-A products generally increased with  $I_f$  values up to 25 mA, with the largest increases observed for UV-13. Given that these four products are expected to run at maximum currents ranging from 500 mA (UV-11) to 4,000 mA (UV-13), it is not surprising that radiant efficiency would improve as  $I_f$  is increased from 5 mA to 25 mA. However, it is expected that further increases in  $I_f$  would eventually reduce radiant efficiency as observed for UV-3 products. For example, the manufacturer's specifications show that the radiant efficiency of UV-11 is 55% when operated at 500 mA and an 25°C; therefore, some drop in efficiency is likely at higher currents.

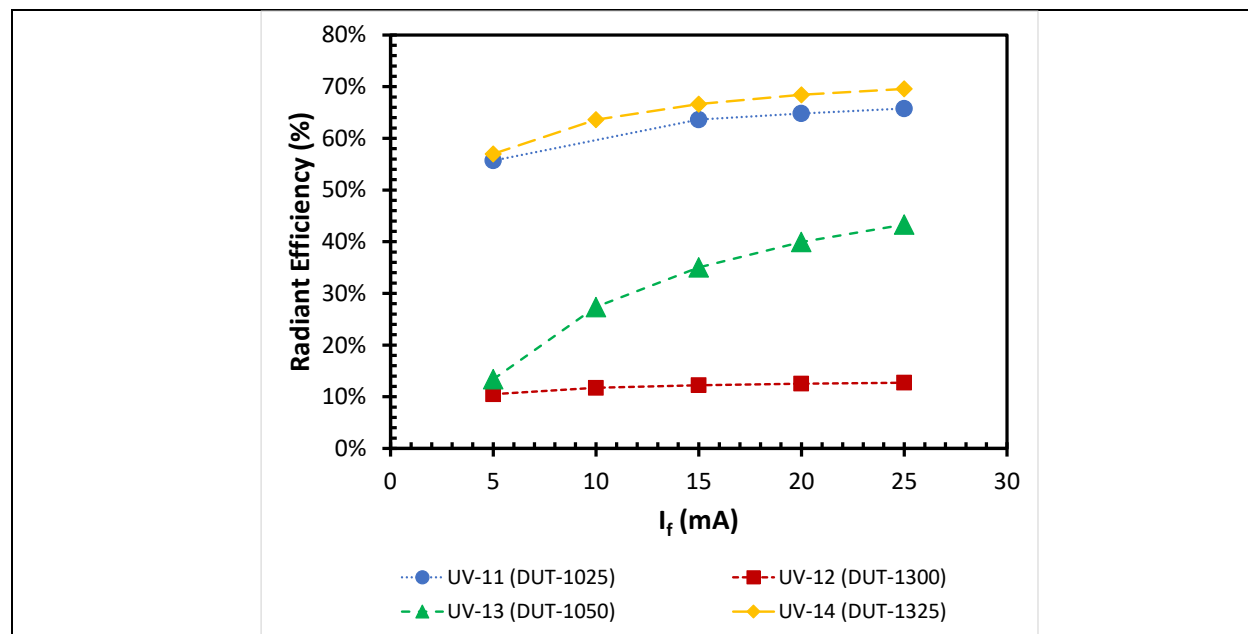


Figure 4-8: Radiant efficiency change with drive current ( $I_f$ ) for a representative DUT of each UV-A product examined in this report.

## 5 Conclusions

UV LEDs are available with dominant wavelengths in the UV-A, UV-B, and UV-C bands. UV-A LEDs are based on InGaN semiconductors, similar to those used in white LEDs, and represent the current state-of-the-art in UV LEDs. High radiant efficiencies are possible with UV-A LEDs with proper design owing in part to the gains made in blue LEDs that power solid-state lighting applications. The maximum bandgap that is possible for an InGaN alloy system corresponds to direct emissions at 362 nm, so producing semiconductors that emit in the UV-B and UV-C bands requires a shift to the less developed AlGaN alloy system. The radiant efficiencies of the UV-B and UV-C LEDs made from AlGaN and examined in this report are low, and values between 2% and 5% were measured across nine different products. The low radiant efficiencies of these products is due in part to electrical issues associated with epitaxy quality and stack resistances, which increase  $V_{th}$  and  $R_{serial}$  for the products. The UV-C products with the highest efficiencies generally had the lowest  $V_{th}$  and  $R_{serial}$  values, with minimal amounts of leakage currents occurring at sub-threshold voltages, which is suggestive of better epitaxy quality. However, improving the overall radiant efficiency of UV-B and UV-C LEDs will require improving not just the electrical performance but also the optical performance at the chip and pad levels. The blue LED that forms the base of the solid-state lighting revolution faced similar challenges 20–25 years ago, and the commercial success of white LEDs can be directly traced to solving these technical issues. It is projected that UV-B and UV-C LEDs will overcome these technical challenges within the next 5–10 years, allowing the technology to fill a market need for compact, robust, and environmentally friendly UV sources and open the path to enhanced capabilities in lighting systems.

## References

1. Young, A. R., Moan, J., Bjorn, L. O., & Nultsch, W. (Eds.). (1993). *Environmental UV Photobiology*. Springer. <https://doi.org/10.1007/978-1-4899-2406-3>
2. Mukish, P. (2021, June 7). *Has COVID-19 pandemic initiated the spark for UVC LED to shine?* 2021 International Ultraviolet Association (IUVA) World Congress, Online.
3. Rea, M. S. (2000). *The IESNA Lighting Handbook* (Ninth ed.). Illuminating Engineering Society of North American (IESNA).
4. Maxson, P., Bender, M., & Culver, A. (2021). *Mercury in fluorescent lighting: Unnecessary health risks and actionable solutions*. [https://cleanlightingcoalition.org/wp-content/uploads/sites/96/Mercury-in-Fluorescent-Lighting\\_FINAL.pdf](https://cleanlightingcoalition.org/wp-content/uploads/sites/96/Mercury-in-Fluorescent-Lighting_FINAL.pdf)
5. U.S. Department of Energy (DOE) Building Technologies Office (BTO) Lighting Research and Development (R&D) Program. (2020, January). *2019 lighting R&D opportunities*. <https://www.energy.gov/sites/prod/files/2020/01/f70/ssl-rd-opportunities2-jan2020.pdf>
6. DOE BTO Lighting R&D Program. (2021, March). *2020 LED manufacturing supply chain*. <https://www.energy.gov/sites/default/files/2021-07/ssl-2020-led-mfg-supply-chain-mar21jul21.pdf>
7. Krames, M. (2021, March 23). *Webinar: UV-C advancements enable innovative germicidal uses displacing lamps in some scenarios*. LEDs Magazine. <https://www.ledsmagazine.com/home/webinar/14198107/uv-c-advancements-enable-innovative-germicidal-uses-displacing-lamps-in-some-scenarios>
8. Schubert, E. F. (2006). *Light-Emitting Diodes* (2nd ed.). Cambridge University Press. <https://www.ifsc.usp.br/~lavfis2/BancoApostilasImagens/ApConstantePlanck/ApCtePlanck2013/LIGHT-EMITTING%20DIODES.e-0521865387-2e.pdf>
9. Hadis, M. (2008). *Handbook of Nitride Semiconductors and Devices*, Volume 1. Wiley-VCH.
10. Tsai, Y. C., & Bayram, C. (2019). Structural and electronic properties of hexagonal and cubic phase AlGaInN alloys investigated using first principles calculations. *Scientific Reports*, 9(1), 6583. <https://doi.org/10.1038/s41598-019-43113-w>
11. Kneissl, M., Seong, T.-Y., Han, J., & Amano, H. (2019). The emergence and prospects of deep-ultraviolet light-emitting diode technologies. *Nature Photonics*, 13(4), 233–244. <https://doi.org/10.1038/s41566-019-0359-9>
12. Peng, Y., Liang, R., Mou, Y., Dai, J., Mingxiang, C., & Luo, X. (2019). Progress and perspective of near-ultraviolet and deep-ultraviolet light-emitting diode packaging technologies. *Journal of Electronic Packaging*, 141(4). <https://doi.org/10.1115/1.4044624>
13. De Santi, C., Caria, A., Piva, F., Meneghesso, G., Zanoni, E., & Meneghini, M. (2021). Degradation mechanisms of InGaN visible LEDs and AlGaInN UV LEDs. In R. W. Herrick & O. Ueda (Eds.), *Reliability of Semiconductor Lasers and Optoelectronic Devices* (pp. 273–312). Woodhead Publishing. <https://doi.org/10.1016/b978-0-12-819254-2.00001-1>

14. Mondal, R. K., Adhikari, S., Chatterjee, V., & Pal, S. (2021). Recent advances and challenges in AlGa<sub>N</sub>-based ultra-violet light emitting diode technologies. *Materials Research Bulletin*, 140, 111258. <https://doi.org/10.1016/j.materresbull.2021.111258>
15. International Ultraviolet Association. (2021). *Far UV-C radiation: Current state-of knowledge*. <https://iuva.org/resources/covid-19/Far%20UV-C%20Radiation-%20Current%20State-of%20Knowledge.pdf>
16. Sliney, D. H. (2021). *Photobiological safety issues—UVGI installations*. 2021 Lighting R&D Workshop. [https://www.energy.gov/sites/default/files/2021/02/f82/ssl-rd21\\_sliney-uvgi.pdf](https://www.energy.gov/sites/default/files/2021/02/f82/ssl-rd21_sliney-uvgi.pdf)
17. International Commission on Illumination (CIE). (2010). *UV-C photocarcinogenesis risks from germicidal lamps* (187:2010). [https://ghdcenter.hms.harvard.edu/files/ghd\\_dubai/files/cancer\\_risk\\_cie187-2010\\_free\\_copy\\_march\\_2020-1.pdf](https://ghdcenter.hms.harvard.edu/files/ghd_dubai/files/cancer_risk_cie187-2010_free_copy_march_2020-1.pdf)
18. ANSI and IES. (2019). *ANSI/IES LM-79-19, Approved method: Optical and electrical measurements of solid state lighting products*. New York, NY: IES.
19. ANSI and IES. (2020). *ANSI/IES LM-85-20, Approved method: Optical and electrical measurements of LED packages and arrays*. New York, NY: IES.
20. Krames, M., Christenson, G., Collins, D., Cook, L., Craford, M., Edwards, A., ... Tan, T. S. (2000). High-brightness AlGaInN light-emitting diodes. *Proceedings of SPIE, Light-Emitting Diodes: Research, Manufacturing, and Applications IV* (Vol. 3938). Yao, H. W., Ferguson, I. T., Schubert, E. F. (Eds.). <https://doi.org/10.1117/12.382822>
21. Trivellin, N., Monti, D., Piva, F., Buffolo, M., De Santi, C., Zanoni, E., ... Meneghini, M. (2019). Degradation processes of 280 nm high power DUV LEDs: Impact on parasitic luminescence. *Japanese Journal of Applied Physics*, 58, SCCC19. <https://doi.org/10.7567/1347-4065/ab1393>
22. Inrad Optics. (2021). *Spectral reflectivity curves*. <https://www.inradoptics.com/capabilities/coating/spectral-reflectivity-curves>

## Appendix A: Initial Benchmarks for UV LEDs

### UV-1

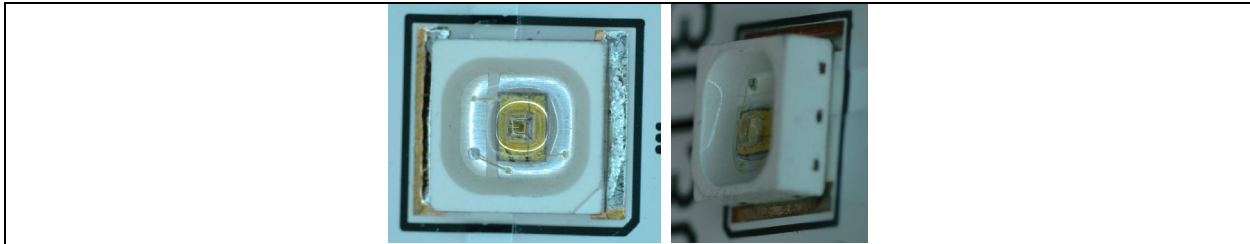


Figure A-1: Front-view and oblique view of UV-1 LED.

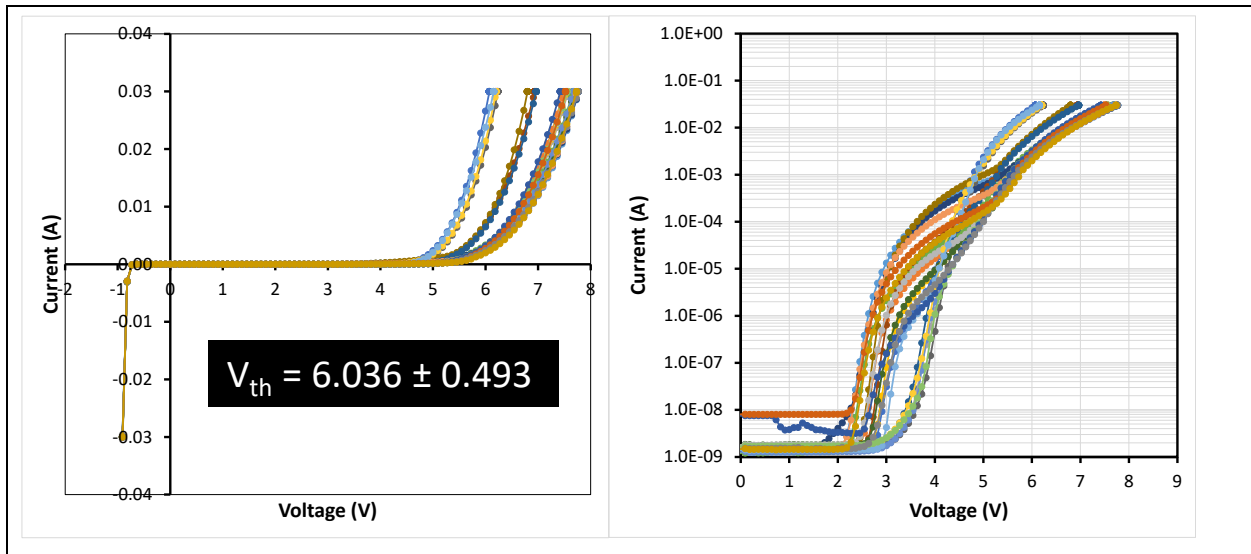


Figure A-2: Initial I-V curves for all 22 samples of UV LED-1. Linear current scale on the left and logarithmic current scale of the right.

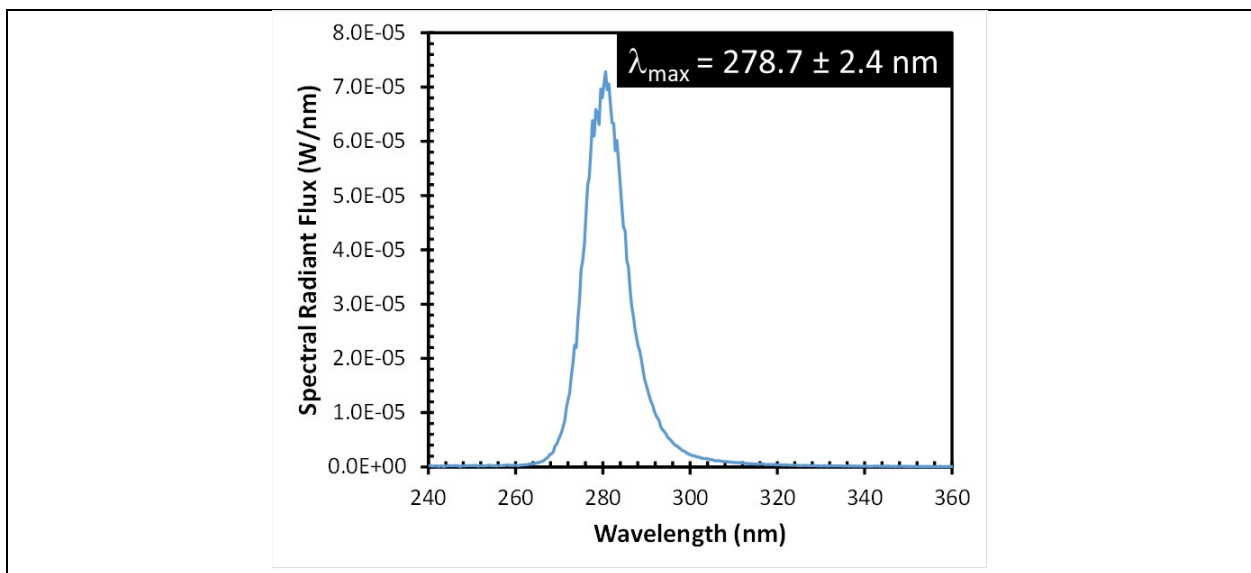


Figure A-3: Initial SPD for a typical UV-1 LED operated at 5 mA.

## UV-2

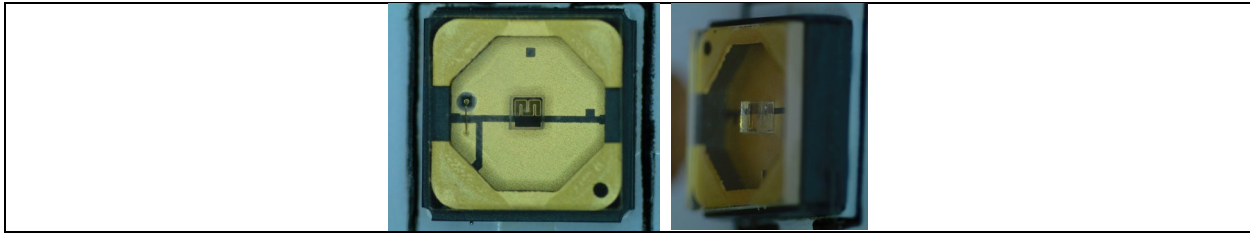


Figure A-4: Front-view and oblique view of UV-2 LED.

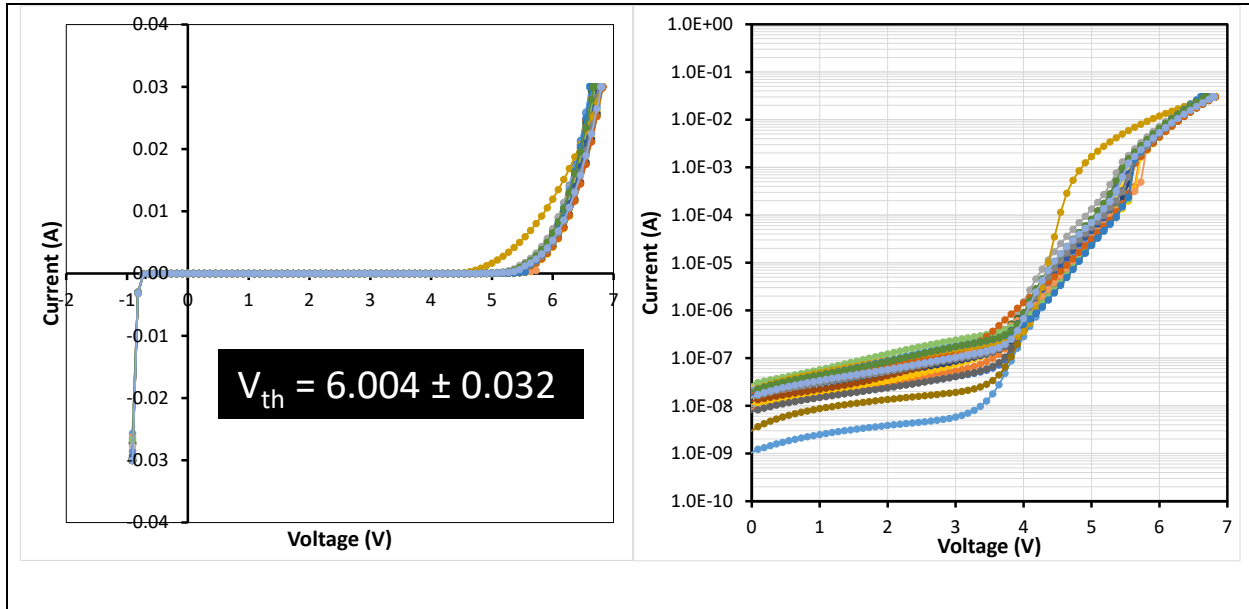


Figure A-5: Initial I-V curves for all 25 samples of UV LED-2. Linear current scale on the left and logarithmic current scale of the right.

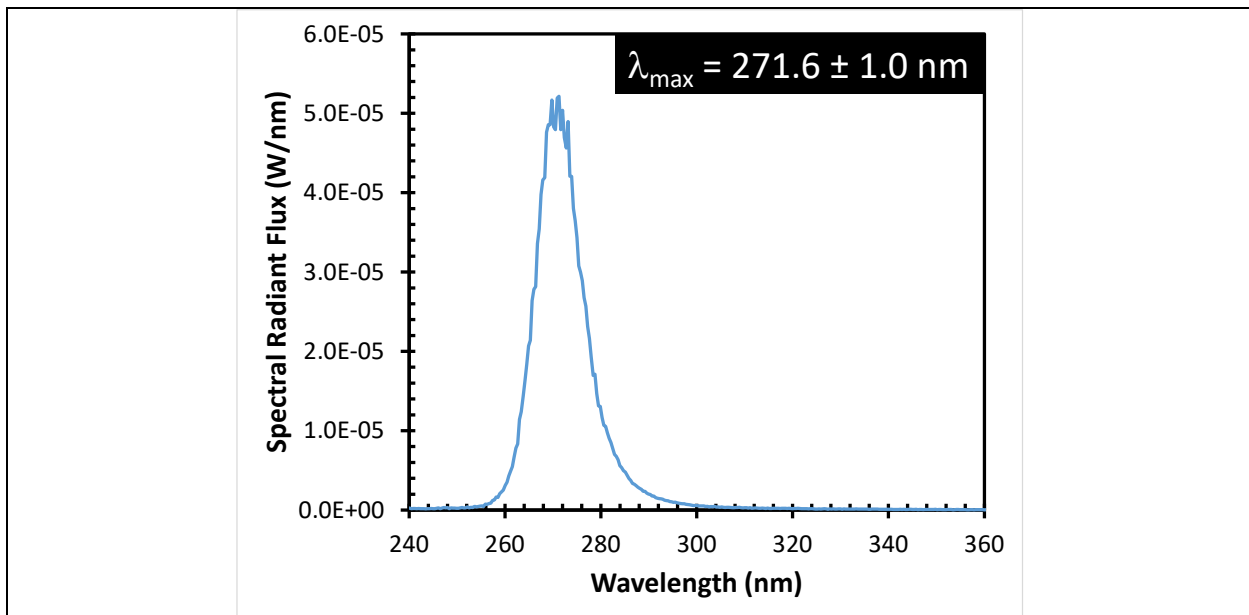


Figure A-6: Initial SPD for a typical UV-2 LED operated at 5 mA.

### UV-3

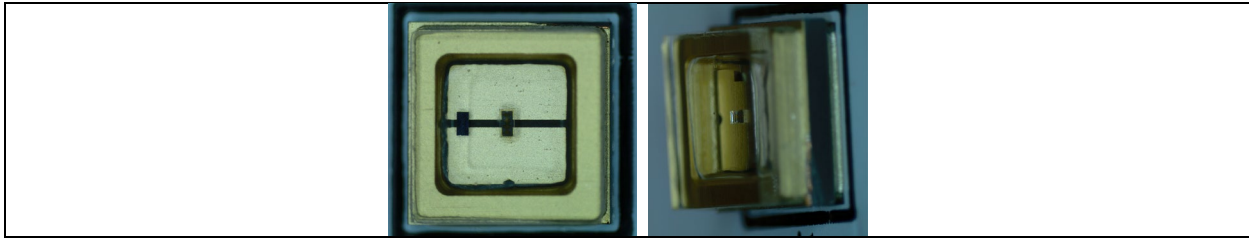


Figure A-7: Front-view and oblique view of UV-3 LED.

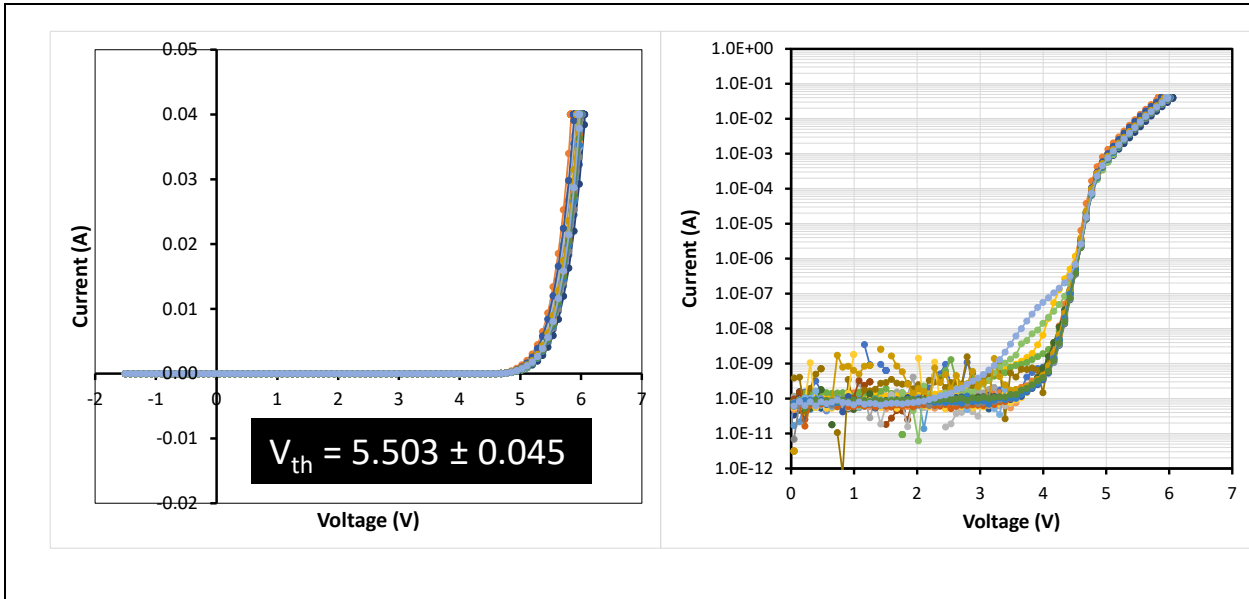


Figure A-8: Initial I-V curves for all 25 samples of UV LED-3. Linear current scale on the left and logarithmic current scale of the right.

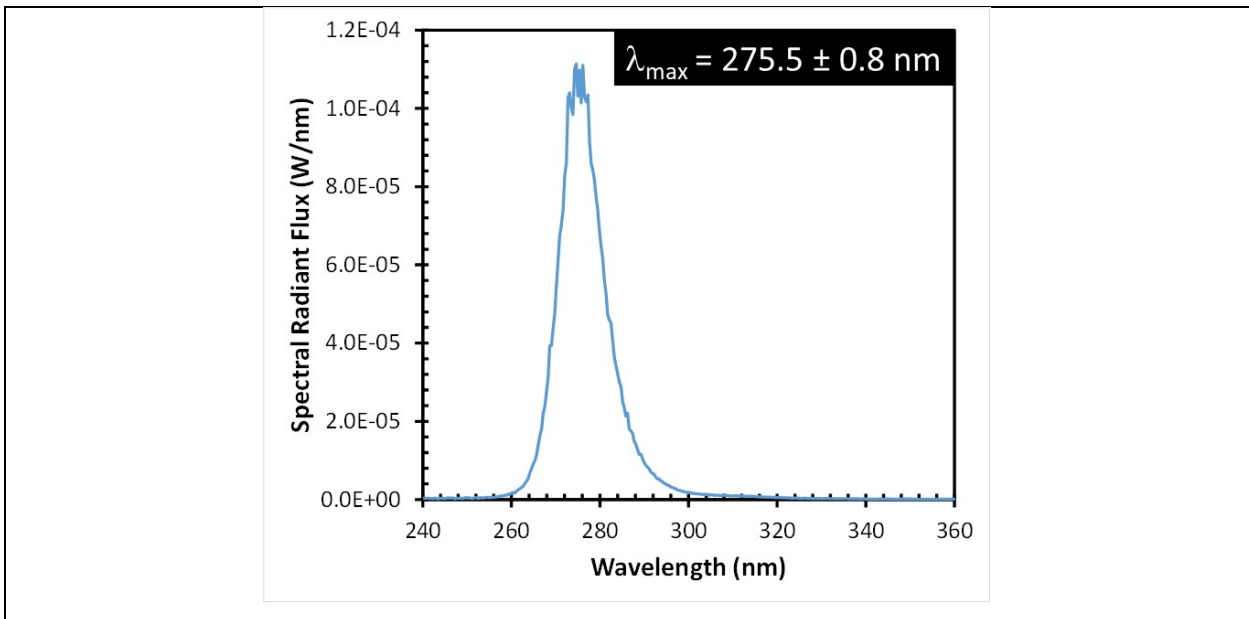


Figure A-9: Initial SPD for a typical UV-3 LED operated at 5 mA.

## UV-4

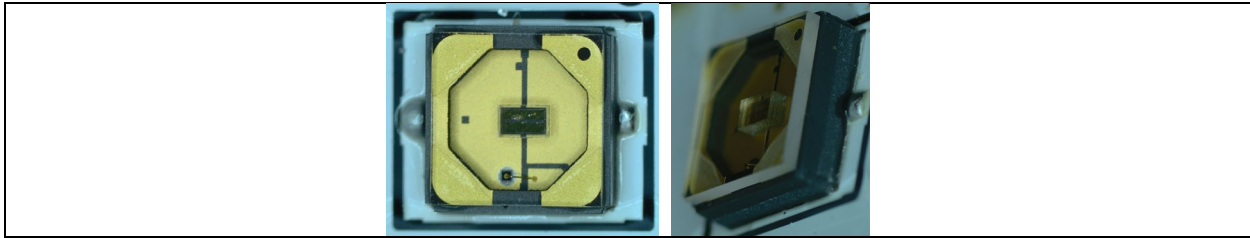


Figure A-10: Front-view and oblique view of UV-4 LED.

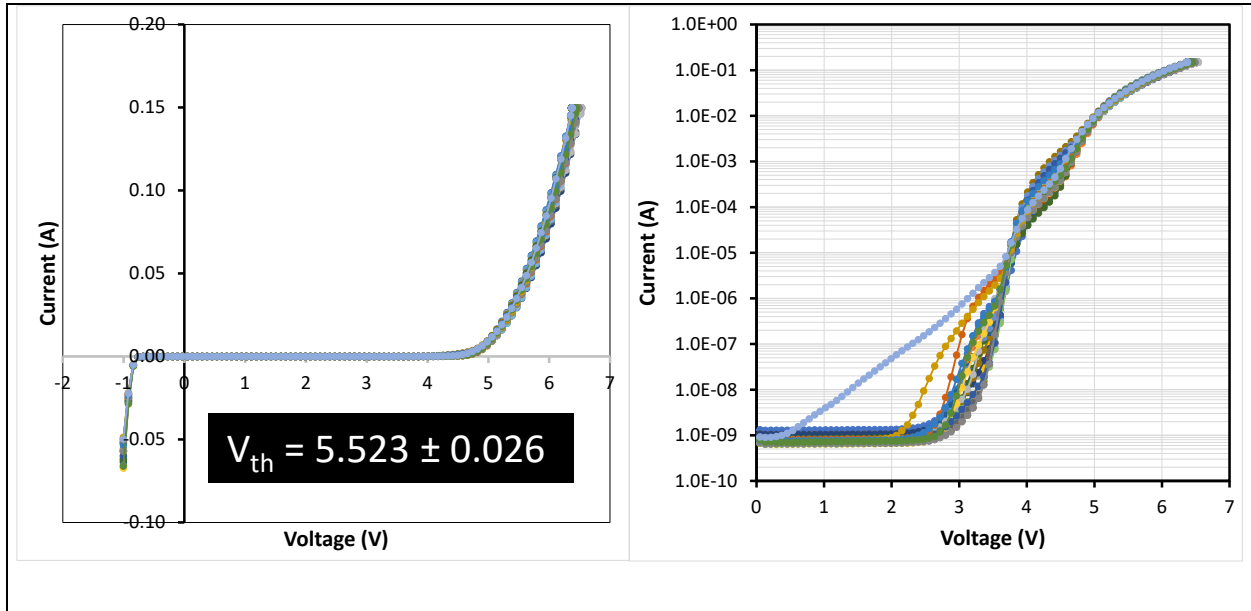


Figure A-11: Initial I-V curves for all 2 samples of UV LED-4. Linear current scale on the left and logarithmic current scale of the right.

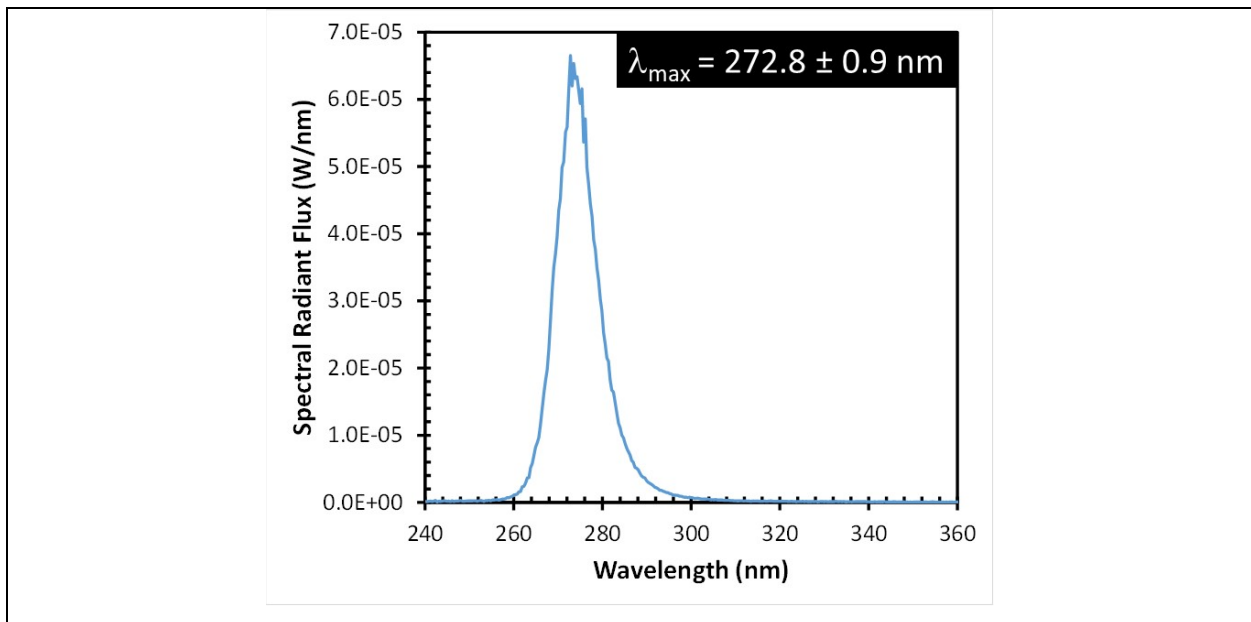


Figure A-12: Initial SPD for a typical UV-4 LED operated at 5 mA.

## UV-5



Figure A-13: Front-view and oblique view of UV-5 LED.

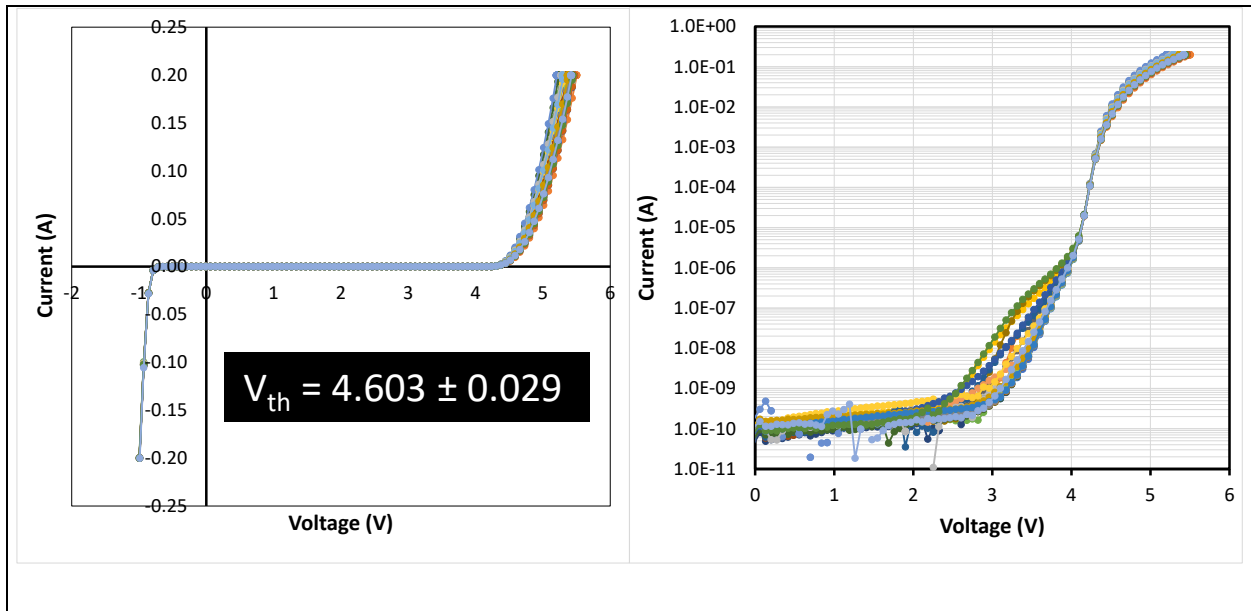


Figure A-14: Initial I-V curves for all 25 samples of UV LED-5. Linear current scale on the left and logarithmic current scale of the right.

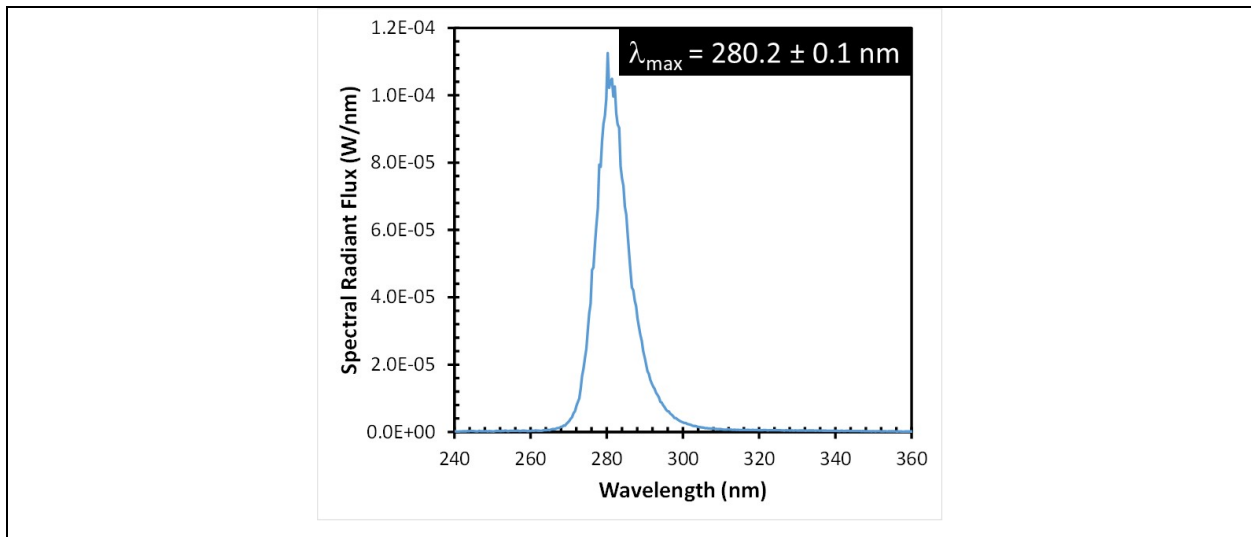


Figure A-15: Initial SPD for a typical UV-5 LED operated at 5 mA.

## UV-6

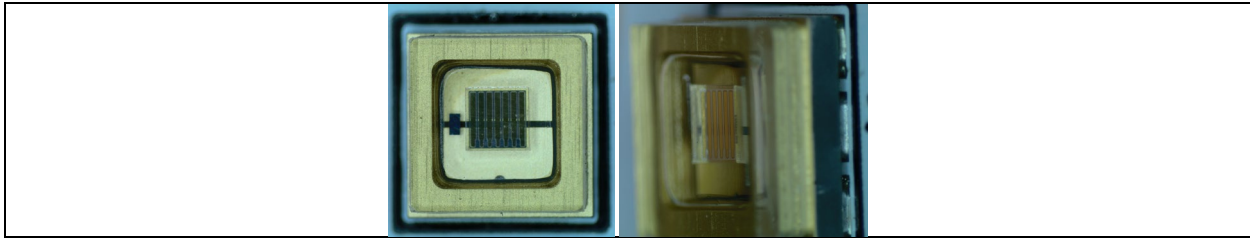


Figure A-16: Front-view and oblique view of UV-6 LED.

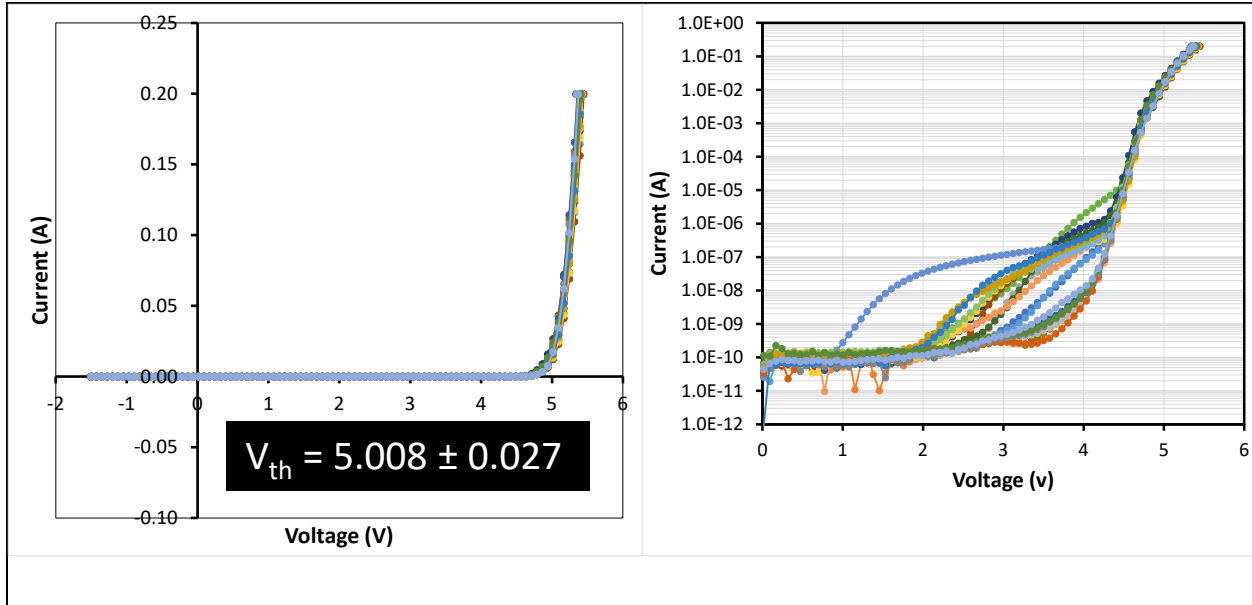


Figure A-17: Initial I-V curves for all 25 samples of UV LED-6. Linear current scale on the left and logarithmic current scale of the right.

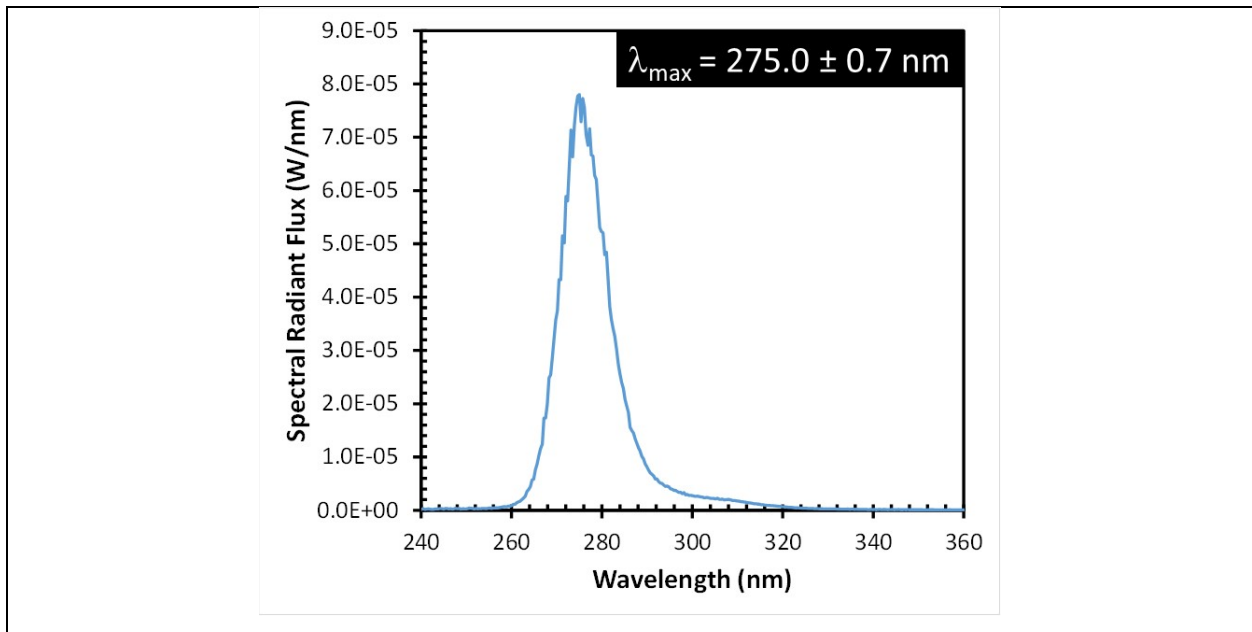


Figure A-18: Initial SPD for a typical UV-6 LED operated at 5 mA.

### UV-7

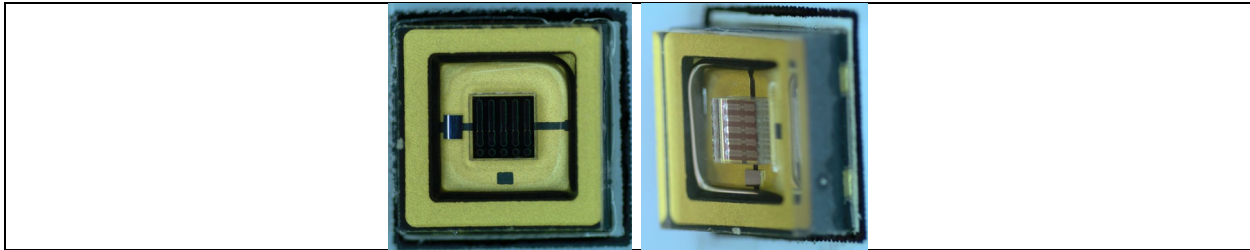


Figure A-19: Front-view and oblique view of UV-7 LED.

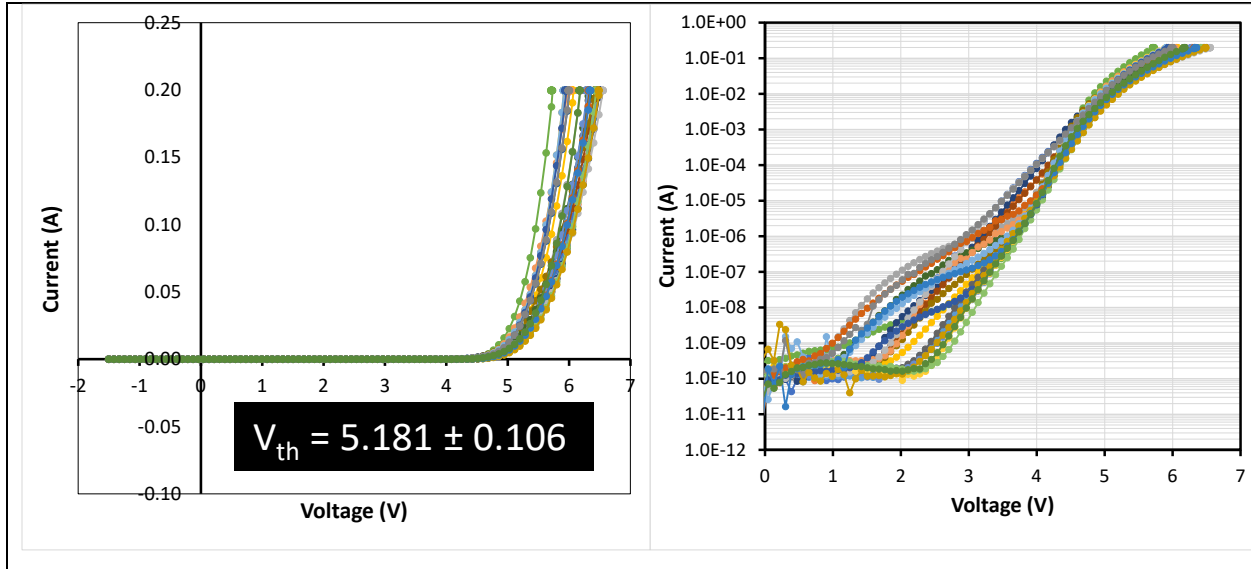


Figure A-20: Initial I-V curves for all 25 samples of UV LED-7. Linear current scale on the left and logarithmic current scale of the right.

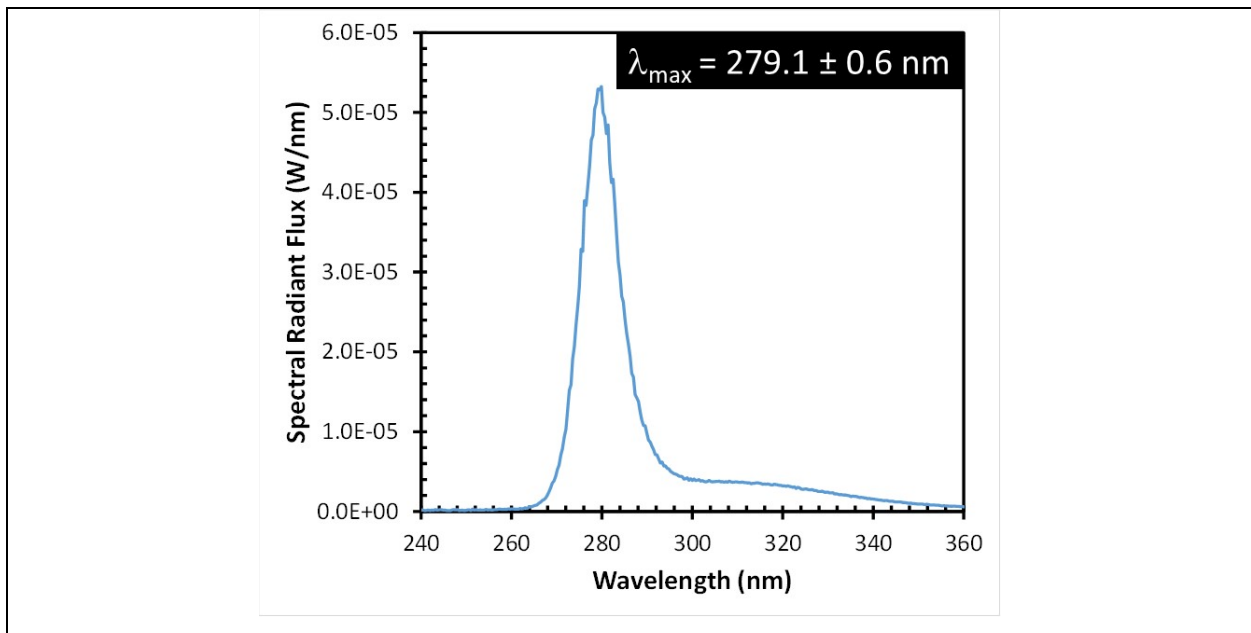


Figure A-21: Initial SPD for a typical UV-7 LED operated at 5 mA.

## UV-8

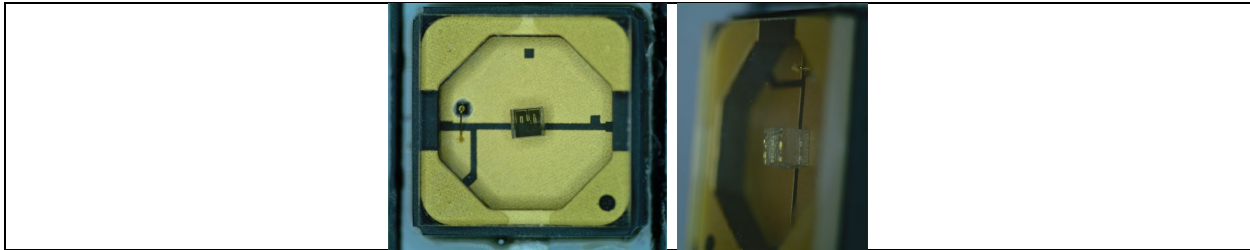


Figure A-22: Front-view and oblique view of UV-8 LED.

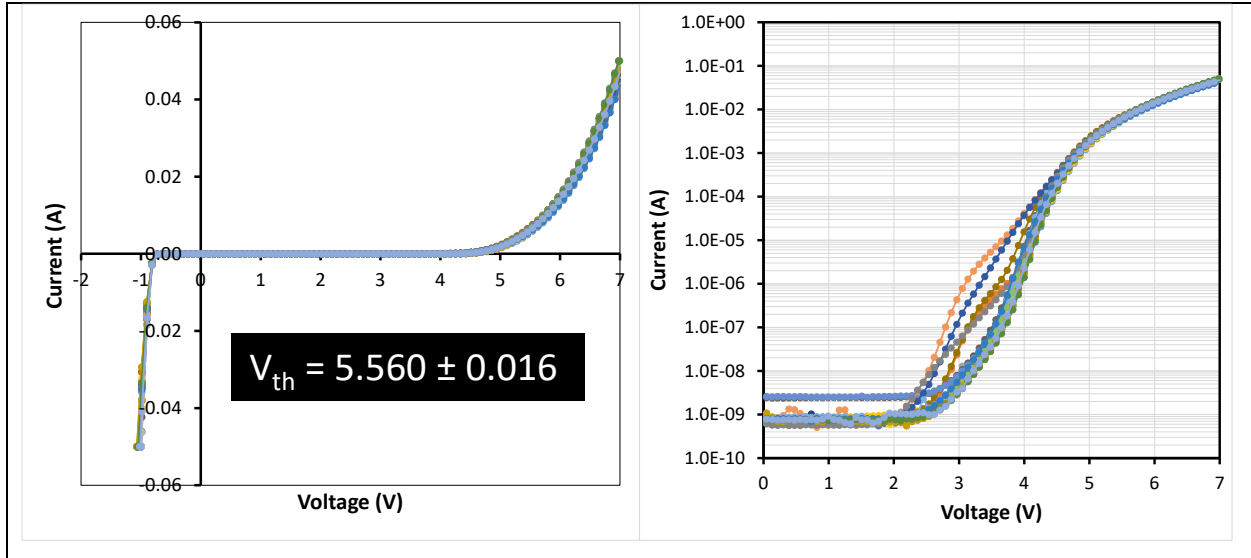


Figure A-23: Initial I-V curves for all 25 samples of UV LED-8. Linear current scale on the left and logarithmic current scale of the right.

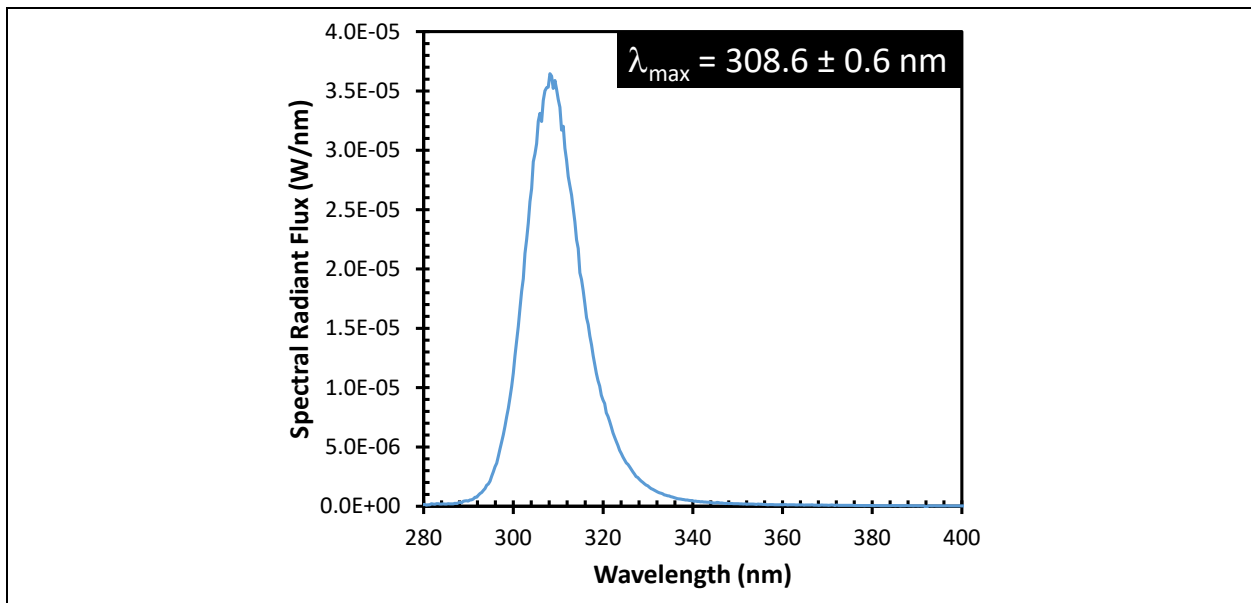


Figure A-24: Initial SPD for a typical UV-8 LED operated at 5 mA.

## UV-9

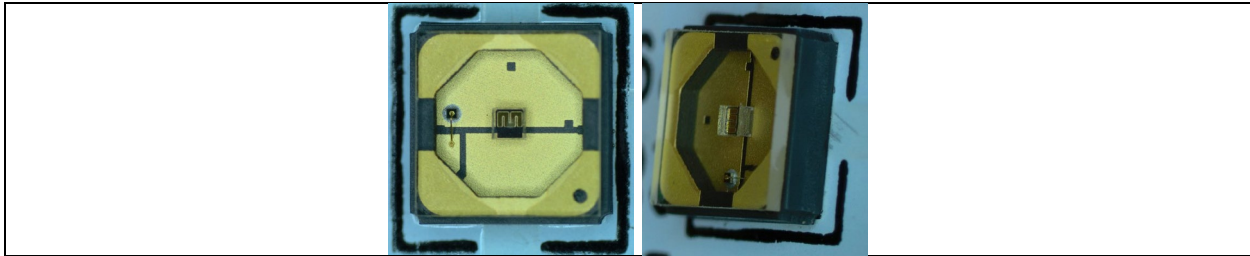


Figure A-25: Front-view and oblique view of UV-9 LED.

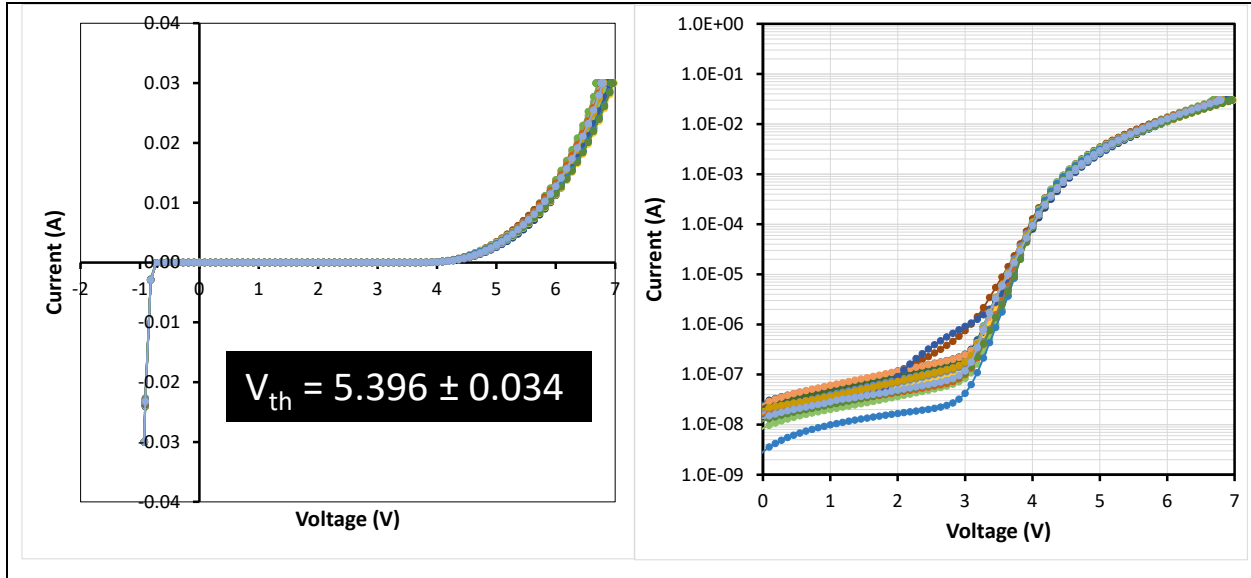


Figure A-26: Initial I-V curves for all 25 samples of UV LED-9. Linear current scale on the left and logarithmic current scale of the right.

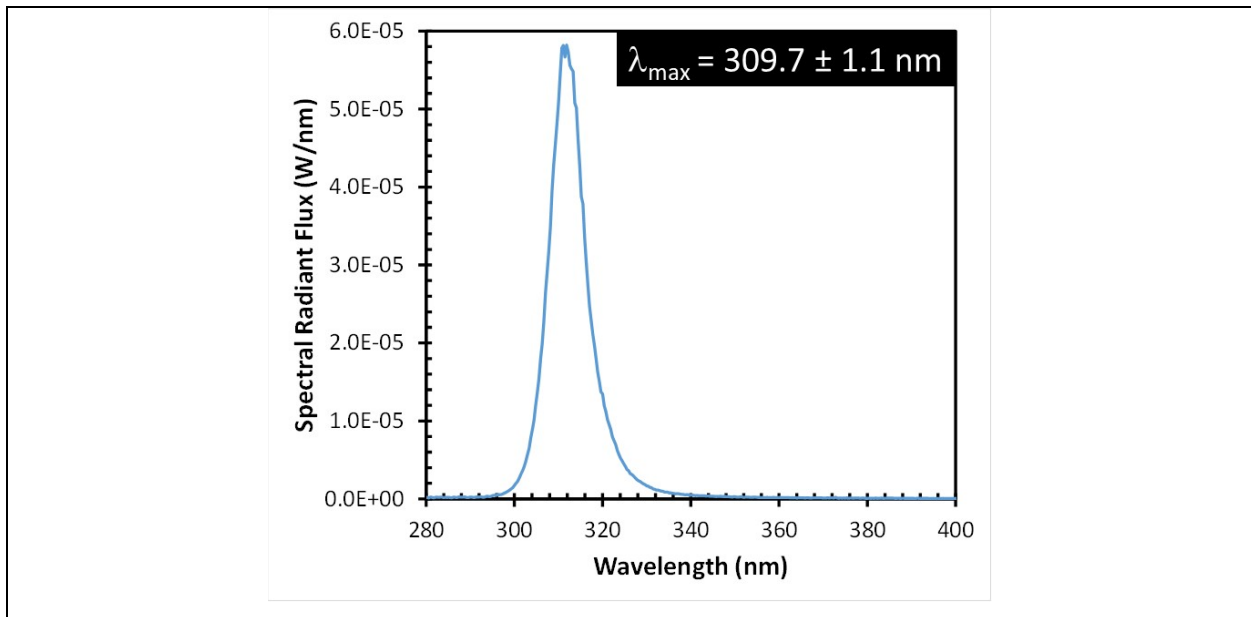


Figure A-27: Initial SPD for a typical UV-9 LED operated at 5 mA.

## UV-11

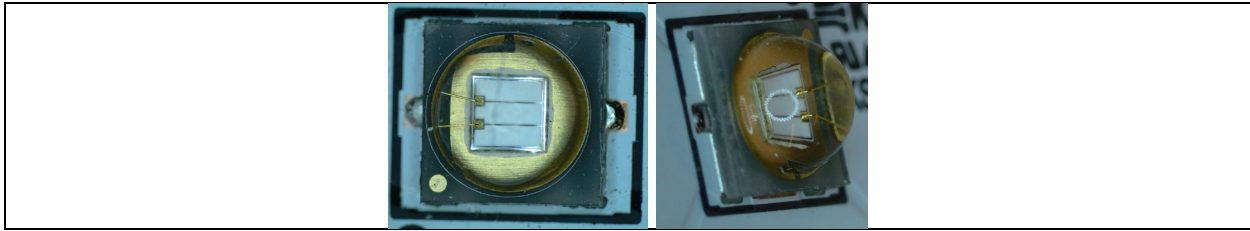


Figure A 28: Front-view and oblique view of UV-11 LED.

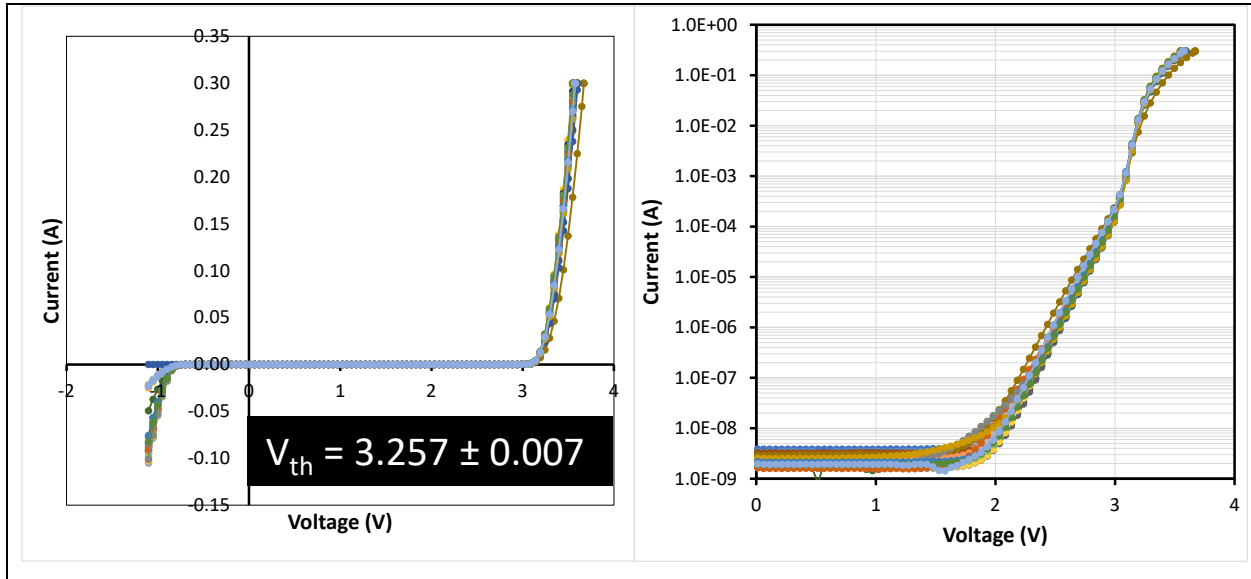


Figure A 29: Initial I-V curves for all 25 samples of UV LED-11. Linear current scale on the left and logarithmic current scale of the right.

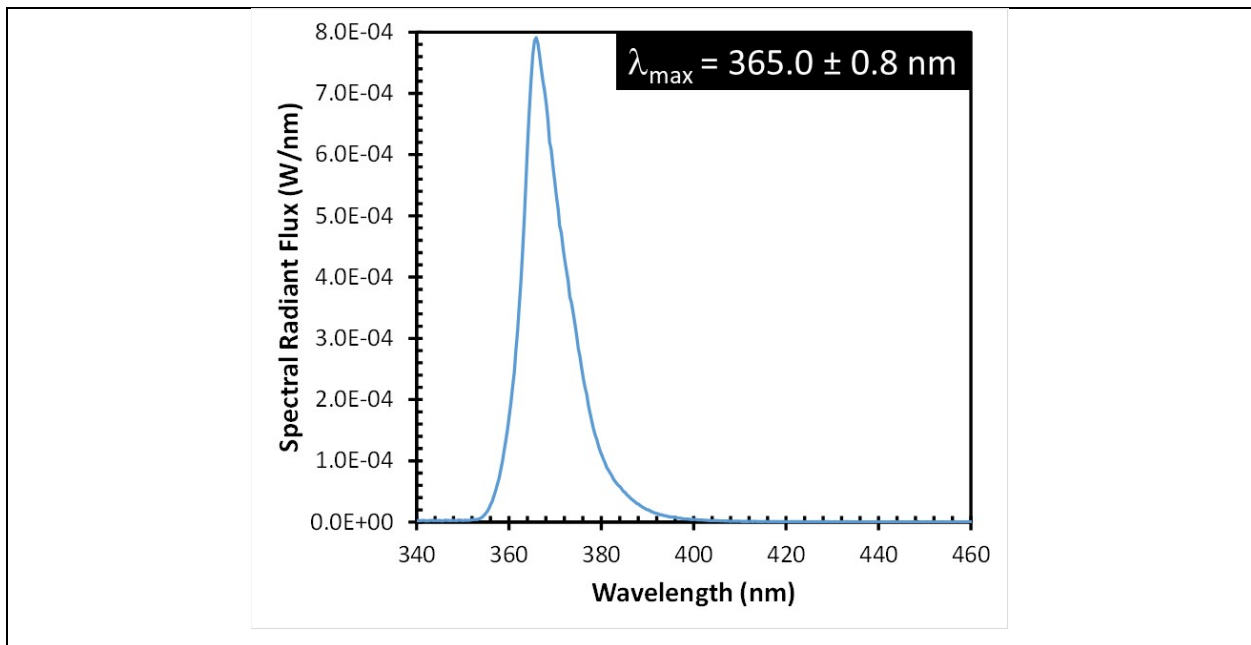


Figure A-30: Initial SPD for a typical UV-11 LED operated at 5 mA.

## UV-12

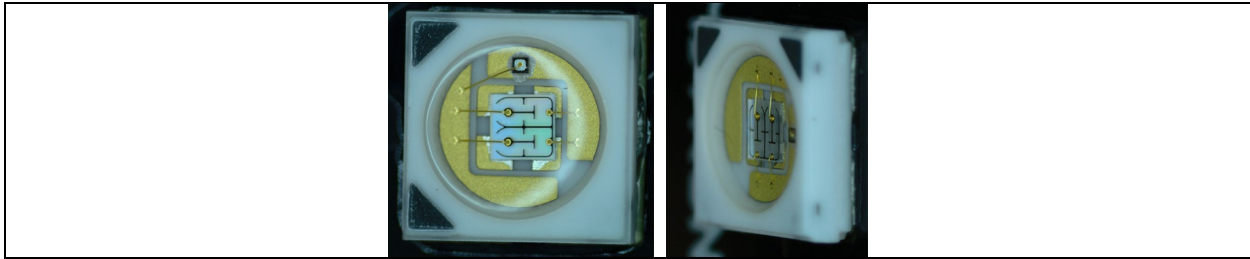


Figure A-31: Front-view and oblique view of UV-12 LED.

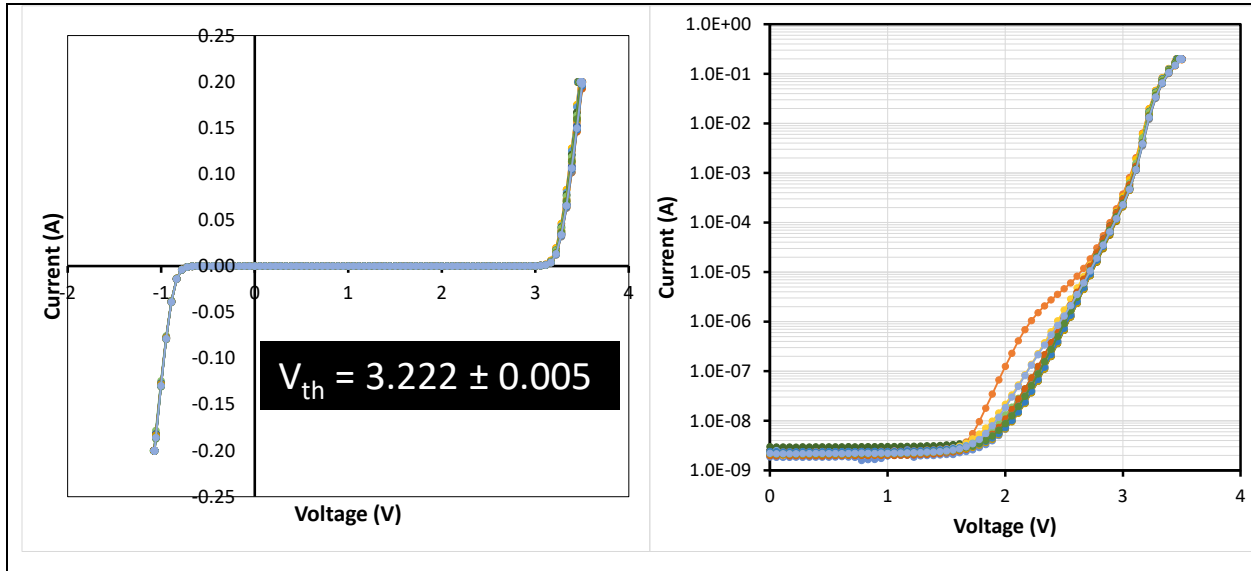


Figure A-32: Initial I-V curves for all 25 samples of UV LED-12. Linear current scale on the left and logarithmic current scale of the right.

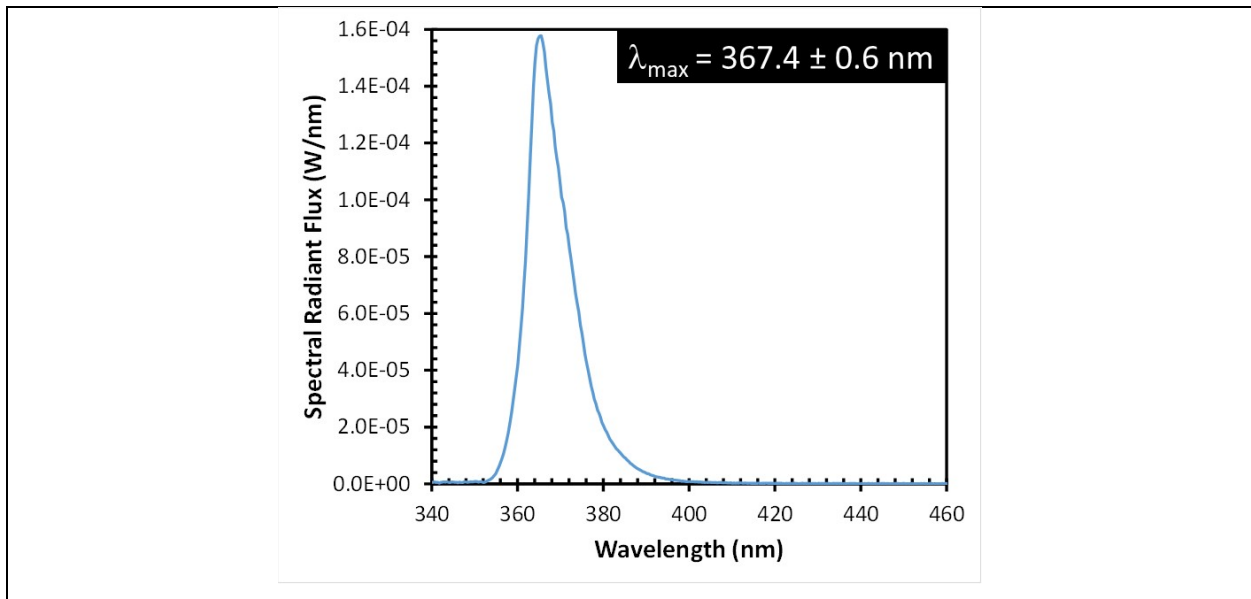


Figure A-33: Initial SPD for a typical UV-12 LED operated at 5 mA.

### UV-13

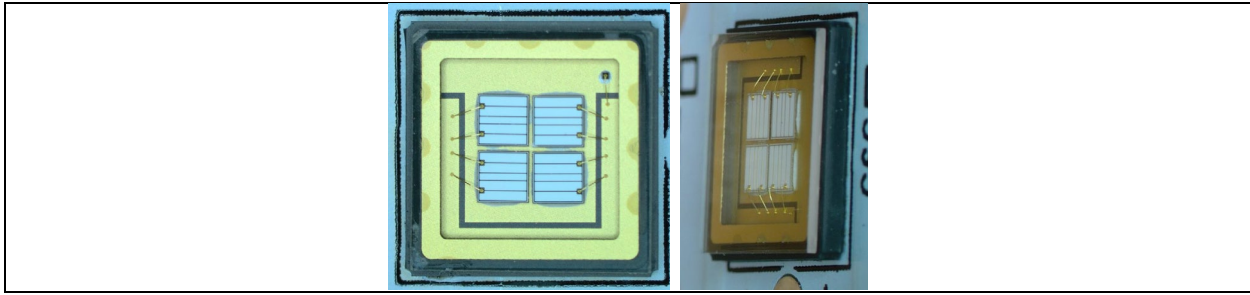


Figure A-34: Front-view and oblique view of UV-13 LED.

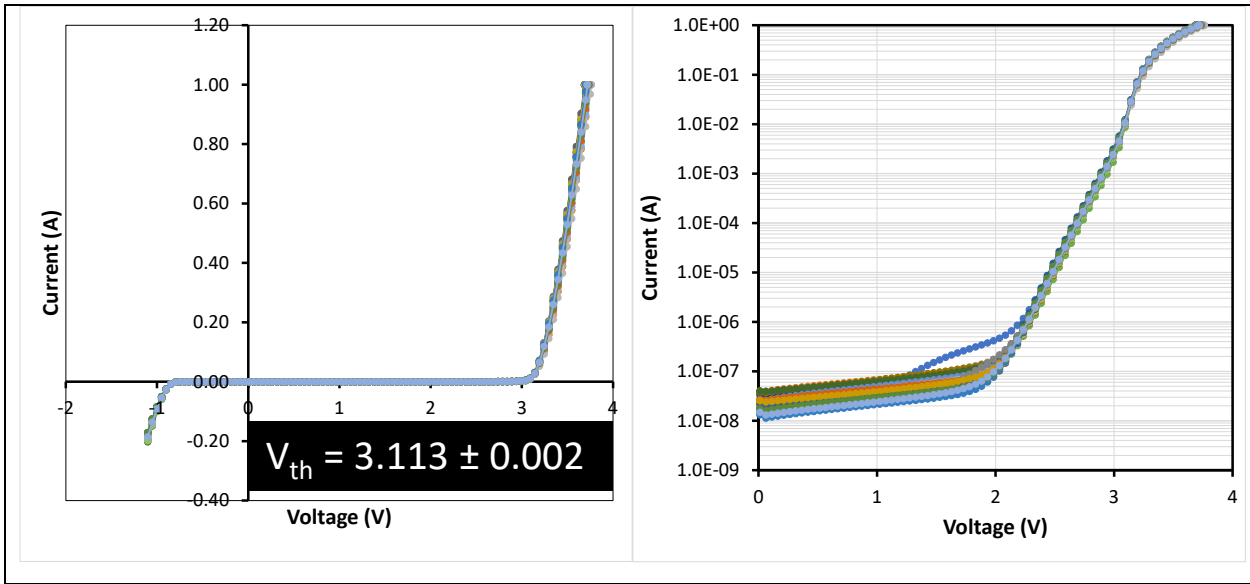


Figure A-35: Initial I-V curves for all 25 samples of UV LED-13. Linear current scale on the left and logarithmic current scale of the right.

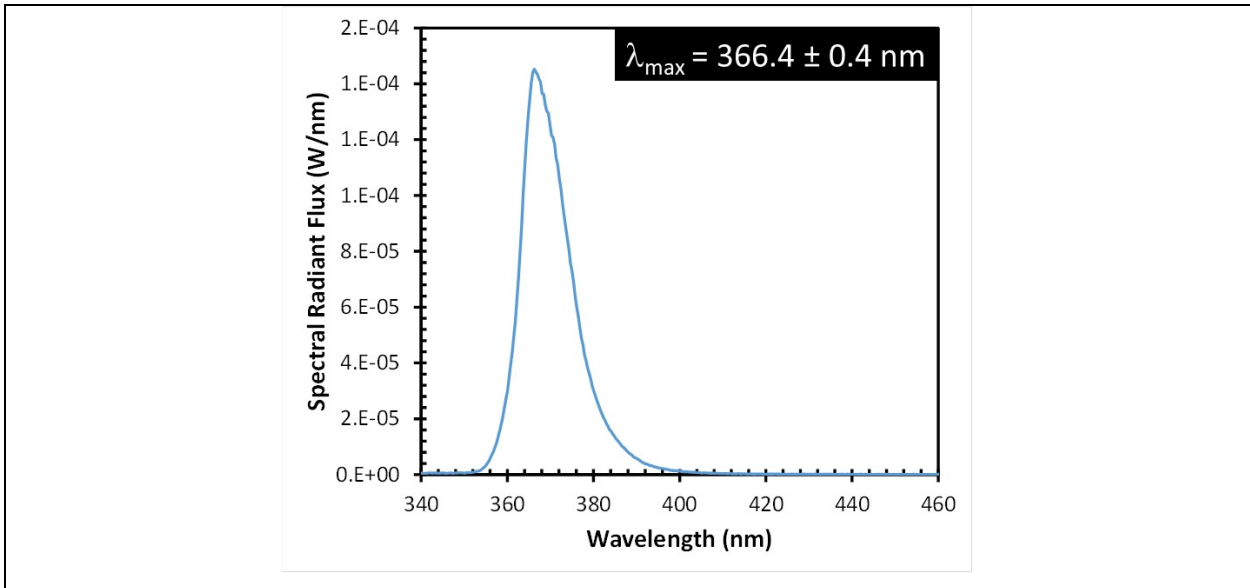


Figure A-36: Initial SPD for a typical UV-13 LED operated at 5 mA.

## UV-14

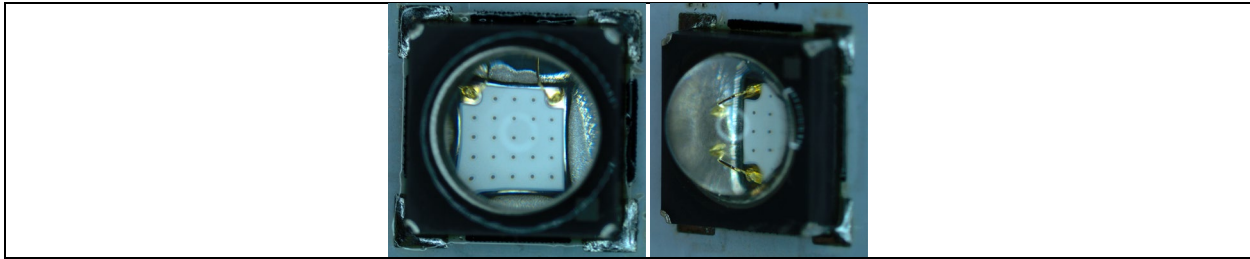


Figure A-37: Front-view and oblique view of UV-14 LED.

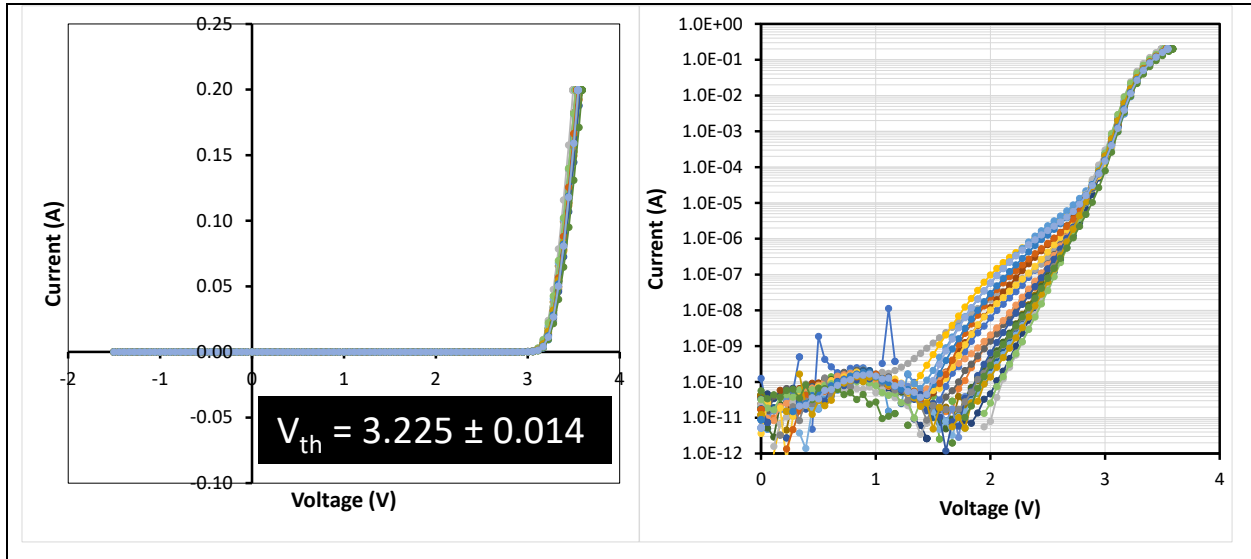


Figure A-38: Initial I-V curves for all 25 samples of UV LED-14. Linear current scale on the left and logarithmic current scale of the right.

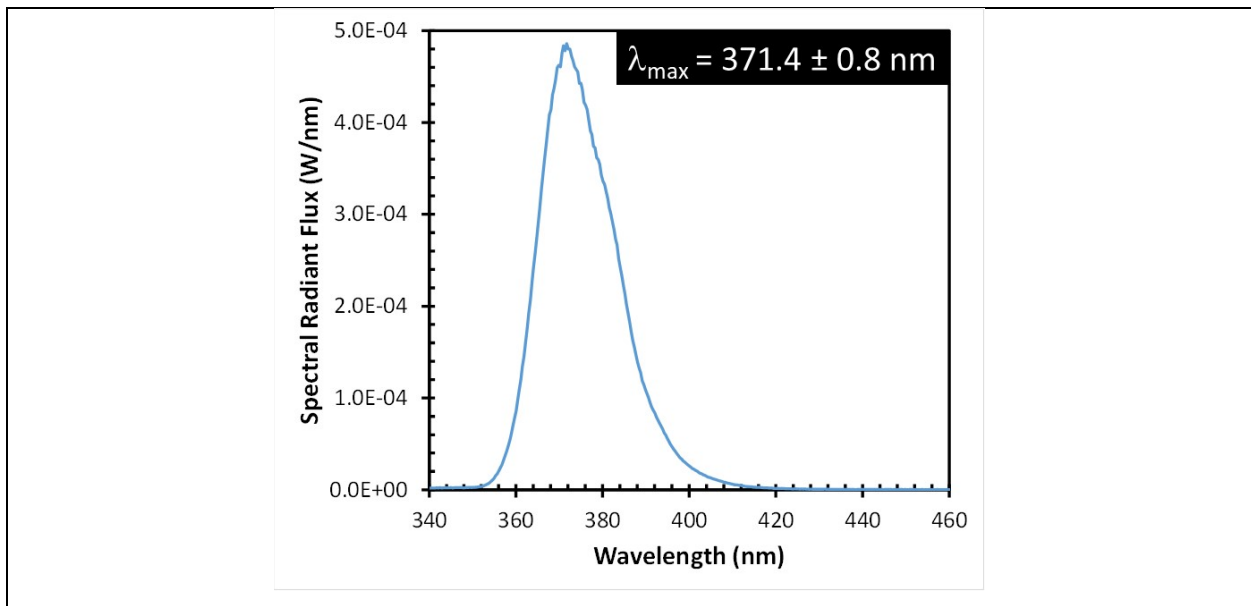


Figure A-39: Initial SPD for a typical UV-14 LED operated at 5 mA.

### White LED-1

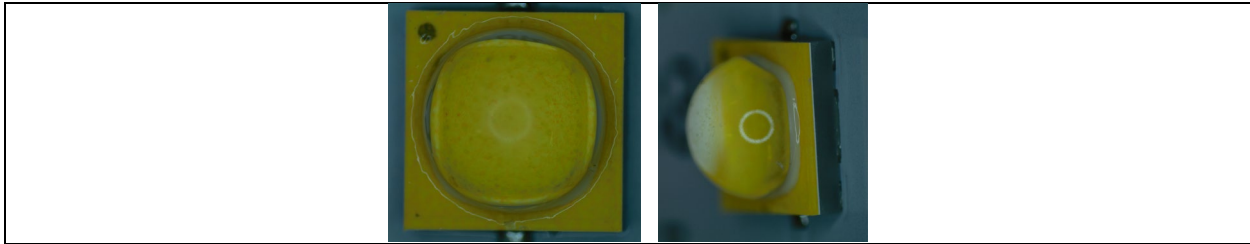


Figure A-40: Front-view and oblique view of white LED-1.

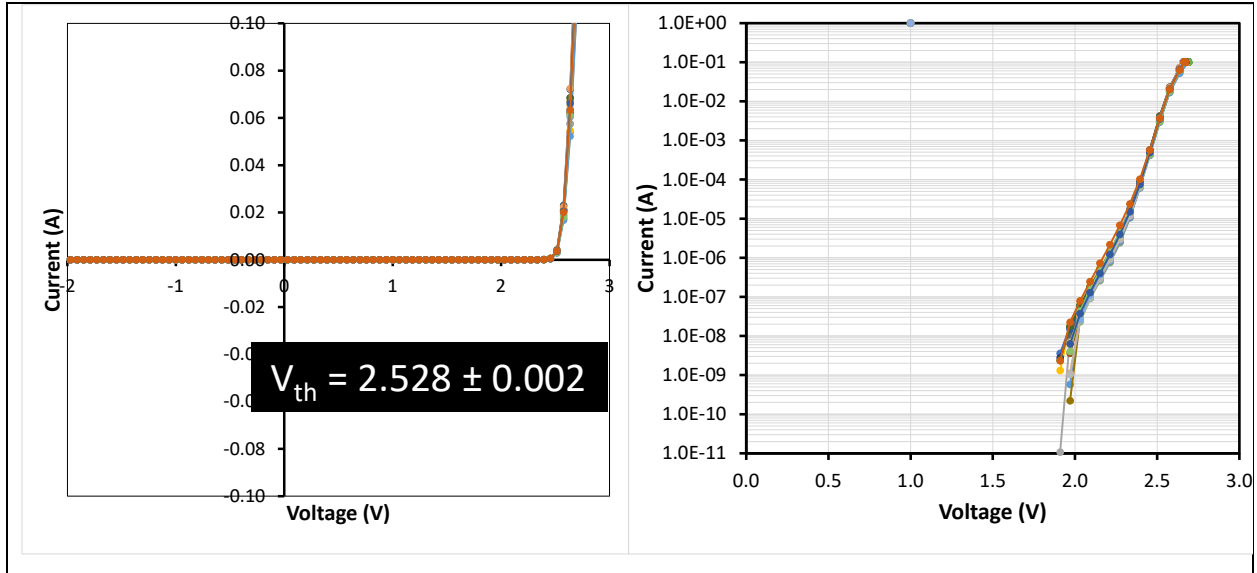


Figure A-41: I-V curves for all 20 samples of White LED-1. Linear current scale on the left and logarithmic current scale of the right.

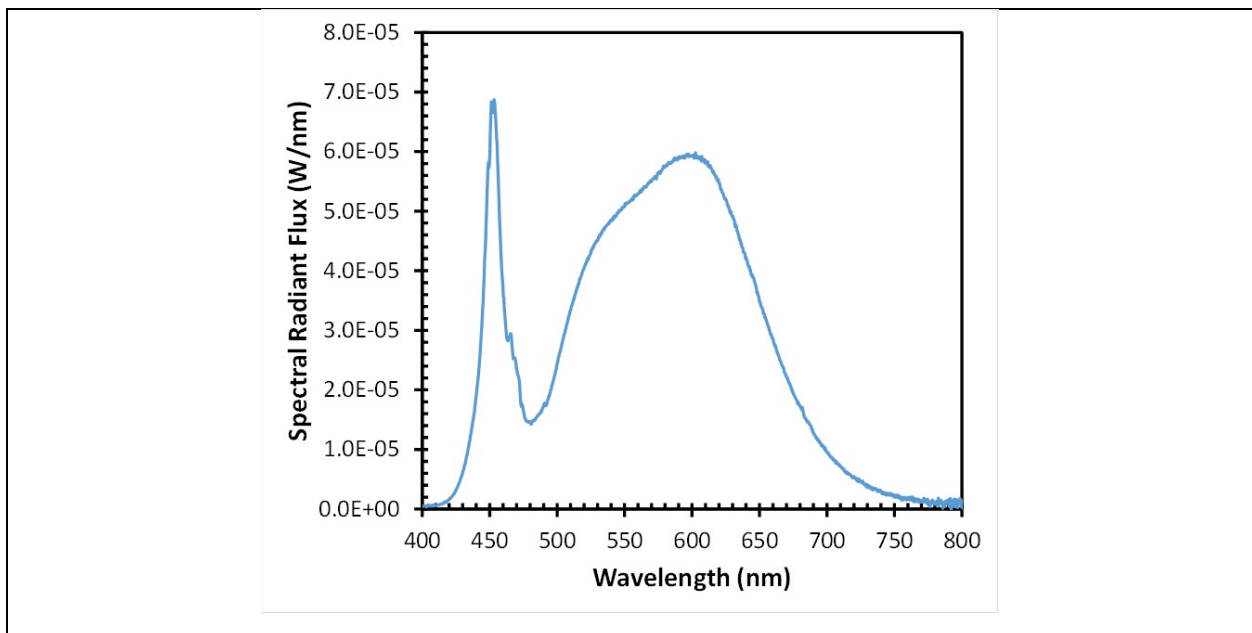


Figure A-42: SPD for a typical white LED-1 operated at 5 mA. CCT value is 3,800 K.

## White LED-2

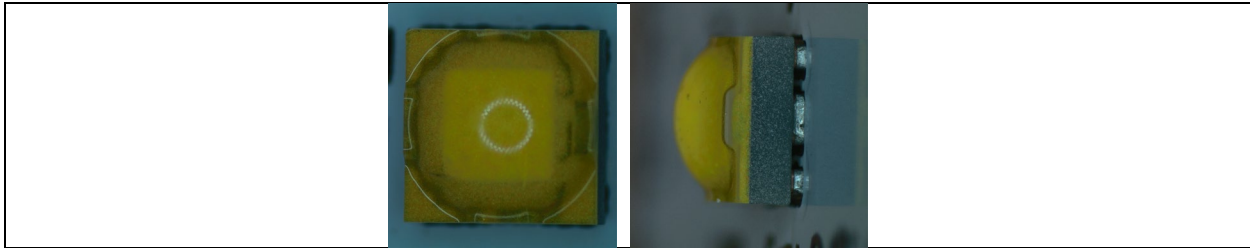


Figure A-43: Front-view and oblique view of white LED-2.

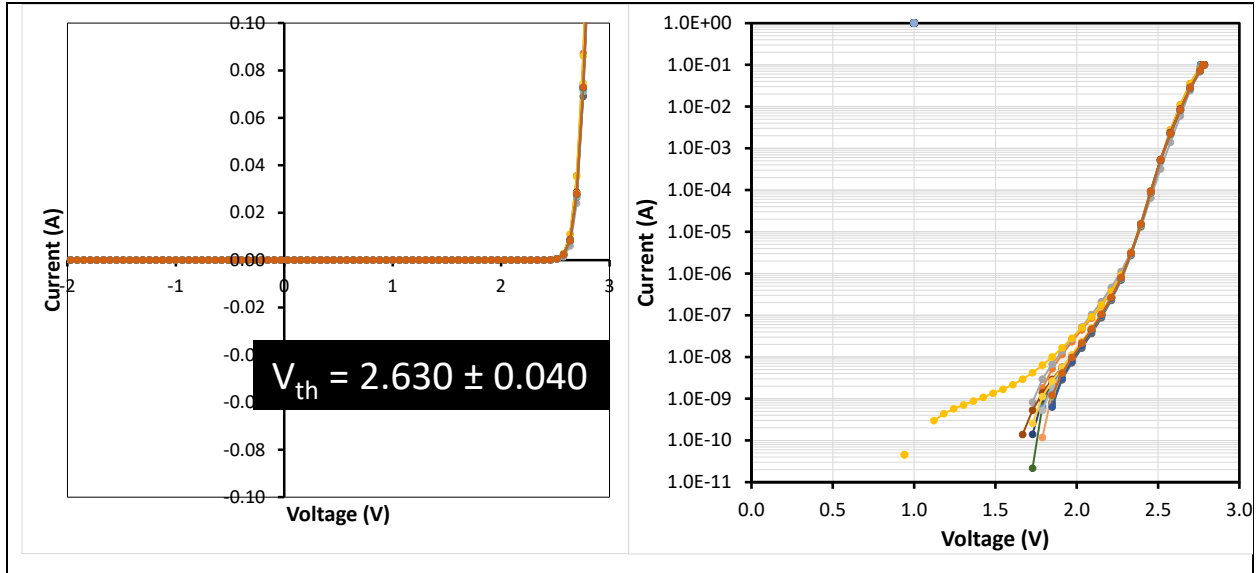


Figure A-44: I-V curves for all 20 samples of White LED-2. Linear current scale on the left and logarithmic current scale of the right.

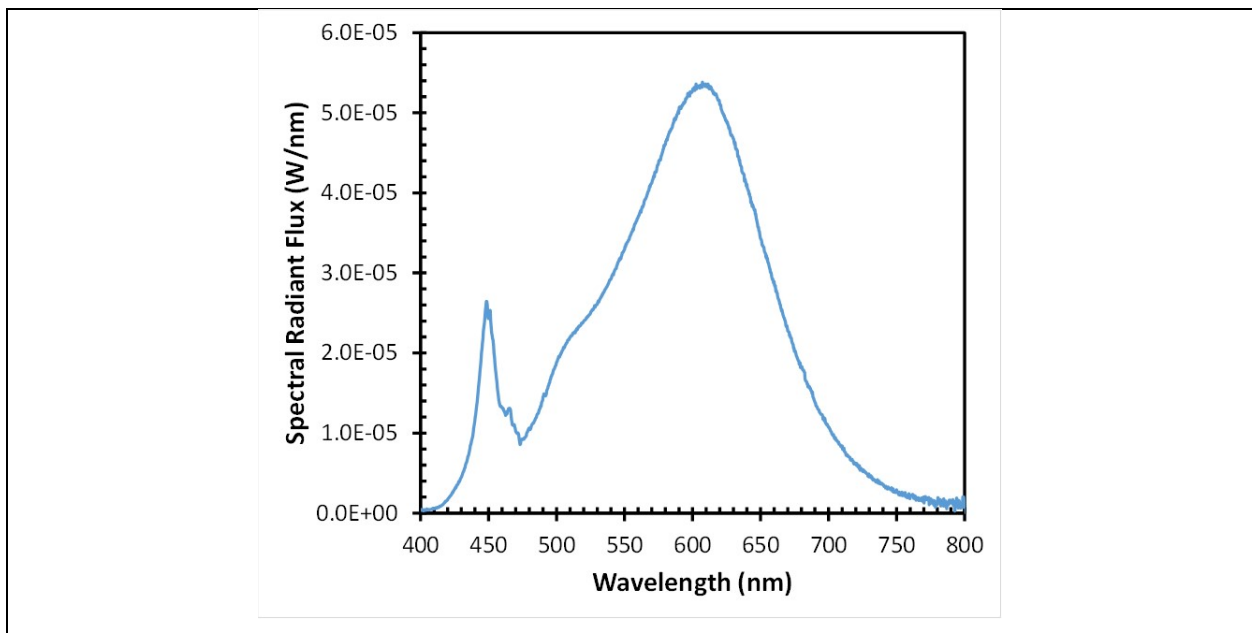


Figure A-45: SPD for a typical white LED-2 operated at 5 mA. CCT value is 2,850 K.

## Appendix B: Initial V(t) Measures for LEDs in This Study

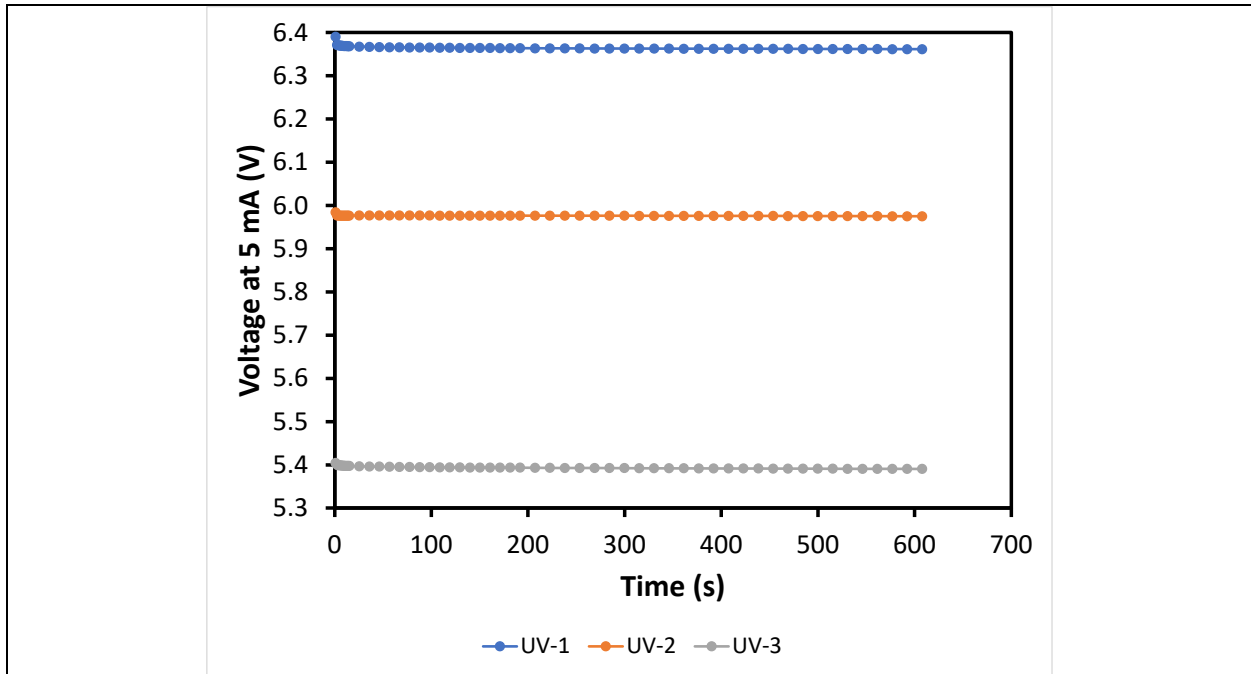


Figure B-1: V(t) graph for low-power the UV-C products UV-1, UV-2, and UV-3.

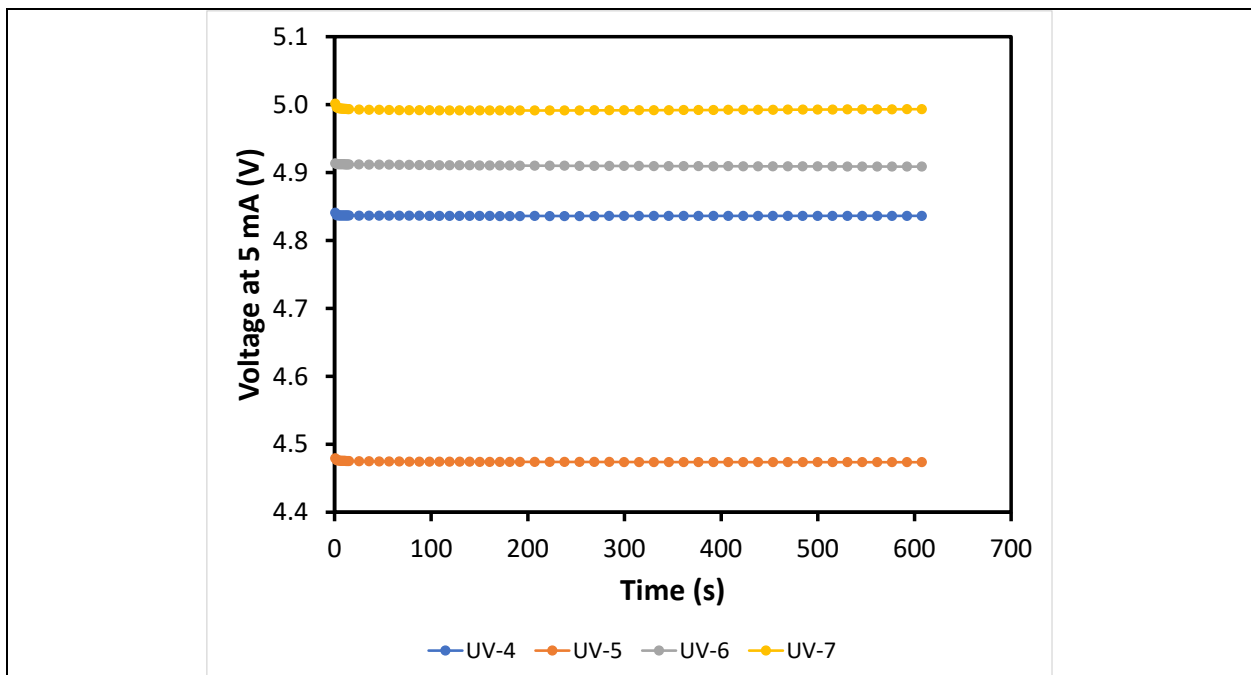


Figure B-2: V(t) graph for the high-power UV-C products, UV-4, UV-5, UV-6, and UV-7.

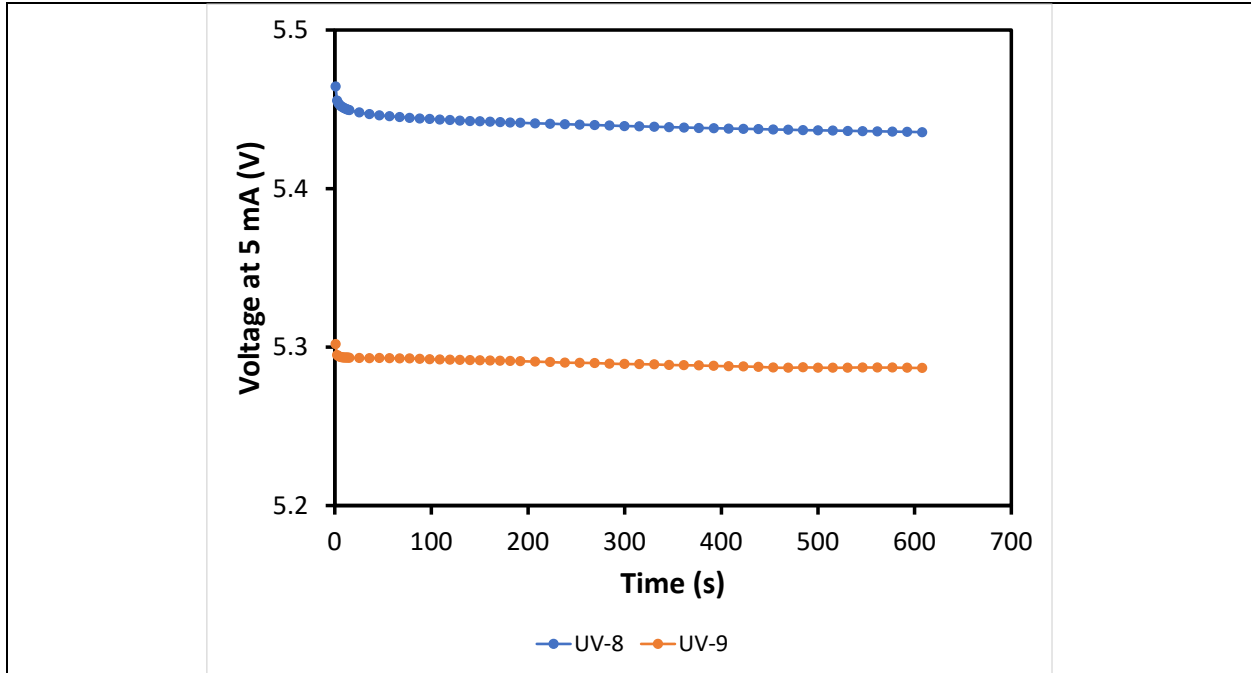


Figure B-3: V(t) graph for the UV-B products, UV-8 and UV-9.

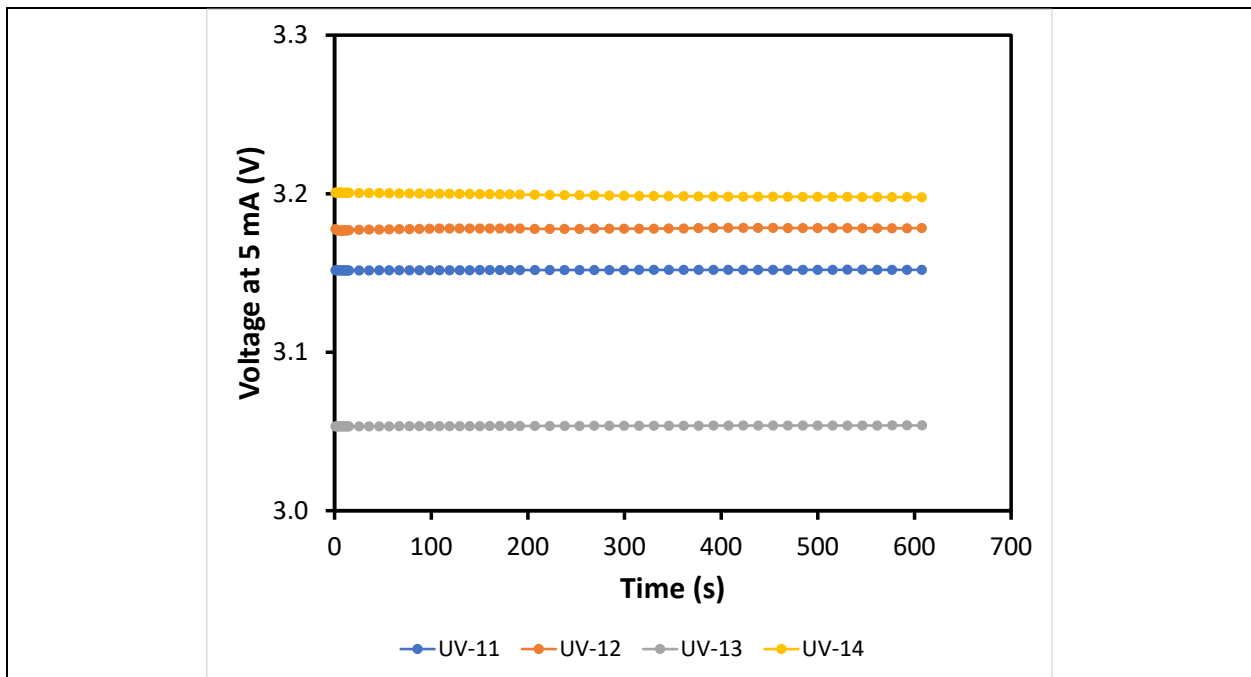


Figure B-4: V(t) graph for the UV-A products, UV-11, UV-12, UV-13, UV-14.

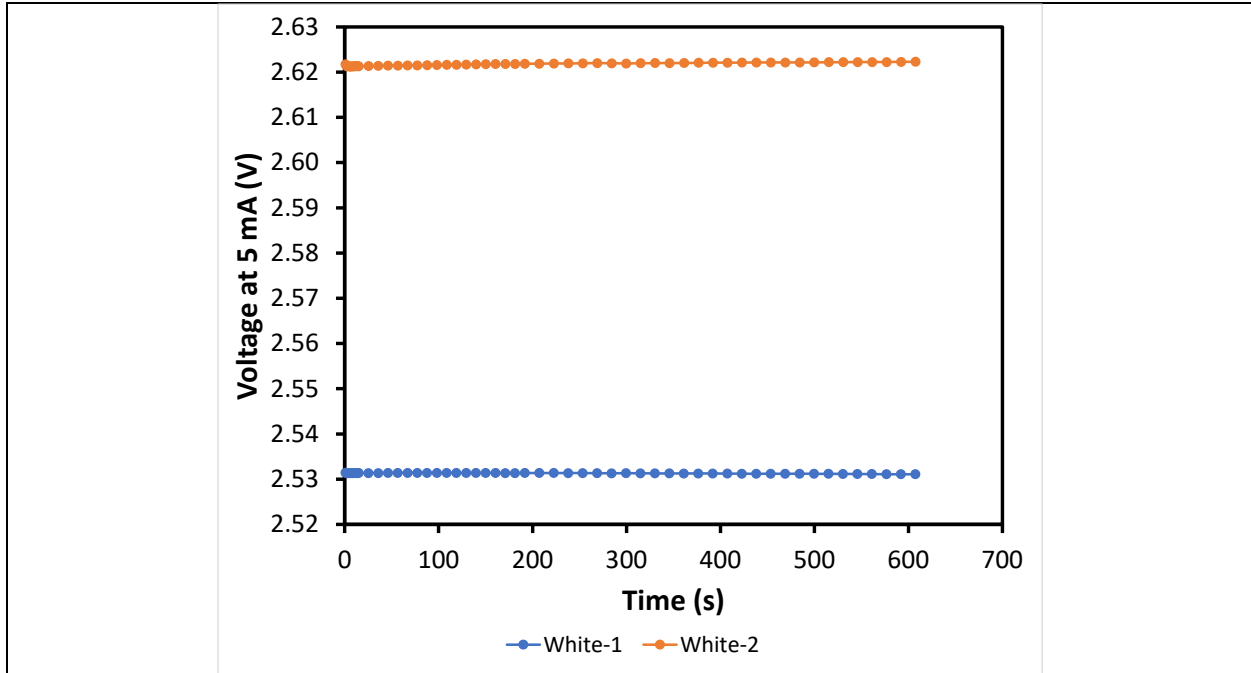


Figure B-5: V(t) graph for the white LED products, White-1 and White-2.

(This page intentionally left blank)

U.S. DEPARTMENT OF  
**ENERGY**

*Office of*  
**ENERGY EFFICIENCY &  
RENEWABLE ENERGY**

For more information, visit:  
[energy.gov/eere/ssl](https://energy.gov/eere/ssl)

DOE/EE-2543 • November 2021